CO_2 Foam Stabilization with Nanoparticles and EOR in Fractured Carbonate Systems

Master Thesis in Reservoir Physics

by

Henriette Trydal Horjen

Department of Physics and Technology

University of Bergen

June 2015

Abstract

This thesis is a part of an ongoing study of CO_2 foam mobility control in the Reservoir Physics group at the Department of Physics and Technology (IFT) at the University of Bergen. The goal of this thesis was to evaluate stabilization of foam and enhanced oil recovery (EOR) using hydrophilic silica nanoparticles and anionic AOS surfactants as foam agents. Foam was generated by co-injection of an aqueous foam agent solution and CO_2 as the gaseous phase. Foam is generated *in-situ* as the two fluids are mixed in the porous medium, resulting in a mobility reduction of CO_2.

Miscible CO_2 and CO_2-foam injection tests using surfactants as a foaming agent were performed to study the effect on tertiary EOR in carbonate reservoirs. The experiments were conducted in strongly water-wet, fractured and un-fractured Edward limestone core plugs. Foam is used for mobility control by blocking high permeable zones, resulting in a delay of gas breakthrough and significantly improve the macroscopic sweep efficiency. Supercritical CO_2 injections increased on average oil recovery by 20% OOIP compared to ordinary water injection. The highest recovery (63% OOIP) was obtained by first injecting supercritical CO_2 followed by CO_2-foam. Foam was generated *in-situ* in cores without fractures, verified by increased pressure drop. Foam generation in fractures was poor, mainly due to lack of generation sites, low stability and high oil saturation.

The limited stability of surfactant-generated foam in presence of oil, combined with high reservoir temperature and high salinity are among reasons why foam is not being widely used as a common EOR method. Nanoparticles are reported to work as foam stabilizers and are chemically stable in a wider range of reservoir conditions than surfactants. Experimental investigations using nanoparticles as foaming agents, without the presence of oil, were therefore conducted in this thesis. The sensitivity in parameters such as gas fraction, total injection rate and injection strategies using nanoparticles to generate foam were investigated. The pressure drop across the core was measured to estimate the achieved mobility reduction factor (MRF) and the apparent viscosity of the generated foam. The result shows that independent of the gas fraction, an increase in injection rate lead to a higher pressure drop. The apparent viscosity of the foam increased with higher gas fractions for some, but not all injections. The inconsistency is caused by a significant hysteresis effect. Common for the injection experiments is that high liquid or high gas fraction generates foam with a lower apparent viscosity.

Acknowledgements

First, I would like to thank my supervisor Associated Professor Martin Fernø at the Department of Physics and Technology at University of Bergen. Thank you for valuable guidance and input during this study.

To Professor Arne Graue, thank you for providing me the opportunity to work on interesting and challenging topic for my thesis, and for giving me the opportunity to travel abroad to conferences for educational purpose.

I would also like to thank PhD Bergit Brattekås and PhD candidate Marianne Steinsbø for great guidance and assistance during the experimental work. You two are great! A thank you goes to fellow master student Thomas Hjartnes for good collaboration.

A special thanks goes to my family, especially my parents, Else Lill and Jan Helge, for always being supportive and motivating me through these years of study. A great thank you goes to Magnus for being an outstanding, patient Word-expert, cheering me up during stressful times.

Finally, I would like to thank the other master students in room 506 for appreciated breaks, laughter and valuable educational discussions. This also goes to all my friends at UoB – thank you for all good memories throughout my studies.

Bergen, June 2015

Henriette Trydal Horjen

Table of Contents

1 Introduction

Typically 5-20% of the oil in a reservoir can be produced with pressure depletion, but in most fields water is injected for displacing the oil (Blunt, Fayers et al. 1993). Even after a successful waterflood, more than 60% of the oil remains in the reservoir. With the present oil price, performing tertiary enhance oil recovery (EOR) on existing fields is more economically beneficial compared to large investments in exploration and development of new fields.

Gas flooding is the most widely used EOR technique (Taber, Martin et al. 1997), and carbon dioxide gas (CO_2) has been used globally, primarily in the US for more than 40 years (Yu, Wang et al. 2014). Miscible CO_2 injections have the potential to provide a more environmental oil production by safely store CO_2 in the reservoir formation, and reduce the emission to the atmosphere. Despite good results from gas injections performed on large scales, the potential for improvement is great. The unfavourable mobility ratio due to the low viscosity of gas leads to gravity segregation and viscous fingering (Holm and Josendal 1974, Burger, Springate et al. 1996). Together with reservoir heterogeneity they all contribute to poor sweep efficiency leaving parts of the reservoir unswept (Koval 1963). These negative aspects can be mitigated by injecting gas in the form of foam. Foam is defined as a dispersion where gas is dispersed in a continuous liquid phase (Hirasaki 1989). It is a field proven EOR technique where foam improves the macroscopic sweep efficiency by reducing the gas mobility, and blocking high permeable layers in heterogeneous formations (Holm 1970, Kovscek and Radke 1994).

Understanding the fundamentals of foams in porous media is crucial for finding the optimal and most successful foam-assisted EOR processes. This has been intensively studied in many research groups. Foam behaviour with regard to gas and liquid fractions, and the interaction with oil present is of great importance for the oil production. Surfactants have been explored for foam generation for decades, but its limited stability in presence of oil and in harsh reservoir conditions paves the way for alternative foam agents. One such alternative is nanoparticles, which has been found to be effective foam stabilizers. Nanoparticles might be the solution for the harsh reservoir environments since they are stable in a wide range of physicochemical conditions (Yu, Wang et al. 2014). They can be used alone (Yu, An et al. 2012) or in synergy with surfactants (Roebrokes, Eftekhari et al. 2015).

Understanding the characteristic and fluid flow in carbonate reservoirs are also of important since more than 60% of the remaining reserves in the world are held in these formations (Whaley 2008). This thesis reports laboratory experiments in fractured carbonate core plugs for *in-situ* foam generation using anionic AOS surfactant and hydrophilic nanoparticles as foam agents in co-injection with CO_2. Using sensitivity analysis, foam stability and quality have been experimentally investigated.

2 Petrophysics in Reservoirs

This chapter gives an introduction to basic parameters in reservoir physics which are important for understanding the experimental results in this thesis.

2.1 Porosity

Sedimentary rock consists of mineral grains of different forms and shapes sedimented together developing pores between the grains. The void space between the grains is measured as porosity and is the ratio between pore volume to bulk volume. Porosity is strongly influenced by the range of grain size, grain shape and grain distribution. This parameter is important for some of the mechanisms studied in this thesis for foam generation since foam is generated in the pores. Experiments on sandstones and limestones outcrop core plugs are conducted. The porosity of sandstone is determined by the sedimentary processes deposition whereas porosity of limestone is mainly the result of changes taking place after deposition. Porosity can be divided into effective and disconnected porosity depending on if the pores are available and unavailable for fluid flow, respectively. In this thesis, the porosity mentioned means effective porosity only since this is the one of concern for the injection processes. Saturation is related to porosity and is defined as a fraction of the pore volume occupied by a particular fluid (Zolotukhin and Ursin 2000).

2.2 Permeability

Permeability is defined as a porous media capacity to transport fluids. Absolute permeability is the measurement of the capacity for flow of a single fluid through a porous formation when the formation is only saturated with the fluid. This parameter can be found by using Darcy's law defined in equation 2.1.

$$Q = \frac{K \cdot A \cdot \Delta P}{\mu \cdot L} \qquad [2.1]$$

where Q is the flow rate, K is the permeability, A is the cross sectional areal of the core, ΔP is the differential pressure, μ is the viscosity of the injected fluid, and L is the length of the core.

For Darcy's law to be valid some assumptions are made; the flow is horizontal and laminar, the porous media is 100% saturated by an incompressible, single fluid and there are no occurrence of chemical or physical interactions between the fluid and the rock. With two or more immiscible fluids present, Darcy's law must be extended to a multiphase flow where the individual phases are dependent on saturation of each fluid. This is called the effective permeability. For practical use, the relative permeability is defined for each phase and is the ratio between the effective and the absolute permeability. The relative permeability connects phase behavior and transport properties of the media and is a very important petrophysical parameter. In this thesis the cores undergo changes from being only saturated with one phase to being saturated with two and three phases during injections. In chapter 5.3 the permeability measurement for the performed experiments is explained in detail. The

parameter is important for being able to compare the results in cores of different rock types with regard to the differential pressure obtained by the generated foam. The cores are also examined for changes in permeability due to adsorptions of foam agents at the rock surfaces.

Just as porosity and permeability are the most basic properties in a single-phase flow, capillary pressure is the most basic rock-fluid parameter in multiphase flow (Kulkarni and Rao 2004). The capillary effects are especially important when the flow rates are low, permeability varies over short distances with large contrasts and permeability differences (Corbett, Ringrose et al. 1992). Water injected into a reservoir is incapable of displacing all the original oil in place because of capillary and surface forces acting in the fluid-rock-system. These forces counteracts the pressure gradient caused by water and significantly affects the oil recovery even on reservoir scale (van Lingen and Knight 1997). This makes secondary and tertiary injections important enhanced oil processes (Skjæveland and Kleppe 1992). Capillary pressure can be defined as the molecular pressure difference across the interface of two immiscible fluids present in a narrow channel and can be found by a simple form of Laplace's equation

$$P_c = p_{nw} - p_w = \frac{2\,\sigma_{nw-w}\cos\theta_c}{R_c} \qquad [2.2]$$

where the first condition, p_{nm} and p_w, is the internal pressure in the non-wetting and the wetting phase respectively. σ_{nw-w} is the interfacial tension between the fluids, θ_c is the wetting angle and R_c is the radius of the pore/capillary tube (Lake 1989). The first condition in equation 2.2 holds if the absence of interfacial tension refers to the two adjoining miscible phases and the second condition hold only for the simple uniform tube geometry.

The capillary pressure plays a supportive pressure role in the case where the displacing fluid is also the wetting fluid. This is for example in a water wet reservoir where water displaces the oil. In laboratory experiments this may on the other hand not be the case where other injection fluids often are used. In this case the capillary pressure does not work as a supportive pressure and a residual oil saturation remains in the reservoir after waterflooding (Kulkarni and Rao 2004).

2.3 Wettability

Wettability is defined as the tendency a fluid has to adhere to a solid's surface in the presence of another immiscible fluid. This parameter can be found by measuring the contact angle between the liquid-liquid's interface and the solid's surface, and is called the wetting angle. The angle reflects equilibrium between the interfacial tension at the fluids interface, and their individual adhesive attraction to the solid. The wettability is a complex function of fluid and solid properties. In a water-wet reservoir the water lays as a water film along the pore walls and oil is found in the middle of the pore volume (Willhite 1986). The cores used in this thesis are water-wet, which is also the wettability that is common for reservoirs.

Interfacial tension (IFT) between to immiscible fluids can be seen as a surface separating two phases. This surface has relative stronger intermolecular cohesion and little or no molecular exchange between the fluid phases. The cohesive forces are stronger than the adhesive and are strongest on the denser fluid side. This results in a sharp change in molecular pressure across the boundary between the two phases. The boundary can be seen as a convex meniscus curve on the interfaces, curving towards the wetting fluid when the fluids are in contact with each other in a capillary glass tube. The magnitude of the IFT represents the work or energy required to keep the two fluids apart in a pressure equilibrium state. For a two phase system with constant temperature (*T*) , pressure (*P*) and mass (*M*) the interfacial tension is given as

$$\sigma = \left(\frac{\partial G}{\partial A}\right)_{T,P,M_{1,2}} \quad [2.3]$$

where σ is the interfacial tension, *G* is the Gibbs free energy and *A* is the interface area (Zolotukhin and Ursin 2000).

2.4 Capillary Number

In a miscible or immiscible displacement of two fluids, four vital drive mechanisms are present; gravity forces, viscous forces, capillary forces and dispersion. The ratio of viscous forces to capillary forces is an important parameter, and is a convenient dimensionless number called the *capillary number,* N_c, defined as

$$N_c = \frac{v\,\mu}{\sigma \cos\theta} \quad [2.4]$$

where *v* is the velocity, μ is the viscosity, σ is the interfacial tension and θ is the wetting angle (Zolotukhin and Ursin 2000).

Capillary number theory predicts that no residual oil saturation can be mobilized until a critical capillary number is exceeded. Chatzis and Morrow found that the critical capillary number for mobilizing trapped oil in a porous media is about 10^{-5} (Chatzis and R. 1984). In enhanced oil recovery, the capillary number is preferably increased by increasing the injection rate or lowering the interfacial tension between the fluids by adding surfactants. Adding polymers to the injected fluid increases the viscosity which could also lead to an increase in capillary number (Zolotukhin and Ursin 2000).

2.5 Mobility

Mobility is considered a key parameter in fluid flow behavior and displacement efficiency. The sweep efficiency of a porous medium is dependent upon the mobility ratio, *M.*

$$M = \frac{(K_r/\mu)_1}{(K_r/\mu)_2} \quad [2.5]$$

where K_r is the relative permeability and μ_1 and μ_2 is the viscosity for the displacing and the displaced fluid phase respectively (Aronofsky 1952).

For miscible displacement the effective permeabilities to both phases are equal, and *M* is reduced to (Habermann 1960)

$$M = \frac{\mu_1}{\mu_2} \quad [2.6]$$

Based on information from laboratory experiments it is believed the mobility ratio may vary over a range between 20 and 0.05 (Aronofsky 1952). From equation 2.5, an efficient and stable displacement is developed if $M < 1$. The displacing fluid has a lower mobility compared with the fluid displaced and the possibility of viscous fingering is low. On the other hand, if $M \geq 1$, which is often the case when using gas, the displacing fluid has larger mobility than the displaced fluid. Injecting gas into heterogeneous reservoirs with high permeable zones leads to poor sweep efficiency caused by viscous fingering. In this thesis, foam is used for enhanced oil recovery and CO_2 mobility reduction. The foam mobility is defined as the ratio between the core effective permeability and the viscosity of CO_2-brine/foam (Mo, Yu et al. 2012).

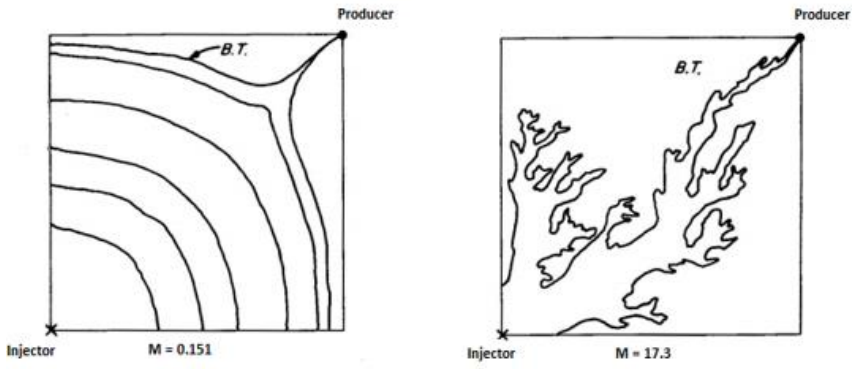

Figure 2-1 Viscous fingering in a quarter five-spot model for two different mobility ratios. For M<1 (left) a stable displacement front has developed. For M>1 (right) viscous fingering has occurred leading to an early breakthrough and poor sweep efficiency (Habermann 1960).

3 Carbon Dioxide for Enhanced Oil Recovery

The goal with Enhanced Oil Recovery (EOR) by injecting a solvent into the reservoir is to increase the local capillary number and lower the residual oil saturation. In Norwegian offshore fields, hydrocarbon gas injection is feasible and a common production strategy because the gas is available directly from the production (Jensen, Harpole et al. 2000). Hydrocarbon gas injection is cheaper and easier compared with CO_2, where CO_2 capture and pipelines for transporting the gas out to platforms is needed. However, the use of CO_2 in EOR is being tested and improved for environmental concerns and better displacement efficiencies.

Injecting carbon dioxide into a reservoir is currently one of the most used techniques for tertiary enhanced oil recovery worldwide (Taber, Martin et al. 1997, Yu, Wang et al. 2014). In USA, it remains an important EOR method in-spite of oil price swings and ownership realignments(Contreras, Durst et al. 2010). A simulation study of CO_2 injection into oil reservoirs on the NCS showed that approximately 63% of Original Oil in Place, OOIP, could be recovered with CO_2 injection compared to approximately 43% OOIP for water injection (Lindeberg and Holt 1994). North sea fields are attractive prospects for carbon dioxide flooding since these fields produce light crude oil, and the reservoirs are less heterogeneous compared with US fields (Skjæveland and Kleppe 1992). The density of CO_2 is similar to the density of the typical light oil making the CO_2 less prone to gravity segregation compared to nitrogen and methane. The gas frees trapped oil by various mechanisms, which will be discussed later, leading to a better sweep of the reservoir. Despite the increased enhanced recovery, the sweep efficiency is low due to the unfavorable mobility ratio between oil and gas. It is well understood that field tertiary recovery efficiencies are determined largely by volumetric sweep efficiency.

CO_2 injections into reservoirs have been used in the US as an enhanced oil recovery mechanism for more than 40 years. The displacement of oil is efficient, but there are challenging improvements in the sweep efficiency which could have a huge impact on the recovery (Hustad and Austell 2004).

CO_2 is commonly used since it, after water, has relatively low cost if it is found near an oil field. Unfortunately, the use of CO_2 causes corrosion and faces a utilization problem with regard to equipment and piping, making it a challenging fluid to use. In addition to this, even though the emission to the atmosphere has increased, it is difficult to obtain concentrated CO_2 (Skjæveland and Kleppe 1992).

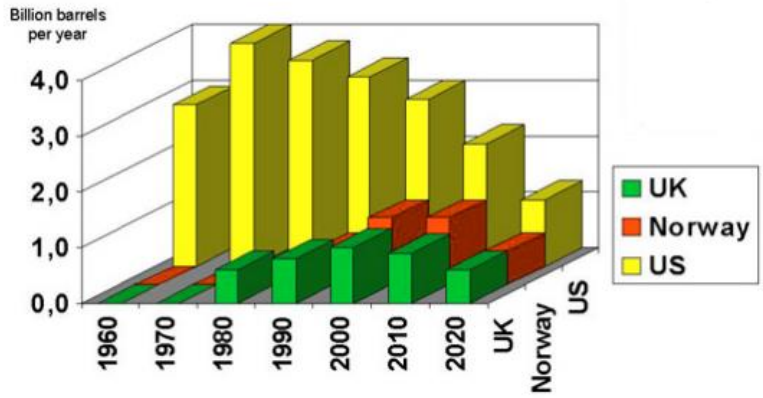

Figure 3-1 Comparison of US and the North Sea Oil production. The US has more than 20 years experience with tertiary EOR compared to Norway and the North Sea (Hustad and Austell 2004).

3.1 The Use of CO2

CO_2 occurs naturally in the atmosphere without any color or odor. As the global population is increasing, the atmospheric concentration of the gas has risen the last few centuries. The demand of fossil fuel also rises resulting in an increase of emission of CO_2 to the atmosphere. Through our interference with the carbon cycle we artificially move carbon from solid storage state to its gaseous state, thus the atmospheric concentration increases (NOAA 2014). Capturing and storing of CO_2 in the reservoir can help the mitigation of global warming concerns. Using CO_2 as injection fluid for enhanced oil recovery can result in a more sustainable oil production. This benefits the human society with capabilities of producing more hydrocarbons as well as capturing and storing CO_2 in underground geological structures. (Dooley, Dahowski et al. 2010) To consider application of CO_2 injection for EOR and in mature oil fields for storage, it is important to have knowledge and understand the thermodynamic properties of the gas and miscibility in a CO_2-oil system. The reservoirs subsurface conditions on the Norwegian Continental Shelf, NCS, are in the pressure region of about 200-300 bar and temperature of 70°C-130°C (NPD 2015). Study of CO_2 phase behavior under these conditions shows that CO_2 will be in a supercritical state. This means the gas will have liquid-like density and gas-like viscosity. High density CO_2 will migrate downward in the reservoir and not only sweep the upper part as a less dense gas like methane would do. CO_2 is often used because it remains a denser fluid over larger areas of the range where reservoir pressures and temperatures are found (Blunt, Fayers et al. 1993). The viscosity of dense CO_2 is between 1-20% of most crude oils at reservoir conditions (Grigg, Svec et al. 2003). Compared to hydrocarbon gases the supercritical state of CO_2 gives a more favorable mobility ratio. The supercritical state is reached after the critical point shown in the phase diagram in Figure 3-2.

The critical pressure is the pressure required at the critical temperature for liquefying the gas. The dense or supercritical CO_2 is reached at pressure 73.0 atm (74.0 bar) and temperature 31°C. CO_2 does not exist in liquid form at atmospheric conditions and can first be in liquid state after the triple point is reached. The experiments in this thesis are performed above the triple point, both as liquefied and supercritical CO_2 gas.

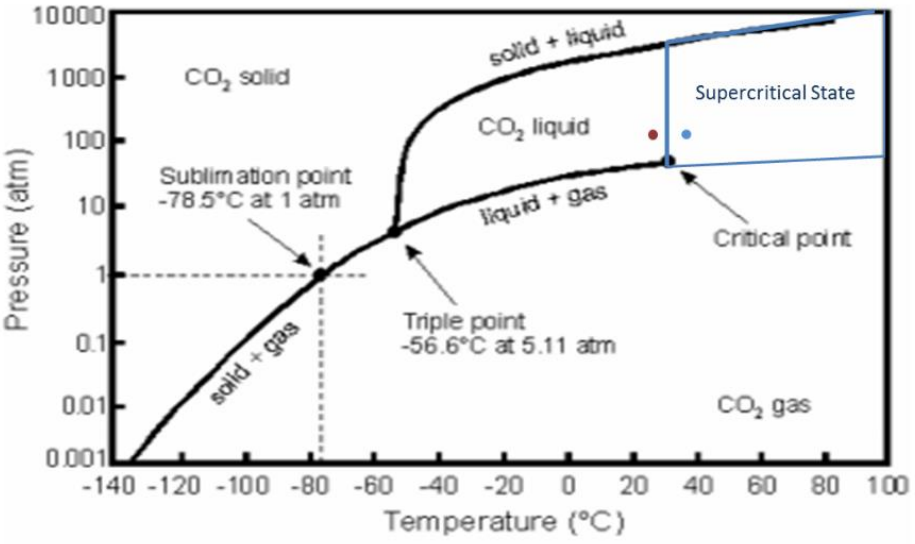

Figure 3-2 Pressure-Temperature CO_2 phase diagram. The red (90 bar, 25°C) and blue point (90 bar, 35°C) illustrates conditions the experiments in this thesis are performed under. Modified from (Picha 2007).

The main challenge injecting CO_2 into a reservoir is the macroscopic sweep efficiency (Skjæveland and Kleppe 1992). The high mobility of gas compared to the other fluids in the reservoir frequently leads to poor sweep efficiency both vertically and horizontally. These problems include gas channeling in high permeable zones and gas coning into production wells (Zolotukhin, A. B., Ursin, J. 2000). CO_2 flooding is considered an inefficient process for EOR in fractured reservoirs based on early breakthrough in the high permeable fractures. The CO_2 tend to follow this high permeable network resulting in poor sweep efficiency (Asghari and Torabi 2008). The macroscopic displacement efficiency can be improved in fractured reservoirs if the mobility of CO_2 is reduced. The viscosity of CO_2 foam is higher than of dense CO_2 and thus has a more favorable mobility ratio during oil displacement. This is the main topic of this thesis and will be explained in more details.

3.2 Miscibility

To understand how injected fluids into a reservoir react with the oil already in place it is important to have a knowledge of how miscibility works. This is an important chapter with regard to this thesis because the experiments are performed at miscible conditions for CO_2. For petroleum reservoirs miscibility is defined as the physical condition when two or more fluids form a single homogenous phase where no interfacial tension between the two fluids is present (Holm 1986). If two fluid phases form after an amount of one fluid is added to another, an interfacial tension develops and the two fluids are immiscible.

In laboratory experiments where CO_2 and reservoir oil pressure is above the Minimum Miscibility Pressure, MMP, miscibility is developed and the flooding of CO_2 increases the oil recovery. CO_2 has the potential to perform either as an immiscible or miscible gas. The nature of its behavior depends on the composition of the reservoir oil and the reservoir conditions (CO2CRC 2015). For a miscible CO_2 injection, the fluid extracts heavier components up to C_{30} from the oil which makes the oil less viscous. This is in contrast to hydrocarbon gas injection where mainly intermediate components like C_2-C_6 are extracted (Skjæveland and Kleppe 1992). CO_2 also develop miscibility with oil at lower pressures than other gasses (Zuta 2010).

The primary goal for a miscible flood injection is to recover the residual oil that remains in a reservoir, often after a secondary recovery. The miscible flood eliminates the interfacial forces between the fluids and makes the trapped oil mobile. It can also sometimes displace oil from regions where the water injection has not swept the area. However, the miscible displacement can leave a sustainable amount of residual oil behind in the reservoir. This occurs at the back of the displacement front due to instabilities caused by viscous fingering, large heterogeneities or water shielding (Muller and Lake). Two main factors affecting the miscible injection performance are oil displacement efficiency at pore level and sweep efficiency on field scale (Healy, Holstein et al. 1994).

Two types of miscible displacement exist: first-contact miscibility and multi-contact miscible displacement. First-contact miscibility is when any amount of the solvent can be injected and will exist as a single phase together with the reservoir oil (Holm and Josendal 1982, Holm 1986). Meeting the conditions for first-contact miscibility are not easy. Good injection gasses are usually very expensive and a continuous injection of the gas is not economically benefitted. The other mechanism, multi-contact miscible displacement, is the reason why oil is swelling. Oil originally bypassed by waterflooding can be recovered by getting in touch with the injected gas. The gas can than dissolve in

the oil phase making the oil swell, or the gas may extract the oil. This method result in efficient displacement, but not as efficient as the miscible case (Zolotukhin and Ursin 2000).

Oil recovery during an ideal miscible displacement is nearly 100%, whereas it is much lower during an immiscible displacement (Takahashi, Okabe et al. 2012).

3.3 MMP - Minimum Miscibility Pressure

Two immiscible fluids might become miscible at a certain pressure. For a miscible displacement process to develop, MMP has to be reached. CO_2 MMP is determined by pressure, temperature, solvent purity and molecular weight of the heavy fractions of the reservoir oil (Lake, 1989).

Since solvent miscibility increases with pressure, ultimate oil recovery should also increase with pressure. However, there is a pressure in which a further increase in pressure only leads to a minimal increase in oil recovery – this is the MMP. Residual oil recovery is observed to decrease dramatically as the system pressure was reduced below MMP (Grigg, Gregory et al. 1997). The MMP vs. oil recovery is illustrated in Figure 3-3 for CO_2 for constant temperature and oil composition.

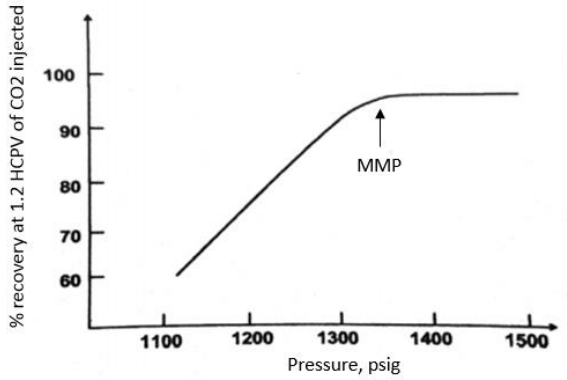

Figure 3-3 Schematic illustration of MMP for CO_2 for fixed oil composition and temperature (Skarrestad and Skauge 2011). The oil recovery is greatly increasing until MMP is reached.

In this thesis, n-decane was used as the oil phase when conducting experiments for EOR. N-decane is a mineral oil composed of a single hydrocarbon component. This oil exhibit a viscosity ratio at room temperature in the range of a typical light reservoir oil on NCS (Graue, Nesse et al. 2002). The simplified oil chemistry of decane provides stable wettability conditions (Brattekas, Haugen et al. 2013).

The MMP for n-decane and CO_2 is shown in Figure 3-4. These results are based on reported experiments using high spatial magnetic resonance imaging (MRI) (Song, Zhu et al. 2011). The signal intensity of n-decane decreased to zero and the interface disappeared reaching the MMP. MMP experiments have also been performed by other researchers and the results are plotted in the same graph, showing fairly consistent values. MMP for n-decane/CO_2 system at temperature 25°C is 59 bar and for temperature 35°C the MMP is 74 bar. All the experiments conducted in this thesis are above the minimum miscibility pressure for a CO_2/n-decane system.

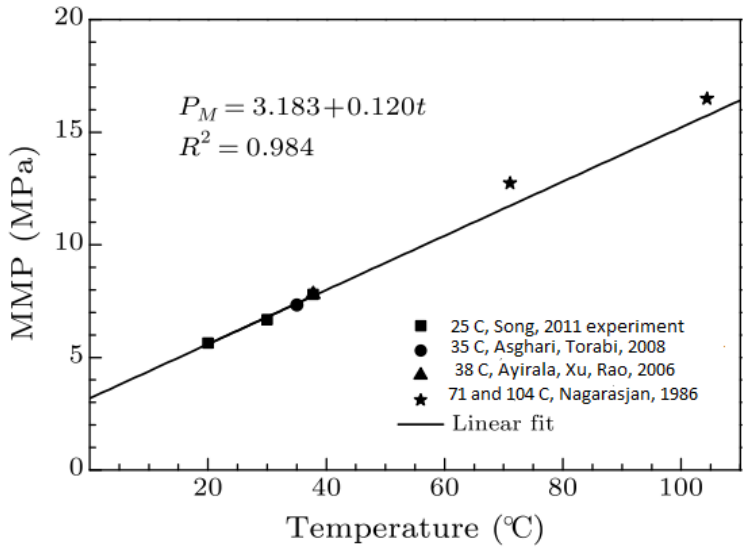

Figure 3-4 MMP of CO_2/n-decane system from 20°C to 37.8°C (Song, Zhu et al. 2011). The values are compared with MMP results measured by (Nagarajan and Robinson 1986, Ayirala and Rao 2006, Asghari and Torabi 2008).

3.4 Diffusion

Numerous theoretical and experimental work have established diffusion as an important recovery mechanism in EOR processes (Burger, Springate et al. 1996). This process has shown especially large impact on laboratory scale. Molecular diffusion is one of the four basic recovery mechanisms when injecting gas into a reservoir. The other recovery mechanisms are viscous forces, gravity drainage and imbibition. CO_2 injection into fractured and whole core plugs have been performed experimentally in this study for enhanced oil recovery. These characteristics are important for the obtained results.

Displacement efficiencies using CO_2 as injection gas depend on the favorable phase-behavior effects from mixing the injected gas and the oil in place. At pore level, the molecular diffusion is responsible for this mixing process to be favorable (Grogan, Pinczewski et al. 1988). The diffusion mechanism describes the mixing of miscible fluids by the transfer of molecules caused by concentration gradients (Haugen and Firoozabadi) illustrated in Figure 3-5.

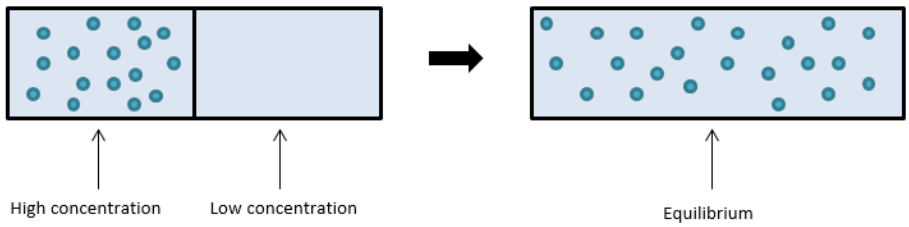

Figure 3-5 Schematic illustration of diffusion. The blue dots are the high concentrated fluid mixed with another fluid shown as light blue color. Over time, the high concentrated fluid diffuses over to the low concentrated area and establishes equilibrium within the fluid.

For an oil-wet reservoir case where CO_2 is injected into the formation, the gas will contact the oil directly (Grogan, Pinczewski et al. 1988). It is observed higher recovery in oil-wet cores then in water-wet cores during tertiary CO_2 injection (Tiffin and Yellig 1983). This is because the oil preferentially wets the rock surface in oil-wet cores, and the oil is a more continuous phase then in water-wet cores. This results in shorter diffusion paths and hence a better recovery then for water-wet cores for similar contact time (Darvish 2007). This is different for a water-wet reservoir case. When the gas is injected as tertiary recovery mechanism, it may contact the oil by diffusion through a blocking water phase (Grogan, Pinczewski et al. 1988). The presence of water reduces diffusional fluxes and lenghts, and consequently increase the amount of oil recovery (Skjæveland and Kleppe 1992). Diffusion can occur in gases, liquids and dense phases and can be a very slow process driven by gradient pressure, temperature and concentration.

The diffusion length is affected by pore-space geometry, microscopic and macroscopic heterogeneities, fluid properties and rock wettability. If the pore network is very tortuous, the diffusion molecules have to travel a longer distance resulting in a slower diffusion rate. According to Grogan and Pinczewski the time required for CO_2 to diffuse a given distance, x, through a water barrier might be scaled by

$$t_{field} = t_{lab} \left(\frac{x_{field}}{x_{lab}}\right)^2 \quad [3.1]$$

Grogan and Pinczewki, 1987, performed experiments determining the diffusion coefficient for CO_2 in contact with decane at reservoir conditions of 25°C and 870 psia (60 bar). They concluded it was the same trend regarding measurements performed under these reservoir conditions as for previous experiments performed under atmospheric conditions. Displacement processes with little contact time, long diffusion path, low diffusion rates, or non-equilibrium effects may reduce the displacement efficiency and hence the oil recovery (Grogan and Pinczewski 1987).

3.5 Dispersion

Dispersion describes the mixing of two fluids in a porous medium during a miscible displacement process. This displacements process is caused by molecular diffusion, local velocity gradients, locally heterogeneous streamline lengths and mechanical mixing within the pores (Lake 1989, Bijeljic and Blunt 2006). The dispersion moves both longitude and transverse. The longitude movement is dominated by dispersivity term under field conditions, whereas the dispersion in the transverse directions is often dominated by the molecular diffusivity term (Perkins 1964).

Due to highly complex geometry of the porous media, prediction of the transport properties is difficult. Even though many experiments and theoretical studies have been conducted, there is a lack of understanding how pore structure controls dispersion. Dispersion and diffusion are often not represented mechanistically at field scale. Mass transfer from a bypassed region to a flowing region is a very strong function of the solvent phase behavior. Capillary-driven crossflow, dispersion and diffusion can contribute to this mass transfer (Burger, Springate et al. 1996). When tracer particles are injected into a porous media the particles will be transported and mixed. This will be done due to random movement between the streamlines within the channels, mixing at pore intersection and due to diffusion-like mixing in the regions with very low velocity (Bijeljic and Blunt 2006). This is illustrated in Figure 3-6.

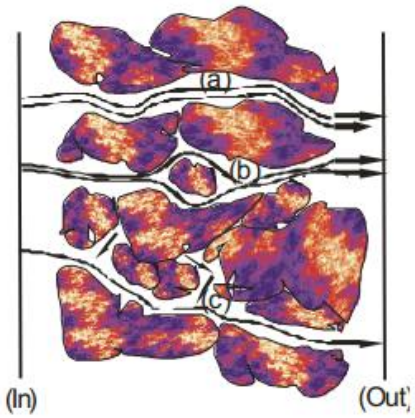

Figure 3-6 Dispersion within a porous medium. Blue and red colored shapes indicate grains. Tracer particles are injected at the inlet indicated by black arrows. The particles are transported by a) random moving along the streamlines, b) mixing at pore intersections, and c) mixing at low velocity region and measured at the outlet (Bijeljic and Blunt).

3.6 Swelling of Oil

Some of the injected CO_2 dissolved in the oil causes the oil to swell. This makes the oil occupy a larger fraction of the pore space. This could lead to oil drops interconnecting, making a continuous pathway of oil. The immobile oil will then be mobile for displacement (Blunt, Fayers et al. 1993).

Campbell did in 1983 a very interesting experiment where a "dead-end" pore filled with oil was recovered by diffusion through a blocking water shield. Initially the oil was separated by a water barrier from waterflooding. As the CO_2 was injected, the oil continued to swell caused by diffusion through the water barrier. After 26.5 hours the oil had swelled enough to push the water barrier away and the oil came in direct contact with the CO_2 (Campbell and Orr 1985).

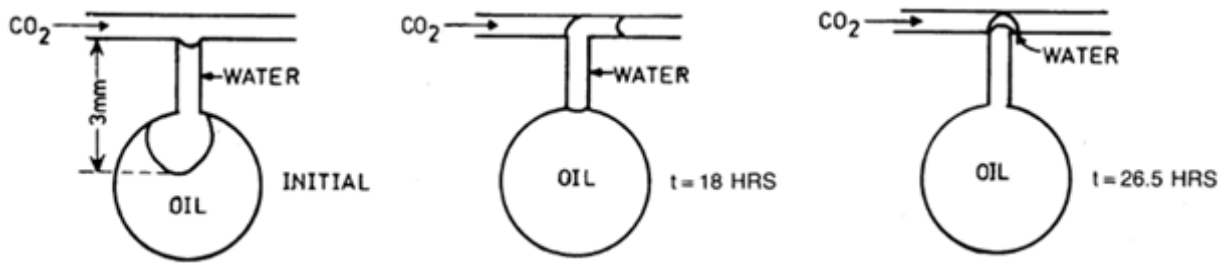

Figure 3-7 Micromodel "dead end pore" oil recovery by CO_2-injection illustrating water shield and oil swelling. Modified by (Grogan and Pinczewski 1987).

Swelling of the oil phase causes a breakdown of the original capillary equilibrium resulting in a redistribution of the phases. For this process to be fully efficient, it is important for sufficient time for the diffusion of CO_2 to swell the oil significantly (Grogan and Pinczewski 1987). Typically during diffusion the oil will swell with 30-40% and the water with 2-7% (Holm and Josendal 1974). The oil swelling depends on the amount of methane in the oil. When CO_2 contacts reservoir oil, it will not displace all the methane. This indicates less swelling of the oil when more methane are present (Skjæveland and Kleppe 1992). Takahashi experienced that the saturation pressure and swelling factor increased as the CO_2 concentration increased for different CO_2 and oil mixtures (Takahashi, Okabe et al. 2012).

4 Foam

Any gas and water injection into an oil filled reservoir ultimately faces gravity segregation. The low-density gas tends to migrate upwards sweeping the upper part of the reservoir, and the high-density water tends to sweep the bottom part of the reservoir. Field studies and laboratory experiments have shown that generation of foam can reduce the mobility of CO_2 injections and mitigate the effects of gravity override, viscous fingering and channeling in high permeable layers. This leads to a delayed breakthrough of the injected gas and a more efficient macroscopic sweep resulting in an increase in oil production (Zuta 2009). A greater pressure gradient during foam injection increases the traveling distance before segregation and essentially improve sweep efficiency. The level of gravity segregation is dependent on the injected CO_2 phase and if formation wettability and reservoir fluids is detrimental to foam stability (Sheng 2013). Foam can affect oil recovery in two ways; 1) stabilizing the displacement process by increasing the displacing fluid viscosity, making a more favorable mobility ratio, 2) by blocking high permeability layers in the reservoir. In addition to these two mechanisms, the gas is in more contact with the oil when foam is developed and interfacial mass transfer between the oil and gas will play an important role in oil mobilizing. This is done through mechanisms already mentioned like dissolution, viscosity reduction, diffusion and swelling of oil (Yaghoobi 1994, Farajzadeh, Andrianov et al. 2010a).

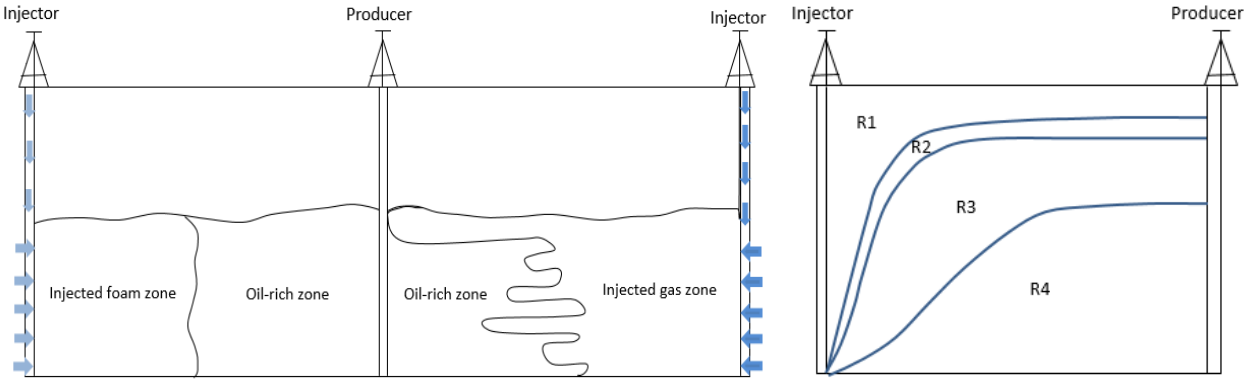

Figure 4-1 Schematic illustration (left) of how an unstable gas injection front behaves with gravity segregation and viscous fingering compared to a foam injection front. A more stable front is developed by foaming of the gas. The gas mobility is lowered giving a better sweep efficiency. Reproduced from (Farajzadeh, Andrianov et al. 2010a). Comparison Illustration (right) of sweep area in a reservoir from injection well to production well during gas and foam injection. R_1 is region already gas swept, R_2 is region where oil production might occur with further injection of gas but might not be cost efficient, R_3 is additional oil recovered by diversion of gas by foam reducing mobility and high permeable layers. R_4 is unrecovered area. Modified from (Farajzadeh, Andrianov et al. 2009).

The following chapters introduce the general basics of foam generation and foam stability with the use of surfactants and nanoparticles as foam agents. These foam agents are used experimentally in this thesis.

4.1 Characteristics of Foam

Foam is used to reduce the gas-phase mobility through formation of stable gas-liquid films (Lake 1989). Foam in porous media is defined as a dispersion of a relatively large volume of gas in a small volume of liquid (Hirasaki 1989). It is a special type of colloidal dispersion where gas is dispersed in a continuous liquid phase. The dispersed phase is referred to as the internal phase, and the continuous phase as the external phase (Schramm 1994). Such dispersion is normally unstable and will quickly break in less than a second unless a foam agent is added to the liquid. The stability is then greatly improved and the foam can persist much longer (Lake 1989).

A foam structure can always be formed in a liquid if bubbles of gas are injected faster than the injected liquid between the bubbles can drain away. Figure 4-2 (left) illustrates a general two-dimensional foam structure illustrating different terms to describe a foam system. The gas phases are separated from each other by thin liquid film defined as *lamella.* The connection of three lamellas at an angle of 120^{o} is referred to as the *Plateau* border (Schramm 1994). Foam flow behavior is dominated by interactions between pore walls and lamellae, where the lamellae are believed to be responsible for the mobility reduction (Zolotukhin and Ursin 2000) (Skarrestad and Skauge 2012). Two types of foam exist; wet-foam and dry-foam. Wet-foam is when the foam is compressing spherical bubbles separated by relatively thick layers of liquid, whereas foam of polyhedral bubbles separated by thin, plane films is referred to as dry-foam (Sheng 2013).

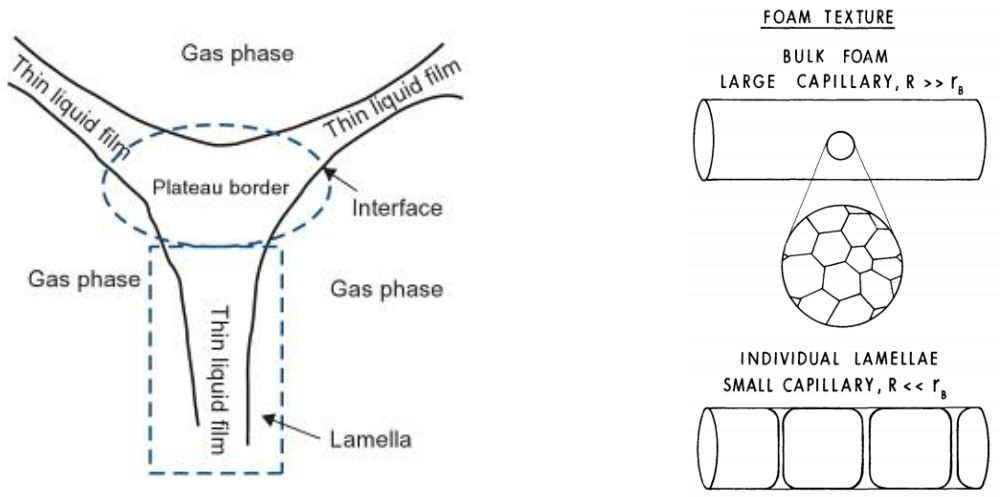

Figure 4-2 A two-dimensional illustration of a general foam system (left) (Schramm 1994). Illustration of lamella configuration in large and small capillaries (right) (Hirasaki and Lawson 1985). R is the capillary radius and r_b is the radius of the foam bubble.

When foam exists as bulk foam, multiples lamellae create a network around the dispersed gas bubbles. This occurs when the capillary radius is large compared to the equivalent radius of the bubbles (Figure 4-2, right) (Hirasaki and Lawson 1985). Foam restricted inside a pore network in a porous medium has a different morphology than the structure of the bulk foam. Individual bubbles of gas separated by lamellae form the confined foam (Skarrestad and Skauge 2012). If the capillary radius is much less than the equivalent bubble radius each lamella is separating two gas bubbles (Hirasaki and Lawson 1985). Foams injected in a porous media undergo constantly dynamic mechanisms of *in-situ* lamella creation and coalescence which will be explained further the following chapters.

4.2 Foam Generation in Porous Media

Foam bubble generation and decay are continuous, dynamic processes. Researchers have identified three fundamental mechanisms for foam generation at pore-level in porous media; snap-off, leave-behind, and lamella division (Ransohoff and Radke 1988).

The snap-off mechanism occurs as the non-wetting phase passes through a pore throat and enters the liquid filled pore. The pressure difference across the interface at the pore throat is greater than the pressure difference at the leading interface resulting in snap-off of the gas bubble (Ransohoff and Radke 1988). The discontinuity of the gas phase is increased, and lamellae are created which influences the flow properties of the gas phase. Given sufficient permeability contrast and sufficient fractional flow of water, gas flowing through a zone with increasing permeability will undergo snap-off because of the capillary pressure reduction (Tanzil 2000). It is found experimentally that snap-off in an increasing permeability region occur regardless of flow rate. A critical flow rate velocity is reported where strong foam is generated above and weak foam below the critical value (Ransohoff and Radke 1988). This foam generation mechanism explains the origin of residual oil saturation since liquid is left behind in the pore throat.

Figure 4-3 Illustration of snap-off using gas injection. A gas bubble penetrates in the narrow throath between two grains (left) and a new bubble is formed (right). P_{cT} is the pressure at the throat, and P_{cF} is the pressure at the leading interface of the gas bubble. Snap-off occurs when $P_{cT} > P_{cF}$.. Reproduced from (Ransohoff and Radke 1988).

Foam is generated by the leave behind mechanism when two gas fingers invade the same liquid-filled pore body from different directions. The two fronts squeeze the liquid between them, create lamella and leave behind a liquid lens. Leave behind produces continuous gas foam, so-called weak foam and is a non-repetitive process that alone cannot account for the reduction in gas mobility seen by foam generation. (Ransohoff and Radke 1988).

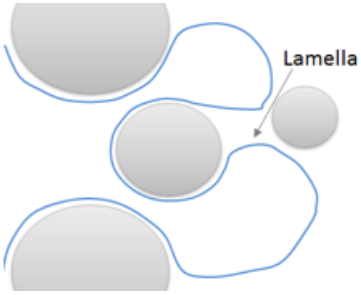

Figure 4-4 Illustration of foam formation by the mechanism "leave behind". Reproduced from (Ransohoff and Radke 1988)

Lamella division is also called secondary foam generation because it only occurs if foam is already existing and is flowing (Ransohoff and Radke 1988). When a lamella enters a pore body with several throats it might spread into different directions and create new lamella. This is provided that pressure gradient is sufficient to mobilize the lamella. Lamella division produces discontinuous gas foam or so-called “strong foam”. This mechanism is similar to the snap off mechanism in the way that a new separate bubble is formed, which can either flow or block gas pathway (Sheng 2013).

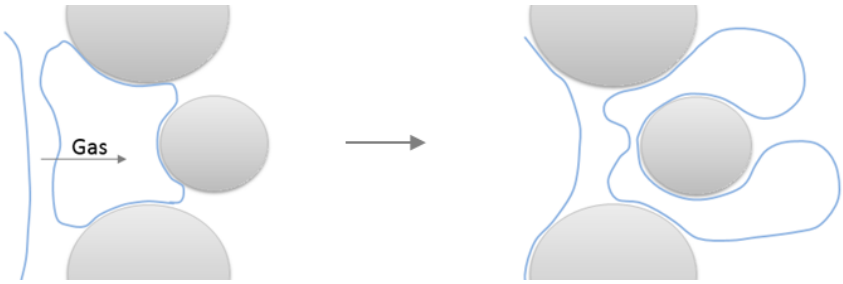

Figure 4-5 Illustration of lamellae division mechanism. Reproduced from (Ransohoff and Radke 1988)

Foam can be divided into two different classes: continuous-gas foam and discontinuous-gas foam. The continuous-gas foam exists as a continuous gas channel uninterrupted by lamella. The mobility reduction compared with pure gas injection is small. The only effect of this type of foam is the small reduction in relative permeability of the gas, and it is therefore often called “weak foam”. The discontinuous-gas foam has a discontinuous gas phase caused by lamellae and there are no continuous gas channels over large distances. For the gas to be able to flow, the lamellae must be transported through the pore system. The resistance in displacing the lamellae causes a large mobility reduction of the gas making the discontinuous foam a “strong foam” (Hirasaki 1989). When the strong foam is formed, the effective foam viscosity is increased and thus the relative mobility of the gas is decreased by up to several orders of magnitude. This again leads to a high increase in pressure gradient and reduction of water saturation (Sheng 2013) (Persoff, Radke et al. 1991). In typical core flood experiments the transition from weak foam to strong foam often occurs as a drastic increase in pressure drop.

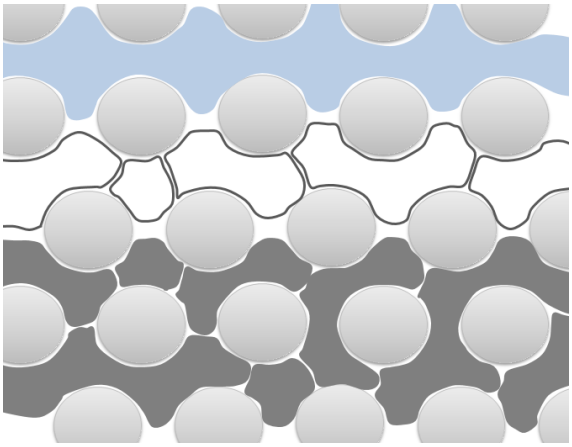

Figure 4-6 Illustration of foam at pore-level of foam in a porous medium. The blue bubbles are continuous gas, the white bubbles are flowing discontinuous gas, and the dark grey area is trapped discontinuous gas. The round, grey areas illustrates grains in the porous medium. Reproduced from (Kovscek and Radke 1994).

4.3 Foam Stability

For foam to be an efficient displacement fluid the lamella must remain stable. The stability is a function of both the petro-physical properties of the porous media and the foam film properties. The strength of the foam is related to the magnitude of the pressure gradient across the porous media (Farajzadeh, Andrianov et al. 2012).

Together with foam generation, the foam also begins to decay due to various processes. Film thinning and coalesce (film rupturing) are two of these processes that are considered in the definition of foam stability. Coalesce occurs due to gas diffusion. When smaller gas bubbles diffuse over to bigger gas bubbles, through the liquid films, the liquid films rupture (Schramm 1994) (Möbius and Miller 1998). The foam film thinning is related to the disjoining pressure. This pressure represents the pressure difference between the gas phase and the bulk liquid from where the lamellae extends (Schramm 1994). When the foam film becomes thinner, the two surfaces of the foam film interacts with each other. The gas pressure in the foam bubbles is always higher than the pressure in the liquid phase. This pressure difference forces liquid to flow towards the Plateau borders (Figure 4-2) causing capillary suction. A high positive value of the disjoining pressure implies strong repulsive forces between the film interfaces making a stable film. Negative values implies strong attractive forces and creates an unstable film. At equilibrium, the disjoining pressure equals the capillary pressure (Farajzadeh, Andrianov et al. 2012). The lifetime of the lamella and corresponding bulk foam becomes short above a critical capillary pressure, P_c^*. This is because the high capillary suction pressure, which is higher than the maximum disjoining pressure, might initiate macroscopic disturbance and result in film rupture. This is illustrated in Figure 4-7.

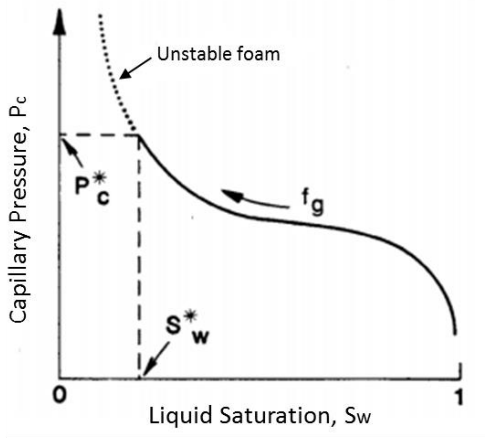

Figure 4-7 Schematic example of gas-water capillary pressure vs. liquid saturation in a porous medium. Foam is unstable above the critical capillary pressure, P_c^*, due to high capillary pressure or limiting water saturation S^*_w below. (Farajzadeh, Andrianov et al. 2012).

Foam films are more stable in high-permeable layers due to the existing low capillary pressure, while the films are less stable in low-permeability layers due to the high capillary pressure environment. Injecting foam into a heterogeneous reservoir with permeability variations forces the injected fluid flow into the low-permeability layers by blocking the high-permeability layers with stable foam (Khatib, Hirasaki et al. 1988). The limiting capillary pressure appears to decrease with absolute permeability, although this is not yet fully understood, especially in a permeability range relevant to petroleum reservoirs (Rossen and Lu 1997).

Gravity influence on liquid layers, separating the gas phases, will cause the liquid to drain. The liquid films then become thinner and the gas bubbles coalesce (Sheng 2013). Low liquid phase saturation would make the foam less stable and higher liquid viscosity will slow down the liquid drainage process. Experiments performed by Sheng *et. al.* 1997, has shown that higher viscosity liquids lead to more stable foams (Sheng, Maini et al. 1997).

Surface elasticity helps stabilize the foam system. This is the fluid mass transfer along an interface between two regions due to surface tension gradient. When a liquid film stabilized by a foam agent undergoes an expansion of the surface area, the local concentration of the foam agent is decreased, resulting in a thinner film. The lower concentration leads to higher surface tension which gives the film flow low energy. The liquid flow provides resistance against thinning of liquid film (Sheng 2013).

The harsh environment in the reservoir with regards to high temperature, high pressure and salinity plays a significant role on the foam stability. No foams are thermodynamically stable, and eventually they collapse. Like any other chemical flooding treatment, high temperature may cause the foaming agent chemicals to thermally degrade and lamella coalescence to prevail. This could make foam propagation deep into the reservoir challenging (Kam, Frenier et al. 2003). Higher temperatures increases liquid drainage and the foam agent solubility increases, resulting in less foam agent in the gas/liquid interface. Higher pressure, on the other hand, helps stabilizing the foam bubbles. When the pressure increases the bubbles becomes smaller. This result in liquid films becoming larger and thinner, leading to slower liquid drainage, making the bubble more stable (Sheng 2013).
In addition to all the parameters already mentioned, the stability of the foam is also dependent on the foam agent and the foam agent concentration.

The average bubble size and distribution of sizes may vary significantly beween types of foams, from the colloidal size (0.01 – 0.1 µm) (Lake 1989)to tenths of millimeters in bulk foam (David and Marsden 1969). The foam stability is not necessary a function of the bubble size, but there might be an ideal bubble size for the variety of individual foam types which are more stable than other sizes. Foams with small bubbles are generally more stable than large bubbles. A uniform distribution of bubble size is more stable than a large variety of sizes (Sheng 2013).

If foam is supposed to be used as displacing fluid, foam films that are stable at reservoir condition have to be created. In the presence of oil, the mechanisms of stability are more complex than in the cases without oil. When foam is intolerant to oil, the created foam in the pores does not control the CO_2 gas mobility efficiency (Farajzadeh, Andrianov et al. 2009). Foam injection is often taking place after a primary waterflooding because large quantities of oil destroy the foam, making the displacement process less efficient. The oil phase is detrimental to foam stability if the oil can enter and spread on the gas/water surface that is creating the foam. Solubilized oil decreases the stability by accelerating the foam film thinning process (Schramm 1994). In a porous medium, the fluids are distributed with

the wetting phase occupying the small pores, and the non-wetting phase occupying the large pores. A small amount of oil may not deteriorate foam stability significantly due to lack of interaction between the fluids while flowing. This is the critical oil saturation where the stability of foam is not significantly affected below the critical oil saturation, but above the value the foam collapse abruptly (Sheng 2013). From core experiments it is reported that foams cannot be generated when the oil saturation is above the critical foaming oil saturation (Friedmann and Jensen 1986, Hudgins and Chung 1990).

4.4 Foam Flow Behavior

This chapter gives an introduction to the terms describing foam flow behavior. These terms are important in the evaluation of the results obtained from the conducted experiments in this thesis.

4.4.1 Foam quality

The foam quality is one of the most important factors affecting foam flow behavior (Mo, Yu et al. 2012). Foam quality is the ratio of gas volume to foam volume (volumetric gas content) at a given pressure and temperature (Grundmann and Lord 1983). In a co-injection of gas and liquid the quality of the foam can also be characterized by the ratio between gas flow rate and total flow rate injected shown in equation 4.1

$$f_g = \frac{q_g}{q_g + q_{liq}} \quad [4.1]$$

where f_g is the foam quality, q_g is the gas flow rate and q_{liq} is the liquid flow rate (Farajzadeh, Andrianov et al. 2012).

Foam quality is closely related to bubble size. When the bubble size becomes larger the generated foam is most likely to become more unstable and the foam quality would become lower (Sheng 2013).

4.4.2 Apparent Viscosity

It is reported that flow properties and apparent viscosity of foam in porous medium are very dependent on the bubble-size and bubble distribution. In other words; they are dependent on the texture of the foam and the texture is highly dependent on the way the foam is generated. The mobility of foam is related to the apparent viscosity (equation 2.6). The apparent viscosity is defined as the relationship between flow rate and pressure drop for foam flowing through a capillary (Hirasaki and Lawson 1985), and can be calculated from equation 4.2.

$$\mu_{app} = \frac{k\,\Delta p}{(u_l + u_g)} \qquad [4.2]$$

where k is the permeability of the porous medium, Δp is the pressure gradient across the whole core and u_g and u_l is the volumetric flow rate of gas and liquid, respectively (Jones, van der Bent et al. 2015).

The apparent viscosity of foam is the sum of three contributors which dynamically change at the gas/liquid interface; the slug of liquid between gas bubbles, the resistance to deformation of the interface resulted by capillary and viscous forces, and the surface tension gradient. The latter develops when the surface active material is swept from the front of a bubble and accumulates at the back of it (Hirasaki and Lawson 1985). These contributors are schematically illustrated in Figure 4-8.

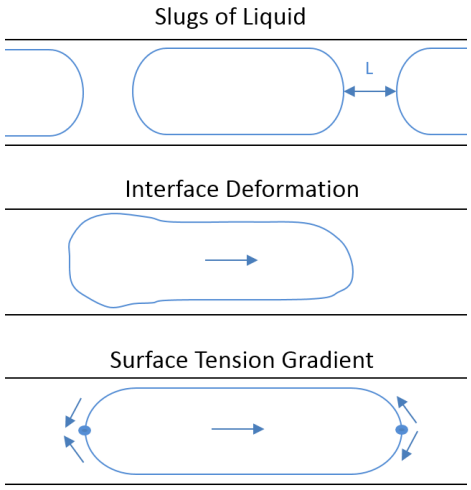

Figure 4-8 Different mechanisms affecting the apparent viscosity of foam in smooth capillaries. Reproduced from (Hirasaki and Lawson 1985).

Foams are, as mentioned, stronger in high permeability layers compared to low permeability layers. When the foam is strong, it has a larger apparent viscosity because gas preferably flows in high permeable channels which help to divert injected fluid into low permeable layers (Hirasaki 1989). Hirasaki and Lawson, 1985, showed that the apparent viscosity increased with the power of 2.0 to 2.5 of the capillary radius when the velocity was kept constant (Hirasaki and Lawson 1985). This is consistent with the observation of Fried where he observed the apparent viscosity increased in proportion with the capillary radius (Fried 1961).

4.4.3 Mobility Reduction

The foam Mobility Reduction Factor, *MRF,* is used to evaluate the effectiveness of the mobility reduction of pure gas when foam is generated. Gas has normally a very low viscosity compared to oil and water, but when foam gas is generated the gas viscosity is greatly increased. The MRF factor characterizes the strength of the generated foam.

$$MRF = \frac{\mu_{app}(foam)}{\mu_{app}\,(gas\ before\ foam)} = k_{rg}^{no\ foam}\,\frac{\mu_{app}}{\mu_{gas}} \qquad [4.3]$$

where $k_{rg}^{no\ foam}$ is the relative permeability of the gas at the end of the gas flood and before foam agents are injected, μ_{gas} is the absolute gas viscosity, μ_{app} is the apparent viscosity of the generated foam (Svorstøl, Vassenden et al. 1996, Farajzadeh, Andrianov et al. 2009).

The MRF factor is often used in commercial simulators like STARS and Eclipse for modelling foam flow behavior since this is based on the reduction in gas permeability and increased foam viscosity. In the software the foam is modeled as a tracer either in the water or the gas phase.

4.4.4 Relative Permeabilities

In a porous medium where foam is generated, the wetting aqueous phase's relative permeability remains unchanged, because the wetting phase resides in the small pores. The gas phase, on the other hand, experiences a significant reduction in the relative permeability caused by the foam blocking all but the least resistive flow paths (Friedmann and Jensen 1986). Experimental observations have shown that even very small concentrations of surfactant foam agents added to the aqueous phase, a great reduction in the relative permeability of the gas phase is achieved. Increasing the surfactant concentration further, decreases the relative permeability until it reaches a critical value. When this value is reached, addition of more surfactants do not contribute to a further reduction (Sanchez, Schechter et al. 1986).

4.4.5 Foam resistant factor

The foam resistant factor is used to evaluate the performance of foam in increasing the gas flow resistance. This factor is defined as the pressure drop measured across a medium where foam is generated divided by the pressure drop for the same system without the presence of foam agents (Duerksen 1986). An increase in the resistant factor indicates stronger foam having a lower mobility. The higher resistant factor, the more effective is the resistance of the foam lamellae (Mo, Yu et al. 2012).

4.5 The Effect of Flow Rate on Foam

When generated foam shifts from weak foam to strong foam, a drastic increase in differential pressure can be seen. Laboratory foam generation experiments with constant foam quality have shown that the pressure drop increases with increasing total injection rate. Figure 4-9 shows an experiment using co-injection of nitrogen gas and a surfactant solution at four different total injection rates with a constant foam quality. The result shows the total pressure drop along the core, ΔP_{total}, and the pressure drop in four sections along the core plug, Δp_1, Δp_2, Δp_3, and Δp_4. The pressure increased dramatically when the total injection rate reached 1.30 cc/min indicating generation of strong foam.

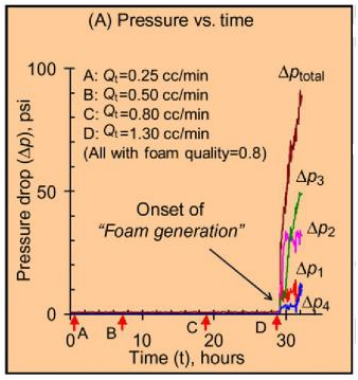

Figure 4-9 Illustration of differential pressure increase in laboratory foam flow experiment. The pressure drop increases with increased total injection rate for a fixed foam quality. ΔP_{total}, is the total pressure drop across the whole core. Δp_1, Δp_2, Δp_3, and Δp_4 are the differential pressure in four sections along the core plug (Sheng 2013).

When strong-foam is generated, the foam is found to follow two distinct flow behaviors. Osterloh and Jante conducted in 1992 foam experiments which identified two foam flow regimes. The two regimes are called the high quality regime and the low quality regime, and distinguish from each other by different independency of the pressure gradient (Osterloh and Jante 1992). In the high-quality regime, the foam flow behavior is near-Newtonian or slightly shear-thickening. In the low-quality regime the foam flow behavior is highly-shear thinning (Sheng 2013). These flow regimes were further confirmed by (Alvarez, Rivas et al. 2001). In the high quality regime, the steady-state pressure gradient is independent of the gas flow rate whereas in the low quality regime the steady-state pressure gradient is independent of the liquid flow rate. The foam behavior is dominated by stability from capillary pressure and coalescence in the high-quality regime and by bubble trapping and mobilization in the low-quality regime. The transition zone between the two regimes is characterized by a specific value of the gas fraction, f_g. It is pointed out that the transition from one regime to another most likely occurs when the limiting capillary pressure is reached (Osterloh and Jante 1992, Kim, Dong et al. 2005). Figure 4-10 illustrates a simplified schematic contour plot of the flow regimes.

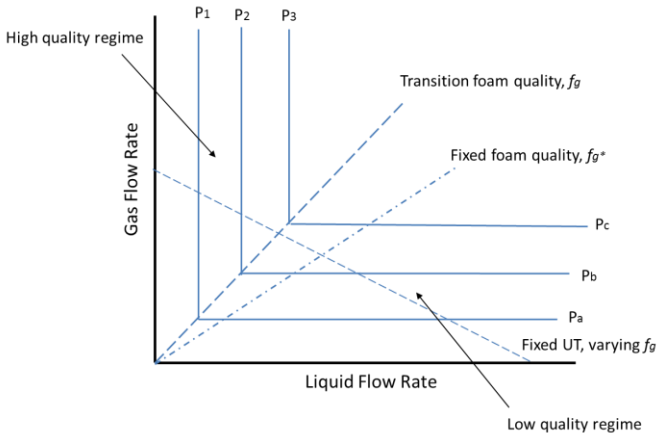

Figure 4-10 Simplified plot showing contours for three different values of ΔP and the two foam flow regimes for strong foams in a porous medium. Modified from (Alvarez, Rivas et al. 2001). When the total flow rate is fixed, U_T, the highest ΔP and the optimal foam quality is obtained at f_g.

4.6 Injection Modes

Foam can be injected into a reservoir mainly in two different ways for EOR purpose; Co-injection and surfactant-alternating-gas (SAG) injection. Co-injection is when both gas and foam agent solution is injected simultaneously. A foam agent is often pre-flush through the porous medium before pre-generated foam is injected in order to satisfy adsorption of the foam agent to the reservoir walls. Co-injecting CO_2-foam may not make the two fluids enter the upper and lower parts of the formation at the same relative rates because of the density differences. SAG-injection is when multiple cycles of gas and foam agent solution is injected separately. The SAG-injection causes a fluctuation in capillary pressure by repeating drainage and imbibition. This naturally helps the creation of fine-textured foams during the injection process. A higher recovery factor has been reported when using co-injection mode than SAG injection with the same amount chemicals used, especially in high gas/liquid ratios (Sheng 2013).

4.7 Fluids Applicable for Foam Generation

A variety of gasses might be used for foam generation; CO_2, steam, and miscible gases like air, nitrogen, or natural gas. The experiments performed in this thesis are exclusively conducted using co-injection of CO_2 as the gaseous phase. The liquid phase is brine with either surfactant or nanoparticle dispersed in the aqueous solution. Since the foam agents often appears as solids, they are dispersed in fluids like brine, distillated water and ethanol. These fluids play a significant role as foam agent dispersing agent in the formation. The fluids can contribute positively or negatively in oil recovery apart from the effect of the foam agent. Research focusing on EOR using various nanoparticles and dispersed fluids showed results where distillated water gave a low oil recovery. Using brine and ethanol as dispersing fluids gave good recovery, while diesel appeared good (Ogolo, Olafuyi et al. 2012).

The generation of foam using surfactants is a well-known technique that has been used for field applications and experimentally investigated for decades. The use of solid particles as foam agents is a more recent option which has aroused great interest. Both surfactant and nanoparticles have been used as foam agents in the experimental study conducted for this work and will be introduced in the following chapters.

4.8 Aqueous Surfactant Solution

Surfactant flooding reduces the interfacial tension (IFT) between oil and water for mobilizing the capillary-trapped residual oil after waterflooding. The fact that oil recovery could be related to IFT was first investigated by (Uren and Fahmy 1927). A trapped oil droplet is displaced when the interfacial tension is reduced to such an extent that the pressure gradient is large enough to overcome the capillary forces holding the oil droplet in place (Lam, Schechter et al. 1983). A large increase in microscopic recovery depends on efficient surfactants that can reduce IFT by a factor of approximately 10^4 (Zolotukhin and Ursin 2000). Experiements conducted by (Taber 1969), (Abrams 1975) and (Zhang, Sayegh et al. 2007) are all important reaserch covering this topic.

The interfacial tension reduction is dominated by alkaline surfactants foam (ASF) where the interfacial tension between the surfactant solution and the oil has a larger drop (Li 2008). In addition to lowering IFT, the surfactants can be used to change wettability, promote emulsification, lower bulk-phase viscosity and stabilize dispersions (Lake 1989). Surfactant together with CO_2 is used to generate a more stable foam for mobility control compared to injecting dense CO_2 and water (Grigg, Svec et al. 2003). When the IFT between two fluids is decreased, the mechanincal energy needed for foam formation is also lowered (Schramm 1994).

Anionic surfactants are the most used surfactants in oil recovery since they are soluble in aqueous phases. They also reduce the interfacial tension efficiently, are stable and relatively resistant to retention, in additon to not being very expensive. If anionic ions are dissolved in an aqueous phase, the surfactant starts to dissociate into a cation (Na^+) and a monomer. A typical surfactant monomer consists of one nonpolar moiety (lypophile) portion and a polar moiety (hydrophile). These represent the tail and the head respectively in Figure 4-11. Increasing the surfactant concentration, the lyophilic moieties start to aggregate into micelles where each micelle contains several monomers. The lyophilic part is orientated inwards and the hydrophilic part is orientated outwards. When continuing increasing the surfactant concentration the critical micelle point is reached, and a further increase result only in an enhanced micelle concentration and not a larger monomer concentration (Zolotukhin and Ursin 2000).

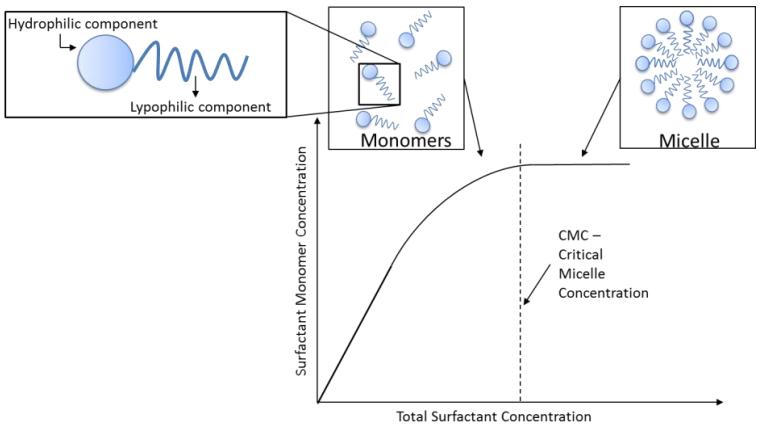

Figure 4-11 Surfactant monomer concentration curve and illustration of a typical surfactant monomer. As the surfactant consentration is increasing the surfactant monomer concentration is also increased until it reaches CMC. A further increase in the surfactant consentration will not increase the monomer concentration significantly. Modified from (Lake 1984).

When a solution contains an oil phase the surfactants accumulate at the interface between the oil and the surfactant solution. The lipophilic moiety attract to the oil phase and the hydrophilic phase to the aqueous phase (Lake 1989). If the oil is greater polarity it will behave as a better solvent for the surfactants. High specific gravity crude oil tend to be rich in organic acids which leads to a lower surfactant oil solubility (Puerto and Reed 1983).

Foam stabilized by surfactants relies on continuous regeneration of lamellae in the small pores of the rock for maintaining mobility control. In some cases, large amounts of surfactants can become unavailable for foam stabilization due to degradation and chemical interference that occurs in the rock surface, called adsorption, at the rock surface (Worthen 2012). The surfactant molecules are mobile and adsorption occur continuously at the CO_2-water interface (Adkins, Gohil et al. 2007). This is much likely to happen under high temperature conditions (Worthen 2012). The adsorption is dependent on the rock wettability, and the anionic and cationic molecules present in the reservoir (Esmaeilzadeh, Bahramian et al. 2011). Because surfactants are expensive it is important to predict the amount needed for a successful flooding. If the adsorption is large, it contributes to a significant decrease in the surfactant concentration, resulting in a lower ability to reduce the IFT. Adsorption is usually a negativ effect, but in the case where the reservoir rock is oil-wet it gives a positive effect by changing the wettability preference of the rock (Zolotukhin and Ursin 2000).

The use of surfactants in field application has several factors reducing its efficiency compared to the promising laboratory tests. The reservoir environments are harsh with regard to high temperature, salinity and rock surface adsorption. This can result in poorer performance of the surfactants (Mo, Jia et al. 2014). The adsorption by reservoir rock is often significant in the field then observed in the laboratory. The ability of the surfactants to reduce the IFT is constrained to certain conditions, and the conditions that can be achieved in the laboratory do not necessary comply what is seen in the reservoir. When choosing a surfactant as foam agent for EOR there are aspects that must be consided. This includes salinity, termal stability, foaming ability, performance in the presencens of oil, reduction of IFT and adsorption. Salinity and hardness of brine is reported to be the most important factor affecting the surfactant-oil-brine (SOB) behavior (Zolotukhin and Ursin 2000).

4.9 Colloidal Silica Nanoparticles Dispersion

Solid particles can be used as emulsifying agents. New technologies enabled use of nanoparticles and micrometer-sized particles as a substitute to the surfactants for foam generation. Nanoparticle-stabilized emulsion have attracted large attention in the recent years due to their specific characteristics and advantages compared to conventional foam generated by surfactants (Zhang 2010). The attention is primarily caused by the nanoparticles long-term stability under harsh reservoir conditions (Mo, Yu et al. 2012). The particles can also be injected into the reservoir formations as tracers or sensors to detect certain reservoir rock and fluid properties (Zhang, Murphy et al. 2014). Nanoparticles are one hundred times smaller than colloidal particles, and foam stabilized with these particles can travel a long distance into the reservoir without much retention.

The first investigation on stabilizing emulsions using solid particles was performed by Ramsden (Ramsden 1903). Espinosa, 2010, later reported foam generation using CO_2 and silica nanoparticles under the absence of surfactants (Espinoza, Caldelas et al. 2010). Foam made by solid particles is stabilized due to particle accumulation at the liquid-liquid interface. The particles can be adsorbed irreversibly at the interface between two fluids due to their high adsorption energy and form highly stable emulsions. These emulsions are potentially more stable than emulsions made by surfactants since the surfactant molecules constantly enters and leaves at the interface. This does not provide long-term stabilization of foam (Zhang 2010) (Yu, Wang et al. 2014) (Worthen 2012) (Dickson, Binks et al. 2004).

The contact angle between the nanoparticle and the interface is the relevant parameter in determining the emulsion type and stability (Safouane, Langevin et al. 2007). Hydrophilic emulsion have contact angle less than 90^o and the majority of the particles resides in the water phase, resulting the interface to bend around the oil phase making an oil/water emulsion. Conversely, hydrophobic particles have a measured contact angle greater than 90^o and the majority of the particles reside in the oil phase, resulting in the formation of a water/oil emulsion (Yu, Wang et al. 2014). Dickson found that the particle hydrophobicity had a significant effect on the emulsion stability and determines the type of emulsion formed (Dickson, Binks et al. 2004) (Zhang 2010). This is consistent with Worthen, 2012, findings that foam stability is strongly influenced by the size and the surface properties of the particles (Worthen 2012). Silica nanoparticles have been used to stabilize emulsion for conformance control by modifying the surface coating (Zhang 2009) (Yu, Wang et al. 2014). These are the types of nanoparticles used in this thesis, with CO_2 as the gaseous phase. Formation of CO_2 foam generated with nanoparticles is desirable because it does not require solvation of surfactant tails or polymer chains by CO_2 (Dickson, Binks et al. 2004, Worthen, Bagaria et al. 2012). Even though the nanoparticles are able to handle harsh reservoir environment, they are still sensitive to temperature, pressure, salinity and concentration. As the temperature increases, the foam becomes less stable and the sweep efficiency decreases, resulting in a lower oil recovery (Liu, Grigg et al. 2005, Mo, Yu et al. 2014).
The nanoparticle concentration is important to achieve stable foam. According to Mo. D, foam can be generated using a concentration as low as 100 ppm. The experiments also showed that nanoparticle concentration of 5000 ppm had the lowest foam mobility and resistant factor (Mo, Yu et al. 2012). The concentrations used experimentally in this thesis are based on these experimental results.

4.10 Foam in Fractured Rocks

There is limited information about foam being injected into fractured rocks. Unlike the foam bubble shape in a porous medium, where the bubble is shaped by the pore configuration (Ransohoff and Radke 1988), the foam bubbles in fractures are deformed as a response to interfacial tension. The gas-liquid interface curvature varies with gas fractional flow (Pancharoen, Fernø et al. 2012). In a porous medium, foam generation is largely due to the snap-off mechanism, and coalescence is controlled by the limiting capillary pressure (Khatib, Hirasaki et al. 1988). In a fractured network, the capillary pressure is lower and the limiting capillary pressure is likely not reached (Ferno, Gauteplass et al. 2014). The foam bubble size within a fractured network compared to a porous medium, is reported to be four times larger as a result of fewer snap-off sites (Kovscek, Tretheway et al. 1995). It is reported finer bubble texture in fractures with increasing foam quality (Kovscek, Tretheway et al. 1995, Ferno, Gauteplass et al. 2014), and finer textured foams cause a larger flow resistance (Ettinger and Radke 1992). Thus, lamella transport through fractures is expected to cause large pressure drops (Kovscek, Tretheway et al. 1995). Haugen, 2014, observed up to 80% recovery from fractured oil-wet limestone core sample when pre-generated N_2-foam was injected, and less than 10% recovery when only gas or water was injected (Haugen, Fernø et al. 2012). Although there are limited information, foam injection has shown promising results in fractured rocks. The foam is blocking fractures and high permeable regions, resulting in diffusion and flow of CO_2 into the low permeable zones (Haugen 2013). A successful field test pilot in naturally fractured reservoir was performed in the Cupiagua in Recetor field area in Colombia, South Africa. Coreflooding experiments using a naturally fractured core sample were designed and conduced before the pilot was started. The results showed that foam could efficiently block the gas flow through the fractures and increase the oil recovery with 15%. The overall result confirmed that the use of foam is a viable mechanism to mitigate gas recycling and improve oil recovery in fractured reservoirs (Sheng 2013). Naturally fractured rock reservoirs account for about 20% of world's oil reserves (Hansford and Fisher 2009). EOR foam experiments have been performed in this thesis in fractured carbonate core plugs.

4.11 Field Application of Foam

The parameters considered to have significantly effect on the foam behavior in field scale application are; oil saturation, foam agent concentration, water saturation, and capillary number. Some of the important screening criteria include high permeability, low salinity and relatively short well spacing. Additionally, high temperatures, generally above 200^{o}C, create challenges for the foam agents (Sheng 2013). It has also been stated that the most important factor for a successful foam application is the foam injection mode (Turta and Singhal 1998).

Serious work with surfactant flooding was not started until the 1960's, even though it was first mentioned by Uren and Fahmy in 1927 (Uren and Fahmy 1927). The first foam field application listed in the literature was conducted in the Siggins field located in Illinois (1964-1967). SAG injection was performed using air as the gaseous phase and a surfactant solution as the foaming agent. This was a successful pilot test confirming that foam could be used for more than soften beard. The water-oil ratio, WOR, was reduced from about 25:1 to 12:1 at the production wells. Estimation from further analyses of the pilot test concluded that the mobility of the injected air was reduced by 50%, and the mobility of the surfactant solution was reduced to about 35% of its original value caused by the reduction in water saturation (Holm 1970).

Most of the surfactant investigation has been performed in the US in water flooded reservoirs. Some of the larger field tests of about 90 to 400 acres (0.4 – 1.6 km^2) have been technically successful with a recovery of 15-30% of the residual oil in place after foam injections (Zolotukhin and Ursin 2000).

The CO_2 foam field verification pilot test, conducted in the East Vacuum Grayburg San Andres Unit (EVGSAU) in 1990, New Mexico, should be mentioned as one of the successful EOR productions with foam generation. The reservoir contained high permeability regions, being the primary cause of channeling and early breakthrough of the injected CO_2. The positive response to the foam injection was evidenced by changes in the CO_2 production rate and oil rate performance at the production well. Reduced injectivity, confirmed by rate and surface injection pressure data, provided indication that *in-situ* foam was generated and mobility reduction was achieved. This reduced injectivity lasted for over three months (Harpole, Siemers et al. 1994).

On the NCS, foam injection has been performed on the Snorre license. This was a foam-assistant-water-alternating-gas (FAWAG) project, and was the world's largest application of foam in the oil industry. The field was under WAG flooding initially, but because of premature gas breakthrough, a foam treatment was performed. One full-scale SAG test and one full-scale co-injection test was performed. The SAG injection was selected and applied, even though better results were achieved by using co-injection. The reason was that the injection pressure was above the fracture pressure in the co-injection mode. The buildup test showed that the foam generated during SAG injection mode was limited, but a strong foam was generated in the co-injection mode. The injection process resulted in a 50% reduction in the gas-oil-ratio (GOR) for two months. It was estimated that the FAWAG treatment contributed with approximately 250,000Sm^3 of oil, and the cost of the treatment was approximately US$1 million (Blaker, Aarra et al. 2002) (Skauge, Aarra et al. 2002). The surfactant used for the foam generation was the same surfactant applied in this master thesis, C_{14}-C_{16} alpha olefin sulfonate (AOS), using equal concentrations of 1 wt%.

5 Experimental Procedures

This chapter describes the experimental preparations, fluids and rock material used in this thesis. The experimental conditions, set-ups and procedures are described in detail to make it possible to accurately reproduce each experiment. The objective for this thesis was to evaluate CO_2-foam using two different foam agent solutions. EOR experiments were conducted using surfactant generated foam, and sensitivity analyses were performed on nanoparticle generated foam.

Table 5-1 lists the different types of experiments presented in this thesis. Seven experiments using supercritical CO_2 and CO_2-foam generated with surfactants were performed in Edwards limestone core plugs for EOR. Nine experiments were conducted generating CO_2-foam with nanoparticles in Bentheimer sandstones. All experiments were performed in the laboratory at Dept. of Physics and Technology, University of Bergen.

Table 5-1 Experimental Overview

Core Material	Experimental Type	Pressure/Temp.
Edward Limestone, fractured	Supercritical CO_2 injection	90 bar / 35^{0}C
	Supercritical CO_2 /surfactant-foam injection	90 bar / 35^{0}C
Edward Limestone, whole	Supercritical CO_2/surfactant-foam injection	90 bar / 25^{0}C
	Nanoparticle-CO_2-foam injection	90 bar / 25^{0}C
Bentheimer Sandstone, whole	Nanoparticle-CO_2-foam injection	90 bar/ 25^{0}C
	Surfactant-CO_2-foam injection	

5.1 Fluid properties

A list of fluids used in this thesis can be found in Table 5-2. Fluid properties at experimental conditions including densities and viscosities are listed where available. The 1.5" diameter sandstone cores were saturated with brine A (2.0 % NaCl). The limestone samples were saturated with two different brines; in partially oil-saturated systems a chalk brine (5.0 wt%, 5.0 wt% $CaCl_2$, 0.05 wt% NaN_3) was used, whereas 100% water-saturated cores used brine A. The surfactant solution for limestones used a third ion composition (2.0 % NaCl mixed with 1.0 wt% surfactant).

The surfactant type and concentration used during supercritical CO_2 experiment on limestone was based on previous experiments conducted by Haugen, 2012 (Haugen, Fernø et al. 2012). For Bentheimer sandstone experiments, the nanoparticles and surfactants were mixed with Brine A, see Table 5-2.The nanoparticle concentration mixture was based on experiments conducted by Di Mo (Mo, Yu et al.). The nanoparticles were discrete, had a smooth, spherical shape and with a narrow particle size distribution. The particles had also been surface modified with a reactive epoxy, silane. It must be noted that the salinities, ionic solutions and used concentrations of foam agents in this thesis have not been optimized for the studied systems. There is a large potential for optimization and stabilization of the studied agents, but this is outside the scope of this thesis. Both supercritical and liquid phase CO_2 was obtained during the experiments. The different properties of the different states are listed in Table 5-2. The notation NP stands for nanoparticles.

Table 5-2 Fluid Properties

Fluid	**Density [kg/m^3]**	**Viscosity [cP]**	**Composition [wt%]**	**Comments**
Chalk brine, 20^{o}C	1.05	1.09	NaCl: 5.0, $CaCl_2$: 5.0 NaN_3: 0.5	$NaN_3$is added to avoid bacterial growth. Used in saturation of limestone cores
Brine A, 20^{o}C	1.03	1.08	NaCl: 2.0	Used in saturation of sandstone cores
Surfactant solution AOS $C_{14/16}$	N/A	N/A	NaCl: 5.0, AOS: 1.0	Used in limestone cores
Nanoparticle solution	N/A	N/A	NaCl: 2.0, NP: 0.5	Used in limestone and sandstone cores.
n-decane, 1bar/20^{o}C	0.74	0.92	$C_{10}H_{22}$	
CO_2 , 100bar/20^{o}C	0.856	0.081	> 99,999% CO_2	Liquid state
CO_2 , 90bar/25^{o}C	0.843	0.015	> 99,999% CO_2	Liquid state
CO_2 , 1bar/20^{o}C	0.0018	0.014	> 99,999% CO_2	Liquid state
CO_2 , 90bar/35^{o}C	0.662	0.051	> 99,999% CO_2	Supercritical state

5.2 Rock materials

The Edward limestone samples was from a quarry near Garden City in Texas, USA were used. The cylindrical core plugs with 1.5" diameter were used for the supercritical CO_2 and the liquid CO_2 experiments. The cores had a relatively narrow range of permeability and porosity despite the common heterogeneous rock material. Limestone is a carbonate rock, and the void system within the rock is characterized by a wide distribution of pore sizes, caused by large variation in distribution of grain sizes and shapes (Craze) (Schweitzer 2015). The rock consists of more than 50% of calcite mineral. (UoA 2005).

Figure 5-1 Example of limestone core plug used in the experiments. The lore length is 7.2 cm and the diameter is 1.5¨ (3,8 cm)

Bentheimer sandstones were used for the sensitivity analyses experiments in core dimensions 1.5". The porous system results entirely from the space between individual sand grains. The pore channels are tortuous and highly irregular (Craze 1950). The sandstone is composed of 95% quartz, less than 2% feldspar and 3% clays distributed homogeneously. This rock type has high permeability ranging from 1100 mD to 3100 mD (Pomeroy , Lacey et al. 1933, Dautriat, Gland et al. 2007). However, the permeability of the cores used in these experimental study had a smaller variation.

Figure 5-2 Expample of sandstone core plug used in the experiment. The core length is 28.8 cm and the diameter is 1.5¨ (3.8 cm)

All core used in this experiments are outcrop core plugs, and are assumed to be strongly water-wet when only saturated with brine.

5.3 Core Preparations and Routine Core Analysis

The core samples were drilled from a large rock block using a water cooled circular saw. The core plugs were washed and dried in a heating cabined holding 60°C for at least 24 hours. In total, 17 core plugs were prepared for the experiments. Seven cores were saturated with oil with irreducible water saturation, while the remaining samples were saturated with brine for foam quality experiments. The cores were weighted before and after saturation. The length and diameter was measured using a slide caliper.

Porosity is a measure of the void space between the grains in a material where fluids can be found. In this thesis, the saturation method was used for finding the porosity of the core plugs. After the cores were dried in the heating cabinet, they were vacuumed in the schematic setup illustrated in Figure 5-3 to a pressure less than 300 mTorr. The saturation brine was also vacuumed. It was important to reach a low pressure for not underestimating the pore volume and leave air behind in the core, resulting in a multiphase system. The cores were saturated with brine for at least 24 hours in the vacuumed apparatus. Since the exact density for the 2 wt% brine solution is unknown, the calculations were based on the density of distillated water which resulted in insignificant higher permeabilities of the cores. This does apply for the oil saturated limestone cores where the density of the chalk brine was known. The brine properties are listed in Table 5-2.

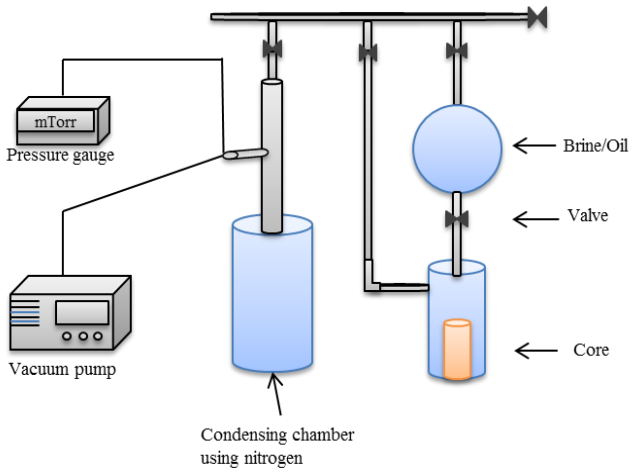

Figure 5-3 Schematic experimental setup for porosity measurement using the saturation method. The core plugs were placed in sealed glas container connected to the vaccum pump. Liquid nitrogen was used in the condensing chamber to avoid water entering the pump.

For finding the porosity, the core samples were weighted before and after saturation. The mass differences correspond to the volume fluid saturated in the pore space assuming the core is 100% saturated. Knowing the density of the saturation fluid the porosity was determined by equation 5.1

$$\varphi = \frac{V_p}{V_b} \cdot 100\% = \frac{(w_{wet} - w_{dry})/\rho_{fluid}}{\pi r^2 l} \cdot 100\% \qquad [5.1]$$

where V_p is the pore volume of the media *[cm^3]*, V_b is the bulk volume *[cm^3]*, w_{wet} and w_{dry} is the weight of the core, *[g],* in saturated and dry condition, respectably, ρ is the density of the saturation fluid, *[g/m^3]*, r is the radius of the core, *[cm],* and l is the length of the core *[cm]*.

The cores were stored in cylindrical plastic boxes surrounded by the respectively saturated brine.

Permeability is a measure of the ability a material has to transport a fluid. It can be distinguished between absolute, relative and effective permeability, the relationship is shown in equation 5.2

$$K_{abs} = \frac{K_{eff}}{K_{rel}} \quad [5.2]$$

The absolute permeability is measured when only one fluid phase is present in the medium (Zolotukhin and Ursin 2000), and it was calculated for all cores using Darcy's law, given in equation 2.1. Liquid was injected with different constant injection flow rates and the corresponding differential pressure was measured.

The experimental setup for the absolute permeability measurement is illustrated in Figure 5-4. The core was placed in a Hassler core holder, where a confinement pressure was set to 20 bar above the pore pressure to avoid the fluid to flow past the core. A Quizix-pump was used to inject the fluid with four different total injection rates. ESI-pressure transducers (range 0-40 bar) and a Validyne pressure transducer (range 0-14 bar) measured the corresponding differential pressures to the different injection rates.

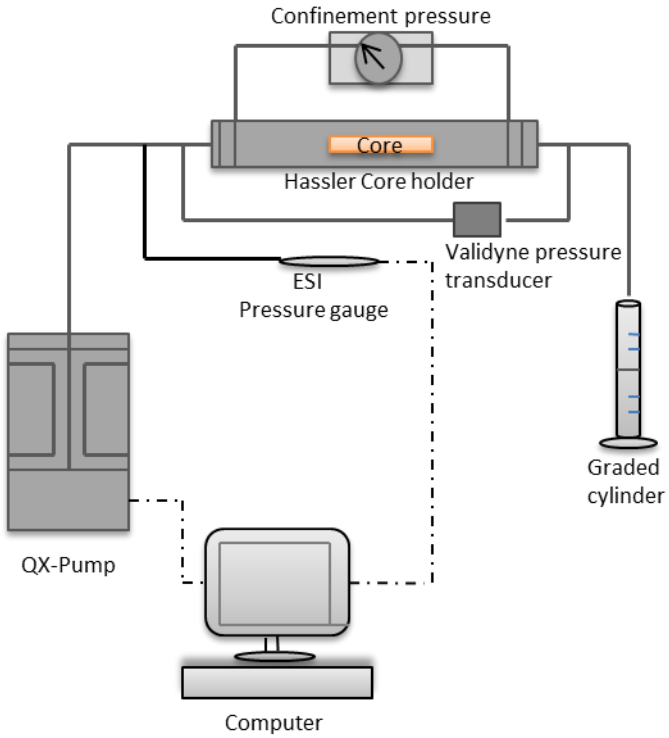

Figure 5-4 Schematic experimental setup for the permeability measurement and oil drainage of the core plugs. All differential pressures were measured using two pressure transducers for comparison.

5.3.1 Oil drainage

For establishing oil saturated cores for the EOR experiments, the cores were oil flooded using n-decane to achieve irreducible water saturation, $S_{wi.}$ The primary drainage was performed with a constant pressure gradient equal to 2 bar/cm at room temperature. 5 PV of n-decane were injected in both directions of the cores to establish a uniform distribution of water along its length. The saturation of water was monitored by measuring the produced volume over time. The saturation data can be found in the result section from Table 6-1.

5.3.2 Fracturing of cores

To study the impact of fractures on oil recovery during CO_2 injection and CO_2 foam, five cores were fractured by artificially cutting the core longitudinally along the center of the cylinder axis using a dry circular saw. The saw was not cooled by water during this process to maintain control of the established oil saturation. Water would have spontaneously imbibed into the cores to displace the oil. After fracturing, the core diameters decreased by 2 mm because of the saw blade thickness. The cores were weighted before and after the fracturing and the new pore volume after fracturing was found by the fraction of the weight difference multiplied by the initial pore volume. This was found based on the assumption that porosity and fluid distribution remained constant.

$$PV_{frac} = PV \cdot \frac{m_{frac}}{m_{init}} \quad [4.3]$$

where $PV\ [cm]^3$ is the initial pore volume, and m_{init} and m_{frac} is the mass of the core before and after fracturing, respectively $[g]$. $PV_{frac}\ [cm]^3$ is the obtained pore volume after fracturing.

The obtained fractures were artificial fractures with smooth surfaces. For maintaining a constant fracture aperture during the experiments, a polyoxymethylene spacer (POM) was placed between the two core halves (Pomeroy , Lacey et al. 1933), as shown in Figure 5-5. The spacer was used to eliminate variation in fracture properties between similar injection tests to improve validity of comparisons. The additional oil volume caused by the spacer was calculated as dead volume and was found by measuring of the open spaces in the spacer.

Figure 5-5 Fractured limestone core with POM spacer showing the fracture aperture. One square in the spacer had measured length 3.1 cm, width 2.6cm and thickness 0.1cm. Its total volume was 0.81 cm³. The length of the spacer was cut to the same length as the core.

5.3.3 Core packaging

In preparing the experiments, each core plug was placed inside a rubber sleeve (Buna-N) in a core holder. Buna-N rubber sleeve was preferred over Viton rubber. This was for reducing etching and sleeve failure from CO_2 diffusing into the rubber sleeve. To reduce the contact between the injected fluids and the sleeve, and thus minimizing the etching process, the core plug was wrapped in aluminum foil and taped. Figure 5-6 shows the wrapping and how the end pieces of the core holder were attached to the core plug with aluminum tape. This procedure was followed for both the limestone and the sandstone cores. Even though aluminum wrapping of the cores were perform, the rubber sleeve still had to be replaced after several pore volumes CO_2 injected. A confinement pressure was applied around the core by using oil as confinement fluid.

Figure 5-6 *(left):* W*rapping of core plug in aluminum foil. The core was taped to the core holder end pieces, ready to be assembled in the core holder. (right): Hassler core holder containing core and end pieces ready to be placed in the experimental setup.*

5.4 Experimental Setups

Two different experimental set-ups were used in this thesis depending on experimental conditions. In all set-ups the cores were placed horizontally in a Hassler core holder using oil as confinement fluid. The gravity forces were neglected due to small dimensions of the core.

5.4.1 Supercritical CO_2 and CO_2-foam injections using surfactants

A total of seven experiments were conducted by injecting supercritical CO_2 into limestone cores, and using material balance for calculations. The objective of the experiments was to compare oil recovery mechanisms within fractured and whole limestone core plugs by using both supercritical CO_2 and CO_2-foam injections generated by surfactants. All tests were performed with a backpressure of 90 bar and temperature of 35°C. The injection rate was 0.83 cc/min (5 ml/h).

Table 5-3 *Overview supercritical CO_2 limestone experiments*

Core ID	State of material	PV [ml]	S_{wi}	$S_{o,iw}$
EDW2	Whole	18.60	0.226	0.774
EDW3	Whole	17.31	0.237	0.763
EDW4	Fractured	17.37	0.240	0.818
EDW10	Fractured	16.67	0.209	0.852
EDW12	Fractured	16.84	0.300	0.754
EDW13	Fractured	21.79	0.245	0.812
EDW14	Fractured	25.37	0.253	0.804

Figure 5-7 illustrates the experimental set-up for the supercritical CO_2 experiments. The set-up was built in a heating cabinet holding 35 °C to maintain a constant temperature. Inside the heating cabinet, denoted by the large square in the figure, the core holder was placed together with the accumulator containing CO_2. The accumulator had to be stabilized to supercritical phase condition before CO_2 was injected into the core. When CO_2 experience changes in pressure and temperature, the fluid phase changes. This is illustrated in Figure 3-2. From 60 to 90 bar and 25 to 35 °C the gas undergoes a change of phase from liquid condition to supercritical condition. Stability within the molecule and thermal stability had to be reached before the experiment could start. A Quizix-pump was set below the CO_2 accumulator for injection of distilled water until 90 bar pressure was reached. When CO_2 is in supercritical state, it is first-contact miscible with n-decane as shown in Figure 3-4. The back pressure regulator (BPR) was also placed inside the heating cabinet to avoid CO_2 phase transitions, which would greatly affect the injection rate with variation in temperature. The BPR was set to experimental conditions using a nitrogen tank. The computer logged the tubing line pressure measured from the *ESI*-pressure transducers, and controlled the injection rates of the pumps. The system was assembled using 1/8 steel tubings.

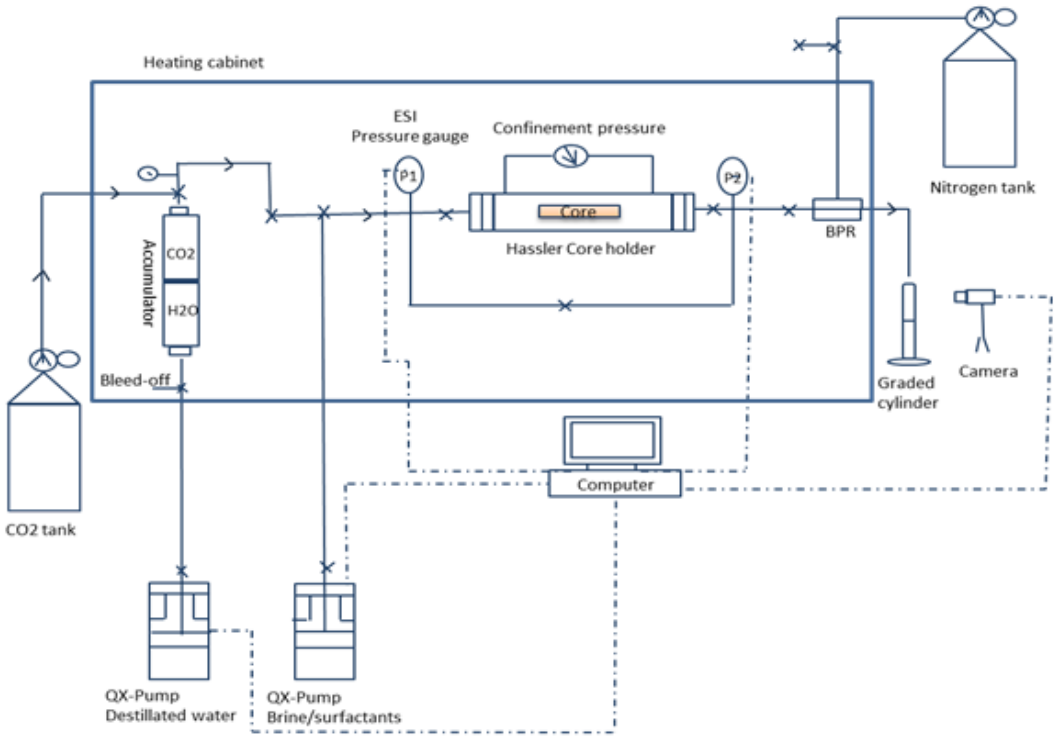

Figure 5-7 *Experimental setup for supercritical CO_2 and CO_2-foam experiments. The large square indicates the heating cabinet holding 35°C. All the crosses on the lines indicate two- or three way valves, and the arrows points in possible flow direction. The dashed lines from the pumps and other electrical equipment indicate data sampling.*

Equipment used:

- Heating cabinet holding 35°C
- Hassler steel core holder
- Hand pump for confinement pressure
- Hassler accumulator containing CO_2, volume 1.0 L
- Back Pressure Regulator controlled by N_2-tank
- CO_2 tank containing 60 bar
- 4 x manometers placed on top of the fluid tanks, the accumulator and the hand pump
- 2 x ESI Pressure Transducer, pressure range 0 – 250 bar, for measuring line pressure
- 2 x Quizix QX-1500 pump for injecting fluids into the lines in the system
- Swagelock – tubings, fittings and valves
- Computers for logging and operating pumps
- Web camera

Procedure

The fractured limestone cores were placed in the core holder with the fracture arranged vertically. The system was saturated with n-decane and pressurized to experimental conditions (P=90 bar, T=35^{o}C). For one core, a water-injection was first performed until no more oil production was observed. Supercritical CO_2 was then injected until no additional oil was produced, before surfactant solution was co-injected with supercritical CO_2 for foam generation. For all the other cores used in the experiments a waterflooding was first performed, then CO_2 or CO_2-foam was injected. Most of the production of oil were observed in the early stages of the experiments. The oil dead volume, tubing volume between the inlet valve and the outlet valve, was subtracted from the oil produced together with the oil volume made by the spacer. All sequences of the experiments were performed at total injection rate 5 ml/h (0.8 cc/min). The confinement pressure was kept at 20 bar above the pore pressure at all times. The oil produced was monitored from a graded cylinder downstream the BPR, and a web camera was used for capturing the oil production overnight.

5.4.2 Liquid CO2 injection & nanoparticles/surfactants for foam generation

Table 5-4 lists the seven sandstone and three limestone cores saturated with brine for evaluating foam quality and stability by utilization of nanoparticles. The objective was to investigate the generated foam stability by changing total flow rates and foam qualities. The experiments were performed at room temperature of 25^{0}C and 90 bar pressure. Under these conditions CO_2 is in liquid state as illustrated in Figure 3-2. A total of eight experiments in whole 1.5" diameter core plugs were conducted. The nanoparticle concentration in the aqueous solution was constant at 0.5 wt%. The total injection rates were varied between 1 - 4 cc/min and the gas fractions (f_g) was varied between 0.1 - 1. In the experiments, gas and liquid were co-injected with flow rates at different gas/liquid ratios holding the total injection rate constant.

Table 5-4 *Overview of sandstone experiments using liquid CO_2/nanoparticles and liquid CO_2/surfactants for foam generation*

Core ID	Perm [mD]	PV [ml]	Injection rate [cc/min]	Foam agent
ST1	2438.3	78.2	1	Nanoparticles
ST2	1725.7	75.3	1, 2, 3, 4	Nanoparticles
ST3	2252.3	76.5	2, 3, 4	Nanoparticles
ST4	2257.6	74.6	1, 2, 3, 4	Nanoparticles
ST5	1456.0	73.8	1, 2, 3, 4	Nanoparticles
ST6	1798.2	70.1	1, 2, 3, 4	Surfactant
ST7	2527.4	63.2	2, 3, 4	Nanoparticles
LM11	22.5	19.9	1, 2	Nanoparticles
LM10	30.3	22.6	1, 2	Nanoparticles
LM14	30.7	21.8	1, 2	Nanoparticles

Figure 5-8 illustrates the experimental set-up used for the cores in Table 5-4. A Quizix pump injected the dispersed nanoparticles at different injection rates into the core. Another Quizix pump was used for stabilizing the accumulator containing CO_2 at 90 bar, and for injecting the CO_2 at different gas fractions. A gas booster was used to achieve a larger volume of gas in the accumulator. The core was placed in a Hassler steel core holder with confinement pressure set at 30 bar above the pore pressure. This pressure was obtained with a hand pump. The outlet pressure was controlled by a *Sigma* pump (ST-pump) where the injected fluids accumulated.

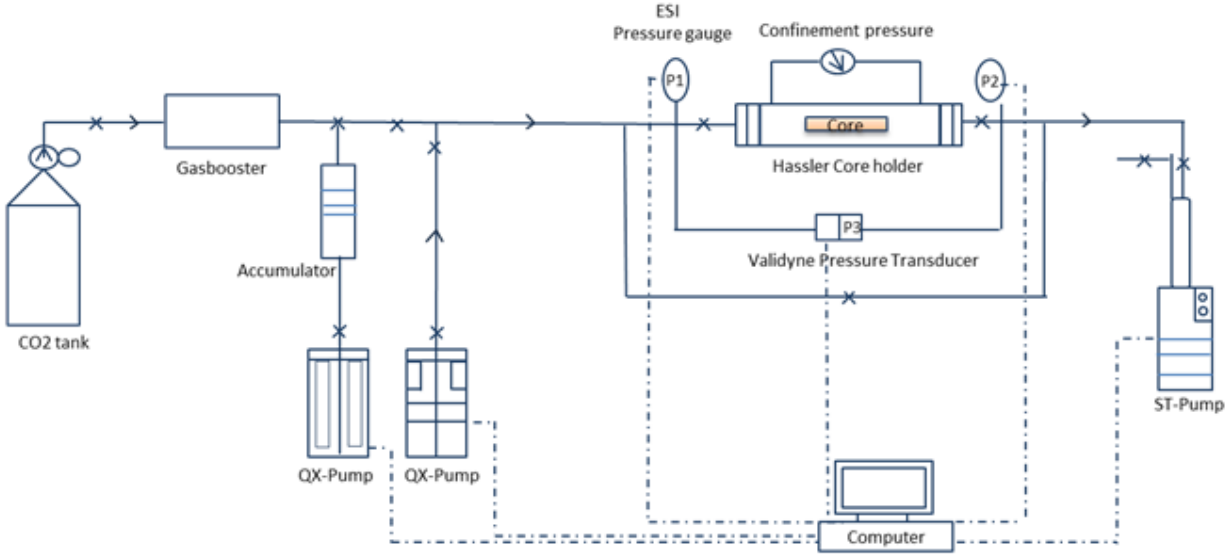

Figure 5-8 Experimental set up for liquid CO_2 and CO_2 -foam experiments. All apparatus are placed in room temperature at approximate 25 °C. The crosses on the lines indicates both three or two way valves, with the arrows pointing in possible flow directions. The dashed lines from pumps and other electrical equipment indicate data sampling.

Equipment used:

- Hassler steel core holder
- Gas booster
- Hand pump for confinement pressure
  Accumulator containing CO_2, volume 1.4 L
- CO_2 tank containing 60 bar
- 3 x manometers placed on top of the CO_2 tank, the accumulator and the hand pump
- 2 x ESI Pressure Transducer, pressure range 0 – 250 bar, for measuring line pressure
- Validyne Pressure Transducer, pressure range 0 – 200 PSI, for measuring differential pressure
- Quizix QX5000-10K and Quizix QX1500 pump for injecting fluids into the system
- Sanchez Sigma 1000 pump for holding the backpressure, volume 1 L.
- Swagelock – tubings, fittings and valves
- Computers for logging and operating pumps

Procedure

In order to evaluate the effect of nanoparticles in CO2-foam generation, a baseline experiment was performed on sandstone cores to establish a benchmark. CO2 and brine was simultaneously injected, with absence of nanoparticles at different volumetric ratios and total injection rates. After the baseline experiment, CO_2 and nanoparticles dispersed in brine were co-injected for foam generation. The same gas fractions and total injection rates as the baseline experiment were used. Each volumetric rate was maintained until a constant differential pressure was achieved. The gas booster was used to increase the CO_2 to experimental conditions (P=90 bar) before filling the accumulator. This was done instead of pressurizing CO_2 with an injection pump after it was transferred to the accumulator. The CO_2 pressure from tank was approximately 60 bar. The *Validyne* pressure transducer logged the differential pressure across the core, while the *ESI* pressure transducers logged the pressure at each side of the core. Produced fluids were collected downstream of the ST-pump, and emptied regularly.

The injection procedure was performed in two different ways. In all cores, with expectance of core ST4, the total injection rate was increased before the gas fraction was changed. Each gas fraction was tested for all injection rates before it was changed. In core ST4, each gas fraction was injected at a constant total injection rate before the total injection rate was increased.

6 Result and Discussions

In this chapter the experimental results are presented and discussed. A total of 17 cores were prepared for the experiments. The routine analysis are presented first, followed by individual experimental results and discussions presented in subsections.

Uncertainties are always present in experiments, and are imported for the credibility of the experimental work. Uncertainties related to the experiments conducted in this study can be divided into two categories; experimental and equipment uncertainties. The overall uncertainty in an experiment is the total of errors related to the many steps in preparing the experiment, and the uncertainties in the equipment. The main contributor related to the errors in this study is the experimental uncertainty. This uncertainty is hard to control, and is related to leakage, BPR, temperature variations etc. The uncertainties related to the conducted experiments are discussed in chapter 7, and will therefore not be discussed further in this section. The equations used for the error calculations are found in Appendix – A.

6.1 Routine Core Analysis

Basic core properties were measured experimentally as explained in section 5.3. Figure 6.1 shows the permeability and porosity variations of the cores used in this experiments. Greater permeabilities are observed in the sandstone core materials compared to the limestone cores. Both rock types were within the same interval of porosity, although the limestone cores had a larger range of variation from 22.4-26.3% in comparison with the sandstone cores (22.7-23.9%). The permeability and porosity variations within the cores of same material was likely caused by heterogeneities. All the core were outcrop cores.

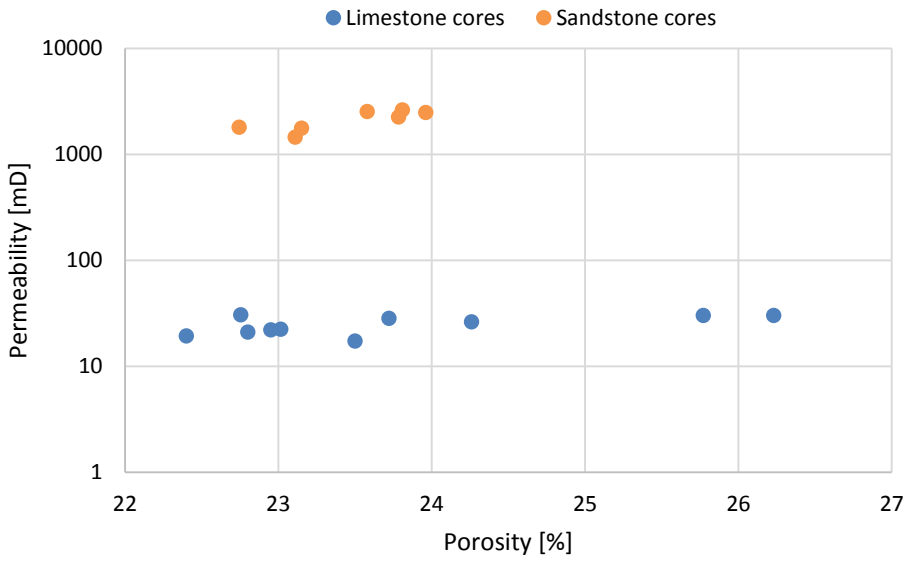

Figure 6.1 Porosity vs. permeability plotted for comparison of sandstone and limestone core plugs used in the experiments. The permeability for the sandstones range from 1700-2600 mD while the range was 17-30 mD for the limestones. The porosities for the cores are similar ranging from 20-25%. Note the logarithmic scale on the y-axis.

Table 6-1 lists the core data for the cores used in the experiments. The permeabilities listed are the permeabilities of the cores matrix, and was measured before the cores were fractured. High flow conductivity through the spacer used in the fractures led to low differential pressures across the cores. This gave high permeabilities, which was difficult to measure due to the small range in differential pressure and accuracy of the pressure transducers.

Table 6-1 Core data

Core plug	Material	Length [cm]	Diameter [cm]	Porosity [%]	Perm. [mD]	S_{iw}	$S_{o,wi}$	State
EOR2	Limestone	7.10	3.75	23.72	28.32	0.226	0.774	Whole
EOR3	Limestone	7.00	3.75	22.40	19.31	0.237	0.763	Whole
EOR4	Limestone	7.20	3.75	23.50	17.30	0.240	0.760	Fractured
EOR10	Limestone	6.70	3.75	24.26	26.21	0.209	0.791	Fractured
EOR12	Limestone	7.20	3.75	22.80	21.01	0.300	0.700	Fractured
EOR13	Limestone	9.00	3.80	22.95	22.16	0.245	0.755	Fractured
EOR14	Limestone	9.35	3.80	25.77	30.28	0.253	0.747	Fractured
ST1	Sandstone	29.40	3.76	23.96	2438.27	1.000	-	Whole
ST2	Sandstone	29.30	3.76	23.15	1725.72	1.000	-	Whole
ST3	Sandstone	28.80	3.77	23.81	2575.90	1.000	-	Whole
ST4	Sandstone	28.10	3.77	23.78	2213.35	1.000	-	Whole
ST5	Sandstone	28.60	3.77	23.11	2027.19	1.000	-	Whole
ST6	Sandstone	27.60	3.77	22.74	1798.22	1.000	-	Whole
ST7	Sandstone	24.00	3.77	23.58	2527.43	1.000	-	Whole
LM10	Limestone	7.44	3.84	26.23	30.29	1.000	-	Whole
LM11	Limestone	7.01	3.96	23.01	22.46	1.000	-	Whole
LM14	Limestone	8.05	3.89	22.76	30.70	1.000	-	Whole

6.2 CO_2 and CO_2-foam injection for EOR by Material Balance

In this chapter, experimental results from miscible CO_2 and CO_2-foam injection for EOR purpose will be presented and discussed. Strongly water-wet carbonate cores for both fractured and whole core materials were examined. The experiments were performed to evaluate the potential for mobility control in fractured carbonates. The literature reports two favourable flow properties in foam injections for EOR processes; 1) stabilizing the displacement process by increasing the displacing fluid viscosity, and 2) blocking high permeability layers in the reservoir. In the presence of a foaming agent, injection of aqueous and gaseous phases in a porous medium could approach a favourable mobility ratio. Blocking high permeable thief zones forces the selective fluid to lower permeability regions, enhancing the oil recovery. The experiments investigate the potential for tertiary CO_2-foam recovery using surfactant as oil producers. CO_2-foam injections were compared to pure CO_2 injections under same experimental conditions. The temperature was kept constant at 35^{o}C in a heating cabinet at 90 bar pressure. Section 5 explains the experimental procedure in detail. N-decane was used as the oil phase and all the experiments were conducted above MMP between CO_2 and n-decane Figure 3-4. All experiments were performed on 1.5" diameter limestone core plugs with total constant injection rate 5 ml/h. The foam was generated *in-situ* by co-injection of CO_2 and surfactant solution at ratio 8:2. The experiments presented in this section were performed in cooperation with fellow master student Tomas Hjartnes (Hjartnes 2015).

6.2.1 Tertiary Supercritical CO_2 Injection

Tertiary supercritical CO_2 injections were performed to serve as benchmark for CO_2-foam injection tests in terms of oil recovery efficiency. Both whole and fractured limestone cores were used for the injections. Table 6-2 lists key core properties and experimental results. The permeability, K_{init}, is the permeability of the cores matrix initially before they were fractured.

Table 6-2 Core properties and experimental data for baseline tertiary supercritical CO_2-injection in whole and fractured cores

Core ID	State of core	PV [ml]	K_{init} [mD]	Avg. Pressure [bar]	S_{iw}	$S_{or, WF}$	$R_{f,WF}$ [%OOIP]	$S_{or, CO2}$	$R_{f,total}$ [%OOIP]
EOR2	Whole	18.60	28.32	93.0	0.226	0.498	35.7	0.358	53.8
EOR10	Fractured	16.67	26.21	91.0	0.209	0.559	29.4	0.325	58.9

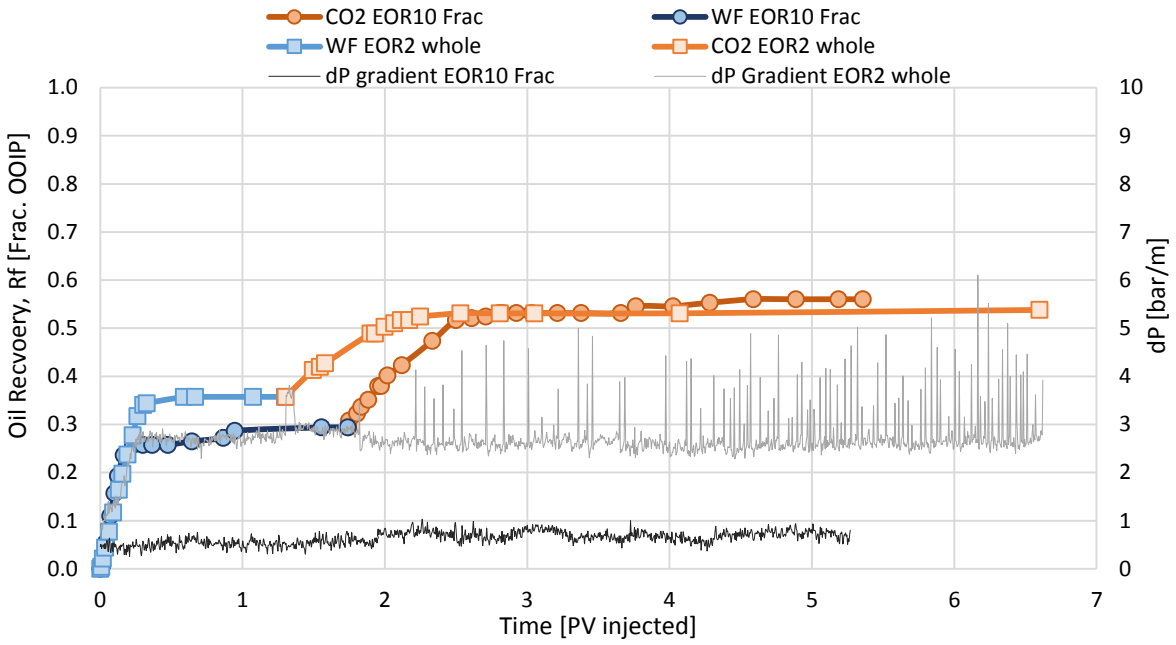

Figure 6-2 Oil recovery, R_f, versus pore volume injected for supercritical CO_2 in whole (EOR2) and fractured (EOR10) limestone cores at constant temperature of 35°C. The lines between the points are only to guide the eye and are not experimentally measured. The differential pressure is plotted on secondary y-axis (bar/m). The injections are distinguish with points of different geometries. Same colors represent same injection fluids.

The results from the supercritical CO_2 injections are shown in Figure 6-2. The fractured core, EOR10, achieved a slightly higher total oil recovery (58.9 %OOIP) than the whole core, EOR2 (53.8 %OOIP). During waterflooding, the two cores had similar production curves because both cores were strongly water-wet and capillary imbibition was the dominant mechanism for the oil displacement. The production graphs were linear before water breakthrough occurred, meaning the amount of water injected was equal to the amount of oil produced. The oil production rates were the same for the fractured system and the whole system until break through was reached. Both cores reached water breakthrough for 0.3 PV water injected. The water displacement was more efficient in the whole core, meaning a better sweep was obtained, leading to a higher oil recovery of 36% OOIP compared to 29% OOIP in the fractured core. Since the cores were strongly water-wet, the obtained recovery was lower than expected. Residual oil was trapped in the middle of the pores after the injection, and the trapped oil drops reduced the water flow. Little to no additional oil was produced after water breakthrough, corroborating the strongly water-wet preference.

When no additional oil was recovered by injection of water, the water was replaced with supercritical CO_2 and an increase in oil recovery was seen, see Figure 6-2. Reaching the maximum oil recovery in whole core EOR2 was faster than in the fractured core EOR10 where a total of 6.5 PV CO_2 was injected (total 10.4 PV). Residual oil saturation in whole core EOR2 was reached after 1.2 PV CO_2 injected (total 2.5 PV). CO_2 breakthrough was expected to be faster in the fractured core, due to the high permeable fracture. However, this was not observed. Tertiary injection processes in cores are dominated by viscous forces (Kulkarni and Rao 2004). However, the oil is also produced by concentration difference between CO_2 in the fracture and oil in the matrix. The recovery continued in fractured core EOR10 due to the diffusion process, which is a slow process. This explains the more time required for achieving irreducible oil saturation in the fractured core. As the size of the matrix becomes smaller, the diffusion effect becomes more important (Hoteit and Firoozabadi 2009). The low recovery for the whole core

EOR2, might be due to water shielding the oil drops, making the contact area between CO_2 and the residual oil smaller. This makes the diffusion process less efficient. When core EOR10 was fractured, dust from the cutting adsorbed to the surface of the fracture. Mixing the dust with oil or water made it sticky and possibly blocked the pores in the fracture. This prevented the injected fluid from displacing the oil, and might be the reason why the oil recovery during water injection was low. When CO_2 was injected in whole core EOR2 the differential pressure remained constant for a short period. It then decreased due to the low viscosity of CO_2 and larger fluctuations were observed. In the fractured core EOR10 this pressure reduction was not seen due to the high permeable fracture. The differential pressure during the production had little significance for this recovery process, due to the diffusion process.

Gas injection into fractured carbonate reservoir can from experience contribute to a 20% increase in oil recovery (Hoteit and Firoozabadi 2009). This complies with was seen in this experiment, where CO_2 injection contributes with a 29% increased oil production in fractured core EOR10. Injecting CO_2 for tertiary oil recovery might performed better in oil-wet cores then water-wet cores since the oil preferably wets the rock, resulting in a more continuous flow than in the water-wet case (Tiffin and Yellig 1983).

Figure 6-3 shows oil production rate for the experiment. The rate is high in the beginning of the water injection, declining towards the transient period until no more oil is produced. When supercritical CO_2 was injected the oil production rate increased again for both cores. This happens after 1.3 PV for core EOR2 and 1.7 PV for core EOR10. Note the slow recovery due to diffusion for the fractured core EOR10.

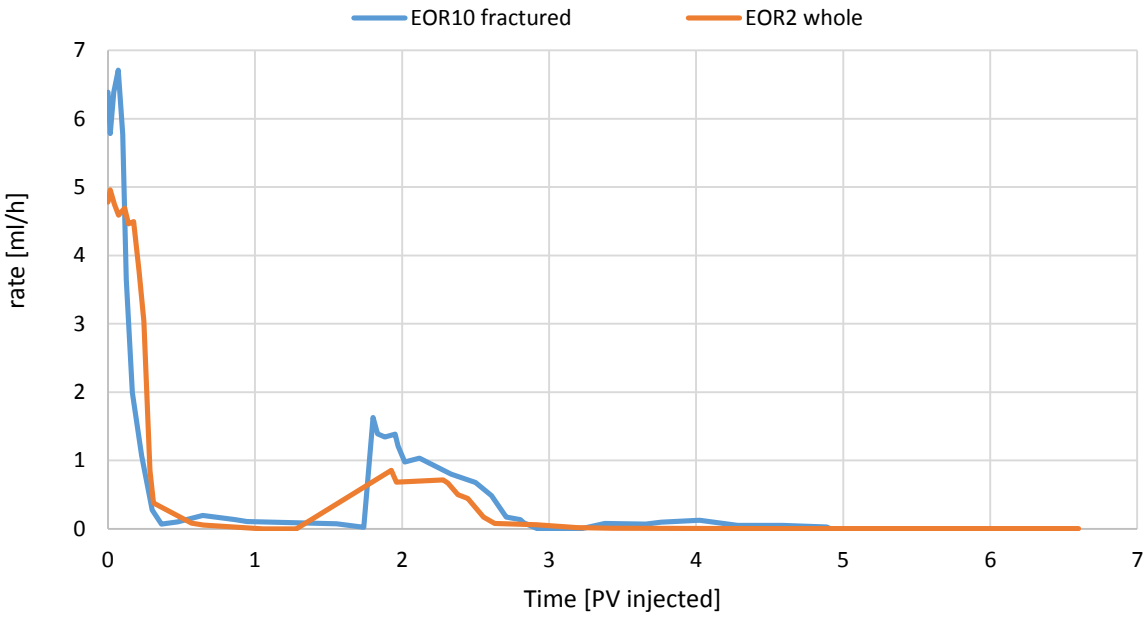

Figure 6-3 oil production rate versus pore volume injected. The fractured core (EOR10) has a higher production rate then the whole core (EOR2). The second peaks in the two graphs represents the injection of supercritical CO_2 resulting in an increase in rate and oil production for both cores.

6.2.2 Tertiary Supercritical CO_2-foam Injection

This chapter present experiments where CO_2-foam was injection in limestone core plugs. The objective was to see how foam performed in whole and fractured carbonate core materials. Table 6-3 lists the core data and the experimental results. The injected fluids total injection rate was 5 ml/h. CO_2 and surfactant solution were co-injected with volumetric ratio 8:2.

Table 6-3 Core properties and experimental data from tertiary CO_2-foam injection in limestone

Core ID	State of core	PV [ml]	K_{init} [mD]	Avg. Pressure [bar]	S_{iw}	$S_{or, WF}$	$R_{f,WF}$ [%OOIP]	$S_{or, CO2-foam}$	$R_{f,total}$ [%OOIP]
EOR3	Whole	17.31	19.31	92.0	0.237	0.487	36.2	0.325	57.4
EOR4	Fractured	17.37	17.30	92.0	0.240	0.638	16.1	0.397	47.7
EOR13	Fractured	21.79	22.16	93.0	0.245	0.632	16.4	0.422	44.1

Figure 6-4 shows oil recovery versus pore volume injected for two fractured limestone core plugs. Both cores experienced a low recovery from water flooding, possibly due to pore blockage of dust as described above. Water breakthrough was observed after 0.3 PV injected for the cores. Both cores achieved approximately the same oil recovery after the water injections of 16.1% (EOR4) and 16.4% (EOR13). The differential pressure remained low and constant for both cores during water injection due to the high transmissibility of the fractures. Both cores showed immediate response in terms of oil recovery when water injection was changed to co-injection of CO_2 and surfactant solution. The additional oil recovery is thought to be driven by the diffusion process in the fractured core. Diffusion processes are effective for high permeabilities and low injection rates.

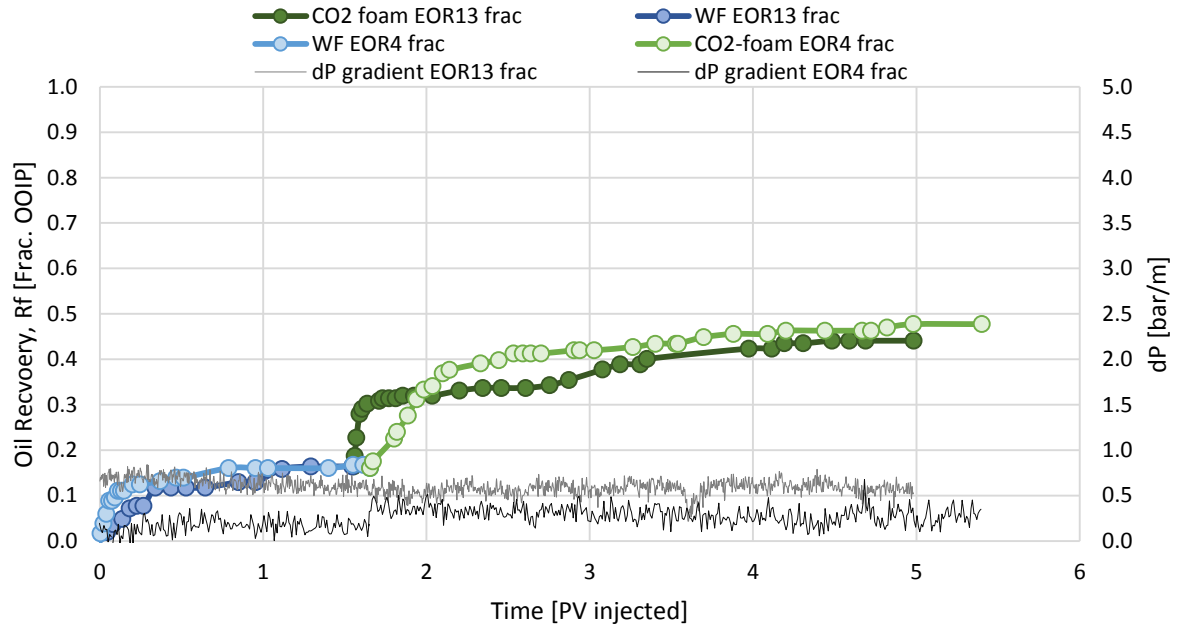

Figure 6-4 Oil recovery versus pore volume injected for tertiary supercritical CO_2-foam injection in fractured limestone core plugs. The differential pressures are plotted on secondary y-axis (bar/m). The lines between the points are not experimentally measures but only for guiding the eye. An increase in oil production is seen when injecting CO_2-foam. However, no foam generation is observed in the fractured systems.

The production rate was observed to be higher than the injection rate during CO_2-foam injection in fractured core EOR13. The reason for this is unsure, but the production may not have been adjusted for a possible oil volume left in the experimental system. The total recovery for the injections were obtained at 47.7% (EOR4) and 44.1% (EOR13). The recovery differences might be due to the cores heterogeneity within pore size distribution.

A small increase in average differential pressure from 0.18 bar/m during waterflooding to 0.31 bar/m during CO_2-foam was observed. Despite the small increase, the pressure was lower than for the pure CO_2-injection in Figure 6-2. Based on this, it is likely that CO_2-foam was not generated in the fractured cores. This might be due to the high permeability fracture. The fractures in the cores were well-defined artificial fractures having smooth surfaces. The foam generation mechanisms from snap-off is only present in the matrix where grains and pore throats are found. Foam is reported to be more efficient in high permeable porous media (Khatib, Hirasaki et al. 1988). This is different from high permeable media caused by large fractures because of the absent of foam generating mechanisms. In a porous medium foam generation is largely due to snap-off. The coalescence is controlled by the limiting capillary pressure (Khatib, Hirasaki et al. 1988). In fractured systems, the limiting capillary pressure is much lower than in porous medium and might not be reached (Ferno, Gauteplass et al. 2014).

A second explanation for the absent foam generation was the high oil saturation present in the cores when foam was injected. Large oil saturations present in the porous media interacts with the foam, making the foam less stable. The oil enters and spreads on the gas/water surfaces creating the foam bubbles, destroying the foam (Schramm 1994). This is why foam injection is normally performed after a water injection (Farajzadeh, Andrianov et al. 2009) (Schramm 1994). If the water injection in the experiments had been more efficient, a lower oil saturation would have been reached, and improving the conditions for foam generation.

Figure 6-5 shows oil recovery during foam injection in a whole limestone core, EOR3 where both oil saturation (S_o) and recovery factor (R_f) are plotted. The total recovery performance was 57.4% OOIP and was achieved after 6.4 PV fluid injected. Water breakthrough occurred after 0.3 PV of water injected and a total recovery of 36.2% OOIP was reached. When the production rate decreased, the differential pressure flattened out due to continuous water flow through the core. Co-injection of CO_2 and surfactant solution was introduced when no additional oil was produced from the waterflooding. An increase in oil recovery was observed together with an increase in differential pressure. In the beginning, the differential pressure had a small increase caused by *in-situ* foam generation in the core. The differential pressure continued to increase during injection, and when reaching breakthrough for 0.2 PV injected, larger fluctuations were observed. Foam generation is a continuous process due to generation and decay of the lamellae (Ransohoff and Radke 1988). This processes could contribute to the large fluctuations in the differential pressure. After 5.1 PV foam injected the maximum oil recovery was reached. The overall displacement efficiency in a reservoir can be considered as a product of the macroscopic and microscopic displacement efficiency (Zolotukhin and Ursin 2000). The macroscopic sweep in the core was improved by the generated foam. Larger fluctuations were observed when the oil saturation decreased, caused by oil left in the pores because of poor microscopic sweep. Unstable foam was generated and the capillary pressure was not stabilized due to inlet effects. These effects could propagate through the entire core because of the small dimensions. The increase in differential pressure might be caused by foam blocking the high permeable channels within the core, forcing the fluid to flow into the matrix. The foam also makes a more favorable mobility ratio between the injected gas and oil in place. The foam generation occur due to the high permeable core where many of the foam generating mechanisms have the possibility to operate (Khatib, Hirasaki et al. 1988). The maximum oil recovery was reached after 5.1 PV foam injected.

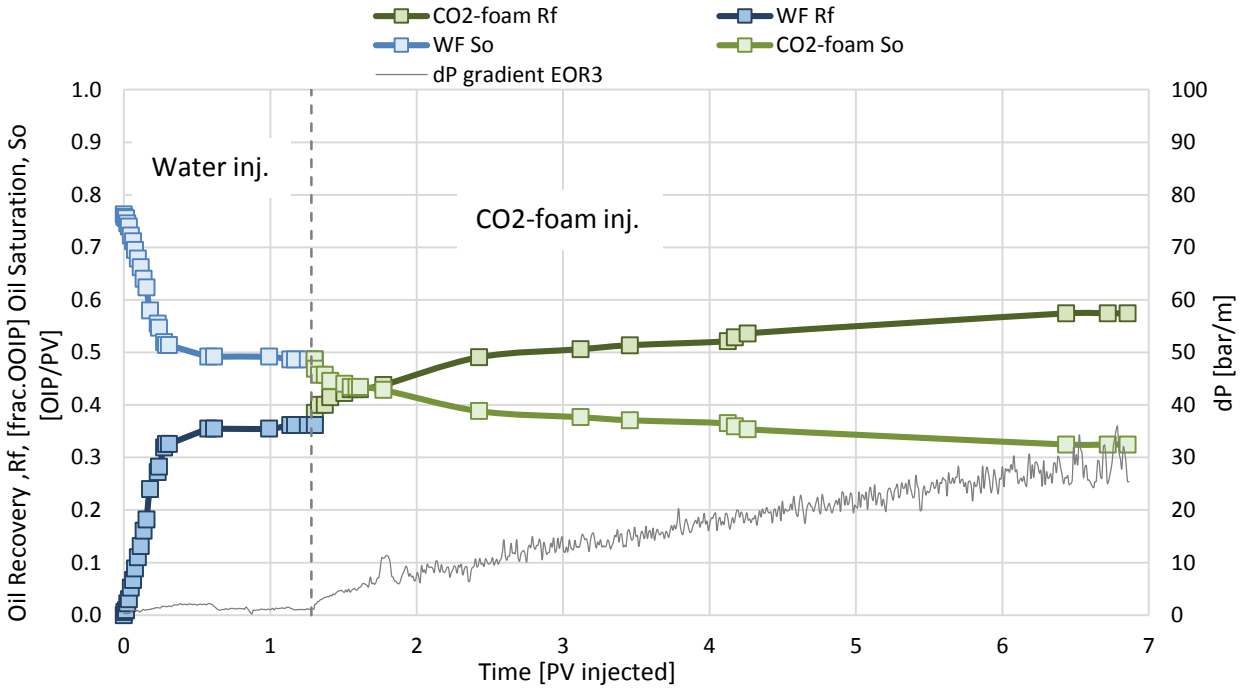

Figure 6-5 oil saturation and oil recovery versus pore volume injected for tertiary co-injection of surfactant solution and supercritical CO_2 in whole limestone core plug. Change of injection fluid is illustrated by the dotted vertical line. Differential pressure is plotted on secondary y-axis (bar/m). Notice the large scale on the secondary axis compared with CO_2-foam injection in fractured systems (Figure 6-4).

Figure 6-6 shows the comparison of CO_2-foam injections in fractured and whole core plugs. The highest recovery was obtained in whole core EOR3 (57.4%) in comparison to the fractured cores EOR4 (47.7%) and EOR13 (44.1%). The difference was mainly an effect of the difference in recovery performance of the water injection and the foam generation. All water injections in the three cores had the same water breakthrough, around 0.3 PV. However, the water flooding was more efficient in the whole core, EOR3, leading to a higher recovery compared with the fractured cores. This was because the pores at the fracture surface most likely were blocked and imbibition of water to produce oil by capillary forces was impeded. When the injection fluid was changed to CO_2-foam, all cores showed an immediate response in oil recovery. The highest CO_2-foam recovery was obtained in fractured core EOR4, where the production increased with 31.6%. In the second fractured core, EOR13, the CO_2-foam contribution was slightly lower (27.7%), even both cores started at the same oil saturation after water flooding. The whole core had only an increase of 21.2%, which might be due to the high recovery during water injection. All CO_2-foam injection tests showed a long production tail caused by diffusion. CO_2 dissolving in the oil, will make it expand and decreases its the viscosity. This increases the microscopic displacement and decreases the residual oil saturation. (Mo, Yu et al. 2012) (Mo, Yu et al. 2014).

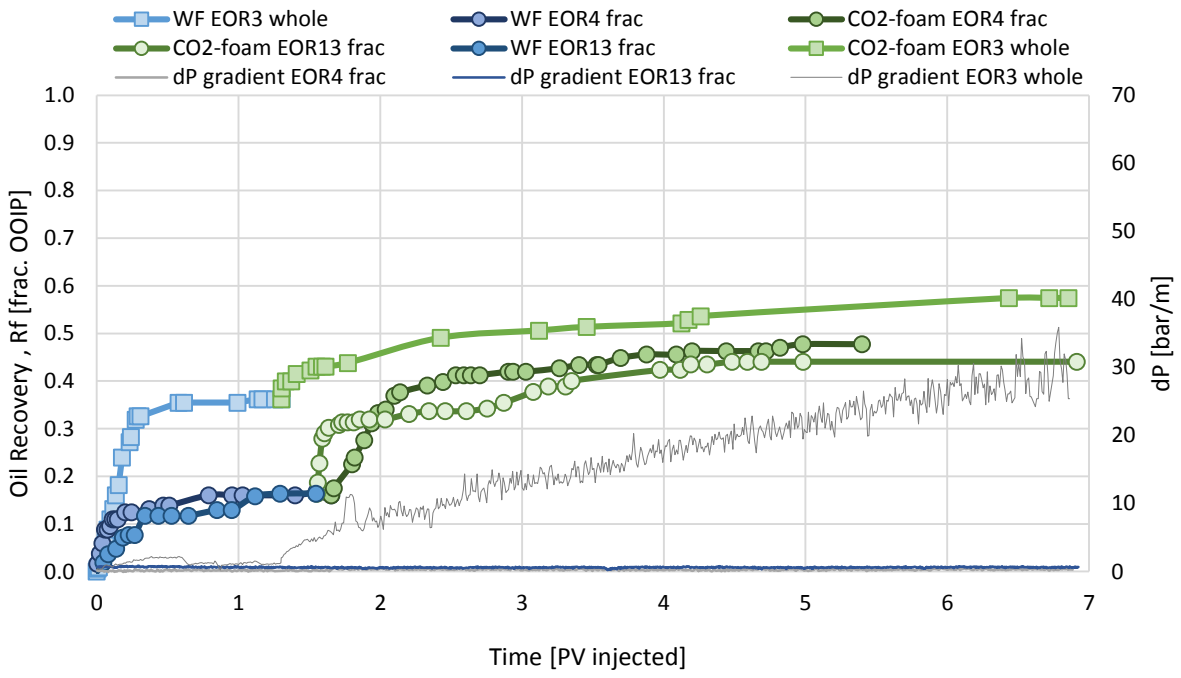

Figure 6-6 Oil recovery versus pore volume injected for fractured (EOR4, EOR13) and whole (EOR3) limestone core plugs for co-injection of surfactant solution and supercritical CO_2. The differential pressures are plotted on secondary axes (bar/m). Foam generation is observed in the whole core compared to the fractured cores where no foam in generated.

The differential pressure during foam injection in whole core EOR3 indicates foam generation, opposed to the fractured cores where no foam generation is observed. This was because the whole core was a high permeability porous medium where the foam generation sites are present to generate foam through snap-off, lamellae division and leave behind mechanisms. As mentioned, foam generally perform better in high permeable channels where the films are more stable due to the low capillary

pressure (Khatib, Hirasaki et al. 1988). A higher recovery could be expected in the fractured cores if foam had been generated. Gas flowing in the form of foam tends to flow through the high permeable and high porosity zones (Apaydin and Kovscek 2000). The foam would blocked the high permeable zones, forcing the injected fluid into the low permeable matrix resulting in a an increase of oil produces. Pre-generated foam could have been a solution for greater oil recoveries, as previous reported from (Ferno, Gauteplass et al. 2014) and (Opdal 2014).

6.2.3 CO_2 injection versus CO_2-foam injection

The effect of CO_2 and CO_2-foam injections in core plugs of the same state (fractured or whole) are compared in this chapter.

Table 6-4 lists the core properties and experimental data obtained for comparison of whole limestone cores EOR2 (CO_2) and EOR3 (CO_2-foam), and fractured cores EOR4 (CO_2) and EOR10 (CO_2-foam).

Table 6-4 Core properties and experimental results from tertiary CO_2 and CO_2-foam injections in fractured and whole limestone core plugs.

Core ID	State of core	PV [ml]	K_{init} [mD]	Avg. Pressure [bar]	S_{iw}	$S_{or, WF}$	$R_{f,WF}$ [%OOIP]	$S_{or, CO2}$	$R_{f,total}$ [%OOIP]
EOR2	Whole	18.60	28.32	93.0	0.226	0.498	35.7	0.358	53.8
EOR3	Whole	17.31	19.31	92.0	0.237	0.487	36.2	0.325	57.4
EOR4	Fractured	17.37	17.30	92.0	0.240	0.638	16.1	0.397	47.7
EOR10	Fractured	16.67	26.21	91.0	0.209	0.559	29.4	0.325	58.9

Figure 6-7 compares CO_2 and CO_2-foam injections in whole limestone core plugs. The recovery development during water injections in the two cores were almost identical, and reached the same recovery of 36% OOIP after 0.7 PV injected. During water injection, the differential pressure across the two cores were similar, with a small increase that flattened out after water breakthrough. Injection of CO2-foam and CO_2 gas increased the oil recovery further. The highest recovery was obtained by foam injection (EOR3, 57% OOIP), while it was lower for injection of pure CO_2 gas (EOR2, 54% OOIP. An earlier breakthrough was observed when injecting foam (core EOR3) compared to injecting CO_2 (core EOR2). The reason for this is unknown. The generation of foam improves the macroscopic sweep, resulting in a higher differential pressure. A secondary oil recovery effect is caused by the foam bringing more gas contact with the oil, enhancing the diffusion process to produce more oil (Farajzadeh, Andrianov et al. 2010a). The above mentioned foam advantages are likely reasons for why core EOR3, compared with core EOR2, achieved a higher oil recovery. When CO_2 and surfactant solution were co-injected in core EOR3, a greater differential pressure was observed, compared to the pure CO_2 injection (core EOR2), indicating generation of foam. The pressure did not stabilize, most likely due to inlet effects as the dimensions of the core plug was small. This effects most likely made the foam generated unstable. Inlet effects describes the behaviour near the inlet of the core, where the surfactant and gas generate foam. The effect can extend a significant distance in the core. Even though the differential pressure continued to increase, the recovery stabilized and no additional oil was produced. Large differential pressure across the core indicate larger foam resistant thus stronger foam (Hirasaki and Lawson 1985). The generation of stronger foam might be due to lower oil saturation which reduces the chances for the lamella in the foam to be destroyed.

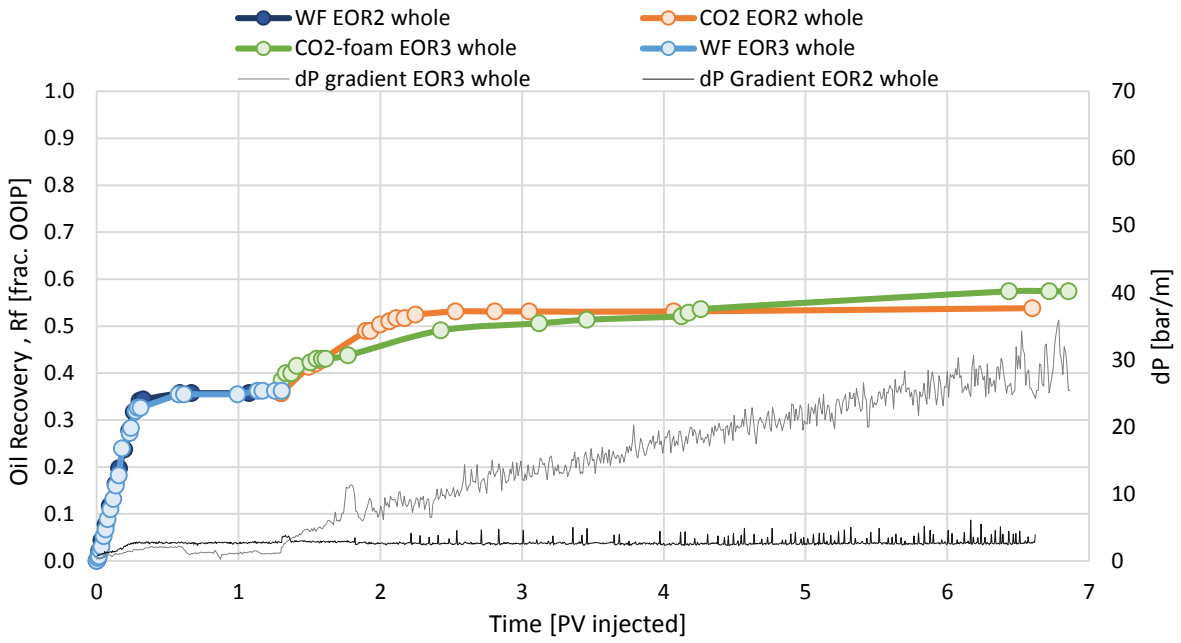

Figure 6-7 Oil saturation versus pore volume injected for CO_2 and CO_2-foam injection in whole limestone cores, EOR2 and EOR3. From injecting CO_2-foam, the recovery is slightly higher than the recovery obtained by pure CO_2 injection. The differential pressures are plotted on secondary y-axis (bar/m). A large differential pressure is observed in core EOR3 due to unstable foam generation.

In Figure 6-8, tertiary CO_2-foam and CO_2 injection in fractured limestone cores, EOR4 and EOR10, were compared. A total oil recovery of 58.9% OOIP was obtained in core EOR10 (CO_2 injection) and 47.7% OOIP in core EOR4 (CO_2-foam injection). An earlier breakthrough was observed in core EOR4 compared to core EOR10 where the water displacement was more efficient. The low recovery in core EOR4 might be caused by more pores plugged in the fracture. The plugging is from the fracturing dust described earlier blocking the pores, and preventing the injected fluid from producing the oil. The recovery after water flooding was lower than expected in both cores since they were strongly water-wet.

When injecting CO_2 (EOR10) and CO_2 –foam (EOR4) a higher oil production rate (see slope in figure) was observed during the CO_2-foam injection. This higher rate was caused by the low oil recovered from the water flooding and less water shielding the oil, due to the low water saturation.

The recovery mechanism for produced oil after injecting about one PV of CO2 is likely to be diffusion due to the slightly increasing oil recovery. Low injection rates and high permeable fractures makes diffusion the main oil producer. The differential pressure for the two injections were quite similar indicating no foam generated in fractured core EOR10, despite the co-injection of CO_2 and surfactant solution. The high oil saturation in the core after waterflooding did likely act as an inhibitor on foam generation. Also, as explained above, the foam generating mechanisms like snap-off is not present in the large fractures. A higher recovery would be assumed when injecting foam into fractured network. The foam would then block the high permeable fractures, forcing the injected fluid to flow into lower permeable zone and thus increase the sweep efficiency. The foam generation would lead to more contact between CO_2 and oil making the interfacial mass transfer between the phases more efficient. This would be important in the mobilization of the oil throughout dissolution, viscosity reduction, diffusion and swelling of oil (Yaghoobi 1994, Farajzadeh, Andrianov et al. 2010a).

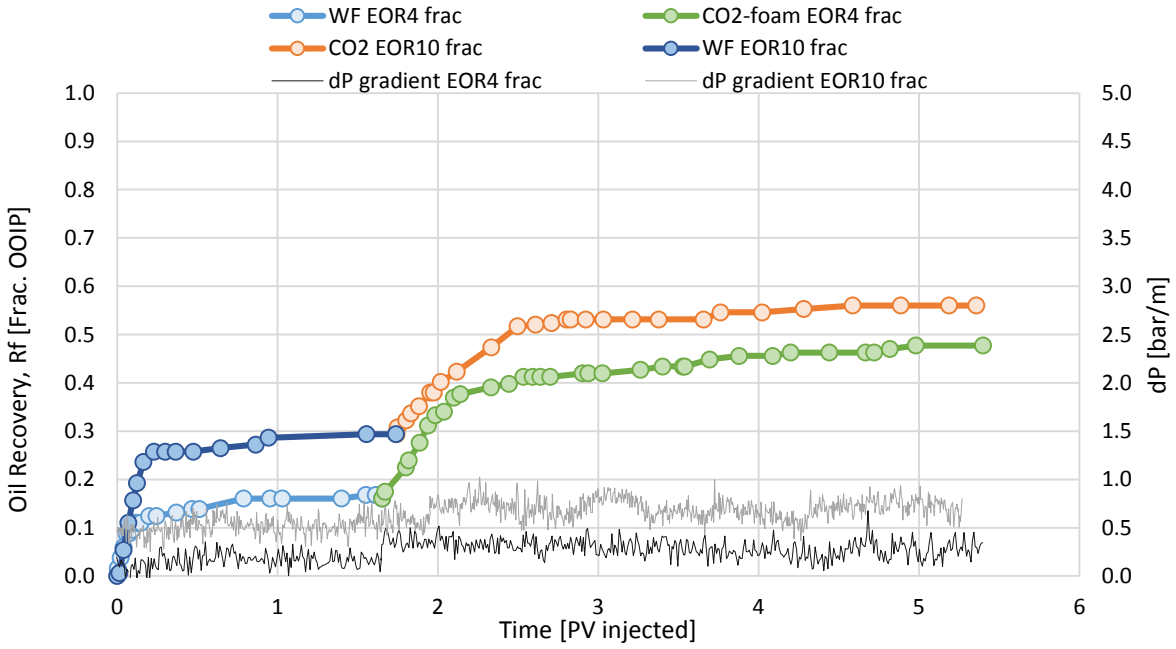

Figure 6-8 Oil recovery versus pore volume injected for CO_2 and CO_2-foam injection, subsequently a water injection in fractured limestone cores at constant temperature 35°C. The highest recovery is obtained in fractured core EOR10 for CO_2 injection. The differential pressure is plotted on secondary axis (bar/m) and are similar for the two injections indicating no generation of foam in fractured core EOR4.

6.2.4 Sequential CO_2 and CO_2-foam injections in Fractured Limestone Core

This chapter present results from tertiary CO_2 and CO_2-foam injections in fractured limestone core plug EOR12. It is, as mentioned, reported that foam perform better at low oil saturations. The objective of the experiment was to investigate how tertiary oil recovery could be affected if CO_2-foam injection was done after a sequence of CO_2 gas injection. Examination of *in-situ* foam generation was also performed. The results were compared to previous EOR experiment conducted by Opdal (Opdal 2014). Table 6-5 lists EOR12 core properties and the obtained results from the experiment.

Table 6-5 EOR12 core properties and experimental results after water-, CO_2, and CO_2-foam injection

Core ID	**PV [ml]**	**Length [cm]**	**K_{init}^* [mD]**	**S_{wi}**
EOR12	16.84	7.2	21.01	0.318

$S_{or,\ WF}$	**$R_{f,WF}$ [%OOIP]**	**$S_{or,\ CO2}$**	**$R_{f,CO2}$ [%OOIP]**	**$S_{or,CO2foam}$**	**$R_{f,CO2foam}$ [%OOIP]**
0.512	26.8	0.372	46.9	0.259	63.1

Figure 6-9 shows the obtained results from the EOR experiment. The core was first water flooded reaching a recovery of 27% OOIP. A linear trend can be seen in the production curve up to the point where water breakthrough occurs after injecting 0.1 PV. This was likely an effect of the high transmissibility through the fracture in the core. The oil recovery from water injection was lower than expected because the core was strongly water wet. When no additional oil was produced from waterflooding, supercritical CO_2 was injected. The injection reached a recovery of 47% OOIP. A delay in the oil production was observed because of an earlier oil production assumed from the core during the injection. The earlier produced oil was possibly a result of oil volumes left in experimental set-up, either in the tubings or the back pressure regulator. During CO_2 injection the differential pressure decreased due to the low viscosity of the gas. When the oil recovery stabilized, CO_2 was co-injected with surfactant solution in ratios 8:2. A production increase was again seen, and the total recovery reached 63% OOIP. The increase in oil production during CO_2-foam injection was due to a more favourable mobility ratio. A small increase in differential pressure was observed, indicating possible foam generation. However, the obtained differential pressure was significant lower than what was observed in core EOR3 (Figure 6-7). The low differential pressure might be caused by small amount of foam generated in the matrix because of lower oil saturation. The generated foam could possibly also be a weak foam which was easily broken, due to high disjoining pressure caused by small capillaries. The obtained recovery was, however, lower than expected and might be caused by blocked pores in the core fracture.

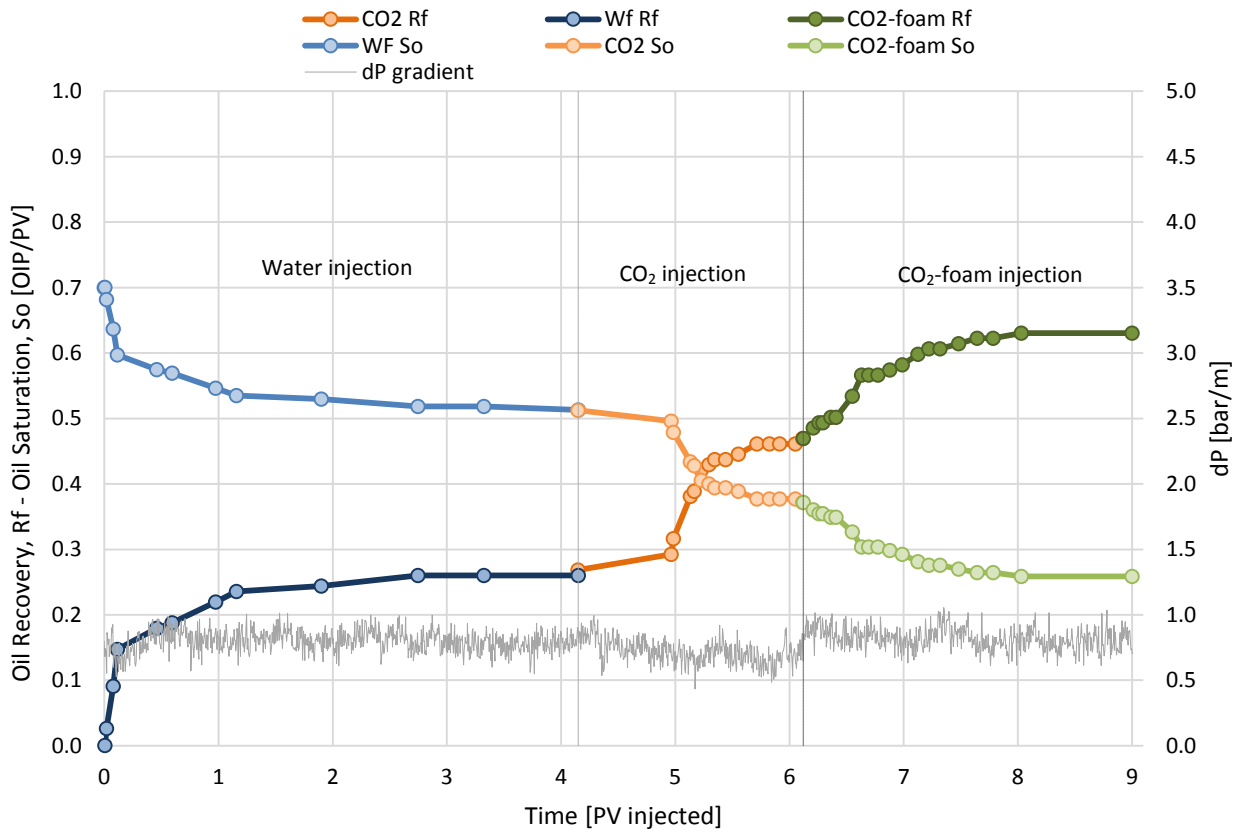

Figure 6-9 Oil saturation (S_o) and oil recovery (OIP/PV) versus pore volume injected for fractured core EOR12. Water was first injected followed by CO_2-injection and co-injection of CO_2 and surfactant solution possibly generating foam. Differential pressure is plotted on secondary y-axis (bar/m). The injection schemes are separated with dashed lines.

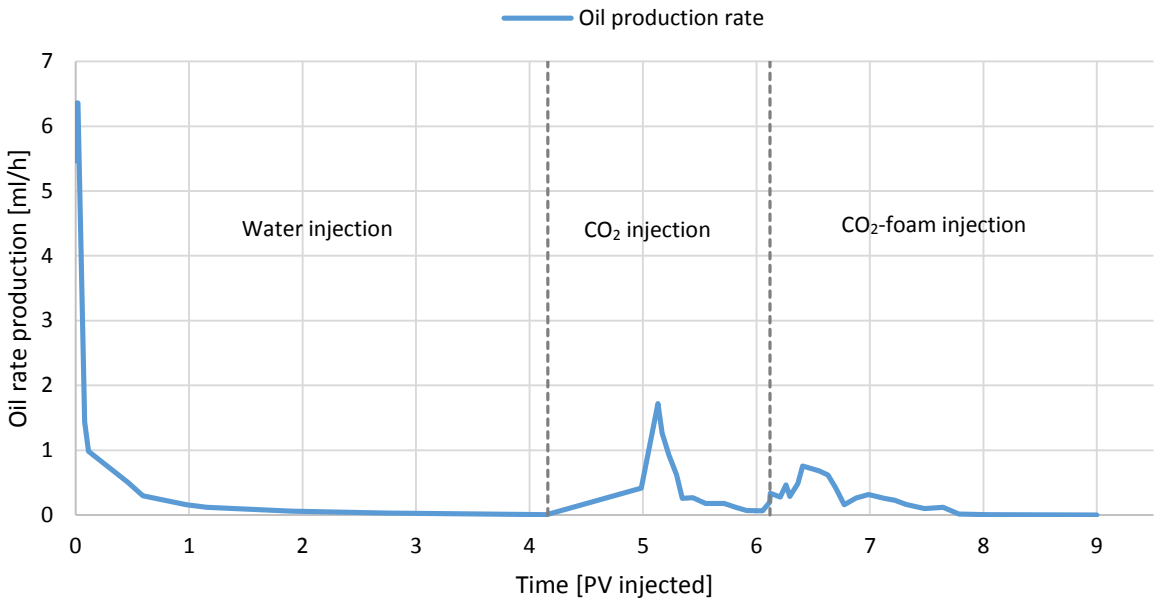

Figure 6-10 Oil rate production [ml/h] versus pore volume injected for the injections of three fluids in fractured limestone core EOR12. Change of fluid injected is marked with dashed lines. An increase in oil production was observed for each time the injected fluid was changed.

The obtained results in core EOR12 was compared with a previous experiment conducted by Opdal (Opdal 2014). The experiment used for comparison (core I.O) was conducted by injecting supercritical CO_2 and CO_2-foam in fractured limestone network using material balance for EOR. Core I.O was made up of three limestone cores stacked together. The first core was whole followed by two fractured cores. The first fracture was placed horizontally and the second vertically in the core holder. Core EOR12 had only one artificially, vertical fracture using spacer. No spacers was used in core I.O which gave a much lower permeability, possibly in orders of several hundred mD, compared with core EOR12. Core I.O was saturated with paraffin oil for the oil phase, whereas core EOR12 was saturated with n-decane. Miscibility between CO_2 and the paraffin oil was assumed.

Figure 6-11 compares the two experimental results in core EOR12 and core I.O. A greater oil recovery was achieved during water flooding for core I.O. compared to EOR12, making it better for foam generation due to the lower oil saturation. The water flooding was more efficient due the lower permeability of the fracture in core I.O, and because of the pore blockage in the fracture in core EOR12. When CO_2 was injected in core I.O, the oil was mobilized from the whole core placed first in the core stack, and displaced the oil in the fractured cores. This was observed by MRI by Brautaset, 2010 (Brautaset, Ersland et al. 2010). The increased differential pressure in core I.O indicated foam generation. The foam was generated in the whole core and moved into the two fractured cores. The foam blocked the high permeable fractures, and made the injected CO_2 more viscous. The generated foam was unstable since the differential pressure was not stabilized due to inlet effects. In core EOR12, the increase in differential pressure was not as significant, compared to core I.O, indicating less foam generated. The large differences in differential pressure between the two cores were caused by the large permeability differences. The foam was shown to be efficient in fractured cores. However, the foam has to be injected in a pours medium where the foam generating mechanisms (snap-off, lamellae division and leave behind) are present. In addition, the oil saturation has to be low.

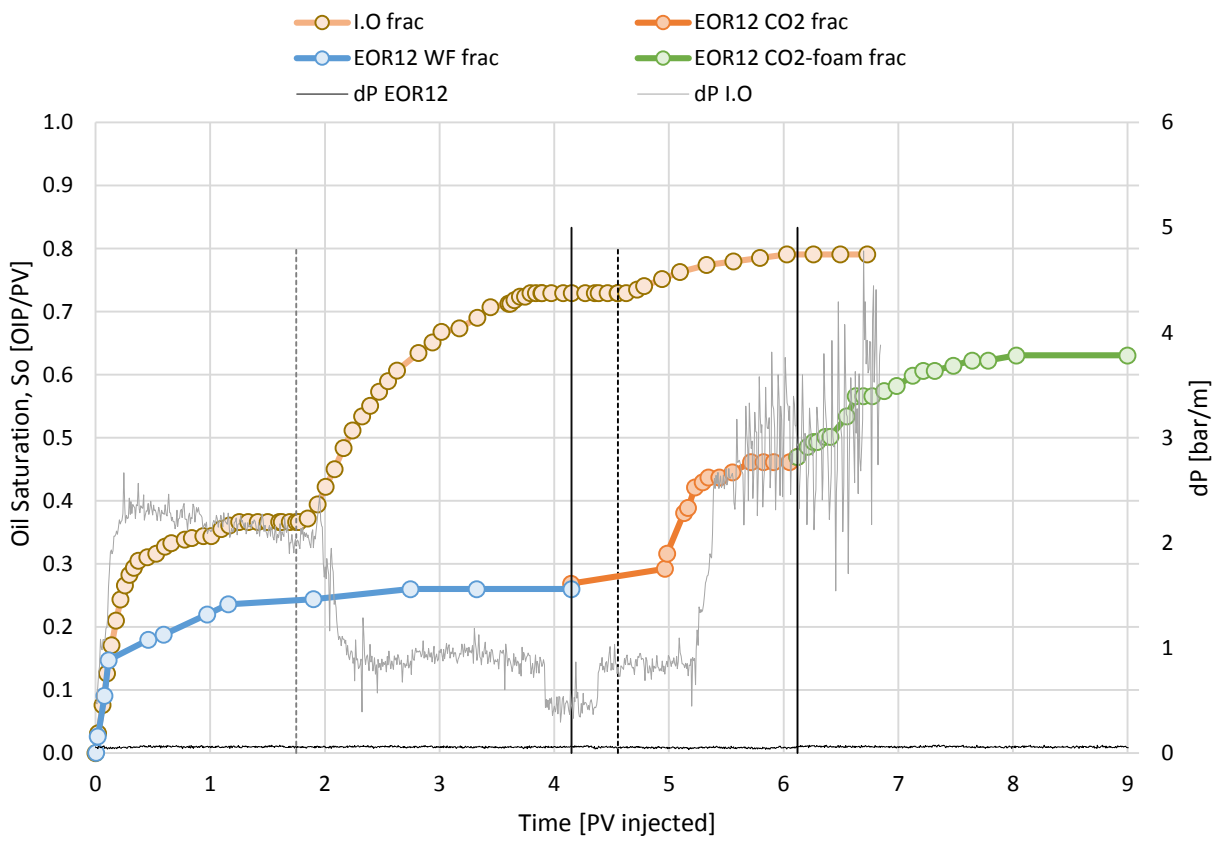

Figure 6-11 Comparison of tertiary CO_2 and CO_2-foam injections in fractured limestone core plugs. The comparison experiment was conducted by (Opdal 2014). Notation I.O represents the comparing experiment. The dashed vertical lines indicates when the injected fluid was changed in the I.O experiment, while the solid vertical line indicates when injection fluid was changed in EOR12 experiment. The I.O experiment obtained a higher total oil recovery, and a higher differential pressure during CO_2-foam injection indicating a stronger generation of foam compared to the EOR12 experiment.

6.2.5 Summary EOR experiment

Table 6-6 and Table 6-7 lists all the core properties and obtained results for the conducted EOR experiments. Oil saturations and oil recoveries achieved from each injection sequence are listes. Core EOR14 was not discussed in the results. This was because the achieved oil recovery was unreasonably low, indicating error in the experimental set-up.

Table 6-6 Measured data of limestone core plugs used in the experiment

Core ID	State of core	PV [ml]	Length [cm]	K_{init}^{*} [mD]	S_{wi}
EOR2	Un-fractured	18.60	7.1	28.32	0.226
EOR3	Un-fractured	17.31	7.0	19.31	0.237
EOR4	Fractured	17.37	7.2	17.30	0.240
EOR10	Fractured	16.67	6.7	26.21	0.209
EOR12	Fractured	16.84	7.2	21.01	0.318
EOR13	Fractured	21.79	9.0	22.16	0.245
EOR14	Fractured	27.32	9.35	30.28	0.253

- The permeability measured is the matrix permeability, and was measured before the cores were fractured.

Table 6-7 Experimental results from EOR experiments conducted on limestone core plugs

Core ID	$S_{or,\ WF}$	$R_{f,WF}$ [%OOIP]	$S_{or,\ CO2}$	$R_{f,CO2}$ [%OOIP]	$S_{or,CO2foam}$	$R_{f,CO2foam}$ [%OOIP]	$R_{f,total}$ [%OOIP]	Injected fluid
EOR2	0.498	35.7	0.358	53.8	-	-	53.8	CO_2
EOR3	0.487	36.2	-	-	0.325	57.4	57.4	CO_2-foam
EOR4	0.638	16.1	-	-	0.397	47.7	47.7	CO_2-foam
EOR10	0.559	29.4	0.325	58.9	-	-	58.9	CO_2
EOR12	0.512	26.8	0.372	46.9	0.259	63.1	63.1	CO_2 + CO_2-foam
EOR13	0.632	16.4	-	-	0.422	44.1	44.1	CO_2-foam
EOR14	0.688	7.8	-	-	0.415	44.4	44.4	CO_2-foam

From the conducted experiments, oil recovery from the water flooding, especially the fractured cores, was lower than expected because of the cores strong water preference. In the fractured cores, the pores in the fracture were likely blocked due to dust. The dust was adsorbed to the pore walls during the fracturing of the cores. This blocking might have prevented the injected fluids to access the matrix, resulting in a lower recovery than predicted. When injecting water prior to CO_2, water shielding might occur. Water shielding is the effect of water films inhibiting CO_2 from contacting the oil phase, leaving residual oil behind in so called "dead-end-pores (Gabitto 1998). The difference in oil production between the cores of same state and injection strategy, can be caused by the heterogeneous limestone material (e.g pore size and permeable streaks) within the cores. All experiments where CO_2 and/or CO_2 foam were injected showed an increase in total oil recovery compared with water flooding. One underlying objective of the experiments was to see what maximum oil could be recovered for each injected fluid. It is, from an economic perspective, important to take into account the amount of pore volume injected to achieve the maximum total recovery. Less fluid injected might give about the same total oil recovery. Taking core EOR12 as example (Figure 6-9), the same recovery by CO_2-foam injection could possibly have been reached for less amount of CO_2 injected prior to the foam injection. The highest total recovery was observed in core EOR12 where both CO_2 and CO_2-foam injections were performed. This indicates the importance of obtaining a low oil saturation before co-injection of CO_2 and surfactant solution is performed.

Experiments performed on core scale are very informative for understanding the enhanced oil recovery processes, but they may be misleading. At small scales, the fluid phases are not as likely to be in equilibrium as they would be in a field-case displacement scenario. This results in optimistic oil recovery efficiency caused by larger mass transfers between two non-equilibrium phases. In actual field flooding, recovery the efficiencies are dominated by large scale bypassing caused by gravity segregation, reservoir stratification and unfavourable mobility ratios. The bypassing effect in fields are therefore several of magnitude larger than on laboratory scale.

Foam injection as a possible EOR method in fractured reservoirs has now been evaluated in limestones. The results indicate that foam generation was weak and, sometimes, even absent during co-injection of surfactant solution and CO_2. It is therefore necessary to consider alternative foaming agents for improved stability and performance. One such alternative is small solid colloidal particles that stabilize the lamella without using a surfactant. Experimental sensitivity analyses investigates the generation of foam using nanoparticles as foam agents in the next chapters.

6.3 CO_2-foam Nanoparticle Stabilization

A series of experiments have been conducted to achieve a better understanding of CO_2-foam generation and behaviour, using nanoparticles and surfactants as foam agents. The objective of this sensitivity analysis was to study the impact of nanofluid and gas fractions on the generation and stability of foam. Co-injections of CO_2 and nanofluid were performed in sandstone core plugs, where gas fractional flow and total injection rates were varied systematically. These results are presented and discussed in addition to injection strategies, mobility reduction and hysteresis effects. The results were also compared to co-injections of nanofluid and CO_2 in a carbonate core plug, and injections of foam stabilized by surfactants in a sandstone core.

A total of seven sandstone and three limestone cores were prepared for the experiments. For experimental preparations see chapter 5.3. The detailed experimental procedure is explained in chapter 5.4, where Figure 5-8 illustrates the experimental set up. All experiments were conducted on 1.5" diameter core plugs with length ranging from 24-28 cm. The experimental pressure condition was 90 bar. Since high temperature and high presence of salt negatively affect the colloidal stability, core-flooding experiments were conducted at 25^0C with only 2% salt concentration present in the liquid phase. This was performed in order to improve the stability of the nanoparticle dispersion (nanofluid). Interaction of foam with oil is not included to avoid confusing foam-oil effects with foam coalescence. The nanofluid concentration was kept constant with 0.5wt% nanoparticles for all the experiments. The developing differential pressure gradients for some of the experiments can be found in Appendix – B

6.3.1 The Effect of Co-injecting Nanofluid and CO_2

Foam generation during co-injections of nanofluid and CO_2 with variable gas fractional flows were evaluated. The foam generations were compared to a baseline injection, where brine and CO_2 were co-injected. The results showed the differential pressures increased for all CO_2 and nanofluid total injection rates, compare to the baseline injections. The foam apparent viscosity showed no shear-thickening or shear-thinning trends, thus, the apparent viscosity were independent of injection rates. The mobility reduction factor showed a large decrease in mobility. The highest reduction was observed for gas fraction, f_g=0.70. This was the same gas fraction as the highest differential pressures and apparent viscosities were achieved for all total injection rates.

CO_2 and foam agent dispersion phase ratio is one of the greatest parameters affecting foam flow behaviour, together with total injection rates. Co-injections of CO_2 and brine, using total injection rates ranging from 2–4 cc/min, was performed as a baseline for the following CO_2-nanofluid injections. The gas fractions (f_g) ranged from 0.1 - 1.0. The injections were performed with increasing rates, starting with rate 2 cc/min, and increasing gas fractions. Stable differential pressure was reached for each total injection rate for the same gas fraction, before the gas fraction was increased.

Figure 6-12 shows the results from the baseline injections (dashed lines). A small increase in differential pressure for all rates were observed until f_g=0.5 was reached. For this gas fraction the highest differential pressures were achieved for all injection rates in the baseline. This is because the two injected phases are most discontinuous at this fraction, resulting in a low relative permeability of the two phases. Above f_g=0.5, the differential pressures decreased slightly due to the higher gas fractions injected. The gas phase became more continuous and the relative permeability became larger, resulting in a smaller pressure drop for f_g>0.5. The similar differential pressures obtained for f_g=1.0 were caused by the injected gas low viscosity flowing through the high permeable core.

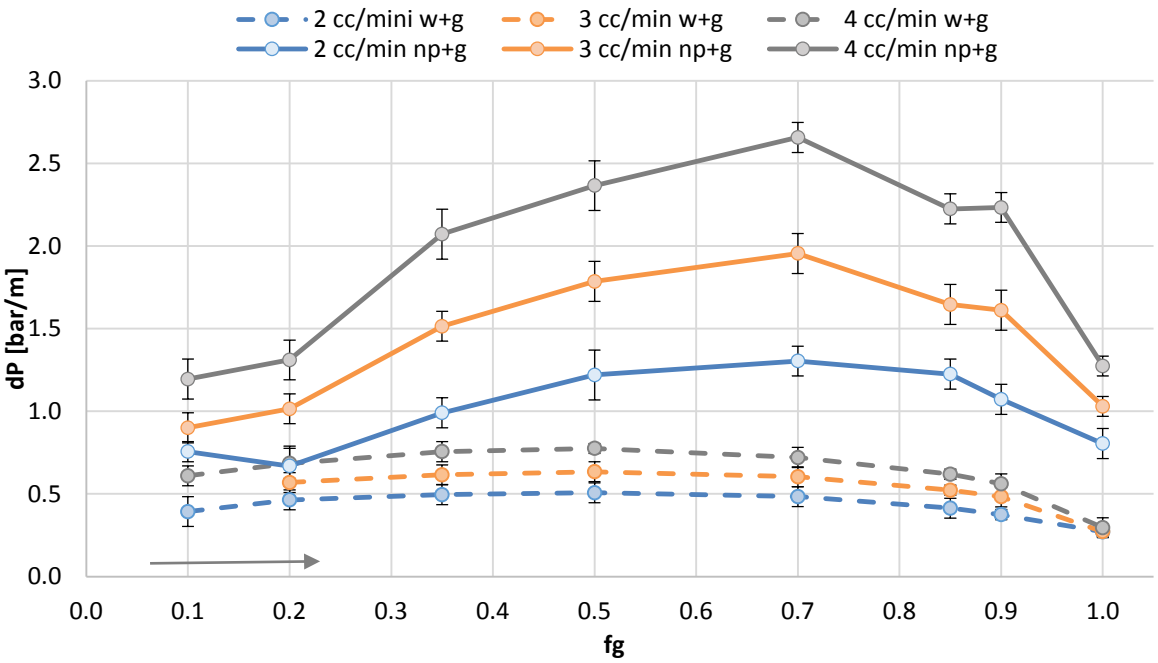

Figure 6-12 Pressure gradient (bar/m) versus gas fraction (foam quality) for co-injection of nanofluid and CO_2 (np+g) (solid line), and brine and gas (w+g)(dashed lines) in a sandstone core plug Three constant total injection rates were used. Same rates are shown with same color. The line joining the points are simply for distinguishing between the data sets, and are not measured values. Injecting np+g, all total injection rates showed an increase in differential pressure until f_g=0.7 was reached, then the differential pressures decreased. The arrow points the way the injections were performed with regard to the injected gas fractions.

When steady differential pressures were reached for all gas fractions (f_g=0.1 – 1.0) in the baseline, the brine was replaced with nanofluid. The nanofluid was delivered at particle size <10 nm. The experiment was repeated in the same core starting at f_g=0.1, using the same injection rates and injection procedure. Figure 6-12 (solid lines) shows an increase in differential pressures when co-injecting nanofluid and CO_2. Larger differential pressure across the core indicates larger flow resistant (Hirasaki and Lawson 1985), and generation of foam. From previous work, larger pressure gradients and flow resistance have been caused by smaller gas bubbles in the foam (Ettinger and Radke 1992). The foam increases the viscosity of the injected CO_2, which leads to more favourable displacement conditions. This further results in an increased oil production in oil saturated porous media (Farajzadeh, Andrianov et al. 2009). When the gas fractions increased, the differential pressures increased for all injection rates until f_g^*=0.7 was reached. f_g^* is defined as the critical gas fraction. For

this gas fraction the largest differential pressures were observed for all three rates injecting nanofluid/CO_2. Rate 2, 3 and 4 cc/min had 169.5, 223.9 and 268.9% differential pressure increase, respectively, compared to the baseline injection (brine/CO_2) at f_g^*=0.70. When gas fractions above 0.7 were continued injected, the differential pressures decreased, indicating a more unstable foam. The foam reached the high quality regime, defined for f_g>0.7. In the high quality regime, coalescence occurred as a result of dry foam. Reaching f_g=1.0, the differential pressures were higher compared to the baseline injections. A possible explanation for this is because the amount of trapped gas is higher injecting foam. Trapping of gas occurs in the intermediate-sized pores since the wetting phase, in our experiment water, occupies the smallest pores (Kovscek and Radke 1994). The pressure difference might also be caused by clogging of the pores caused by adsorption of the nanoparticles to the rock walls.

Figure 6-13 shows steady differential pressures were achieved for all baseline injection rates. Three total injection rates were performed for each gas fraction. Each plateau in the graph represents the steady state for one injection rate.

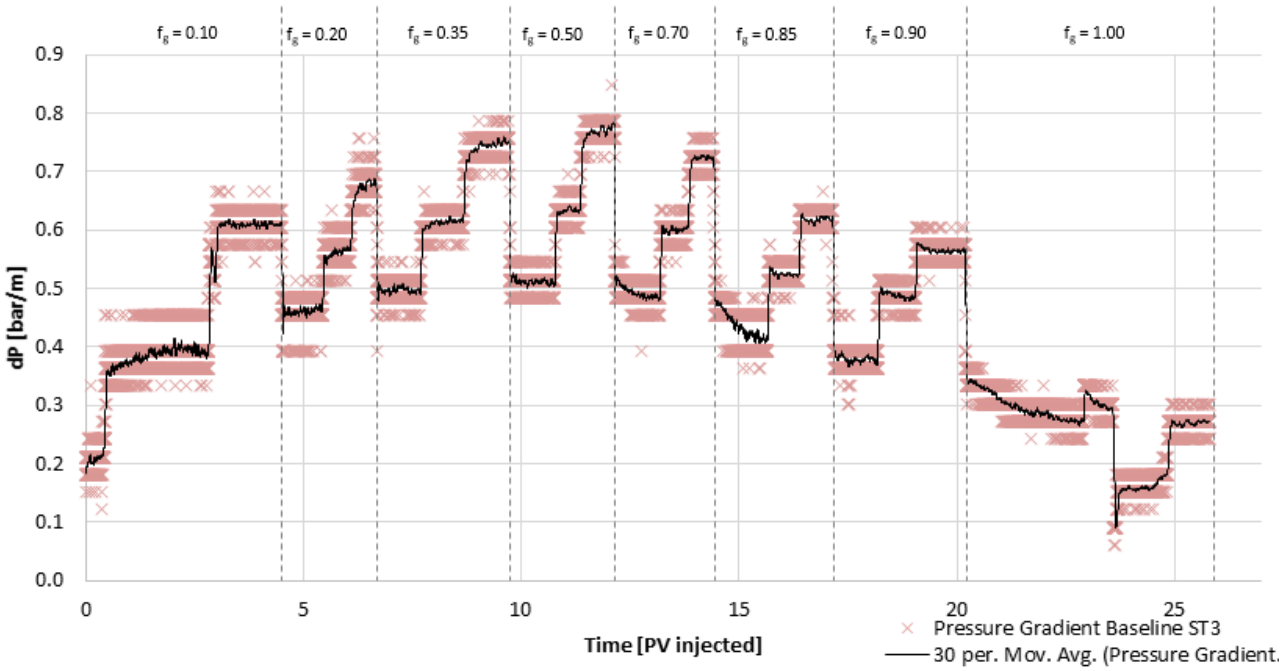

Figure 6-13 Differential pressure gradient vs. pore volume injected for co-injection of CO_2 and brine in sandstone core. Each plateau in the graph represents a total constant injection rate within the given gas fraction, where steady differential pressures were achieved.

The differential pressure gradient for the foam injection (CO_2/nanofluid) is shown in Figure 6-14 (red line). The injection is compared to the differential pressures obtained for the baseline injection (grey line). A large decreasing pressure tail was observed when gas fraction f_g=0.1 was injected. This was caused by the transition from injecting gas fraction 1.0 in the baseline. The core was dried out by the pure CO_2 injection before it was re-saturated with liquid fraction 0.9, and a decreasing pressure was observed. However, a larger differential pressure was achieved comparing the baseline and foam injections, which indicated foam generation. Injecting foam, an average of 2.14 PV surfactant and CO_2 was injected for achieving pressure steady state. This average was calculated without the first injection with gas fraction 0.1, since this injection had a large deviation from the other injections. The foam injections required twice as many pore volume injected, compared to the baseline. Possibly this is caused by the foam generation mechanisms, which needs to reach a steady state between generation and coalescence before steady pressure is reached. Larger fluctuations were also observed for the foam injections, compared to the baseline, which might be caused by the mechanisms for foam generation since this is a continuous process.

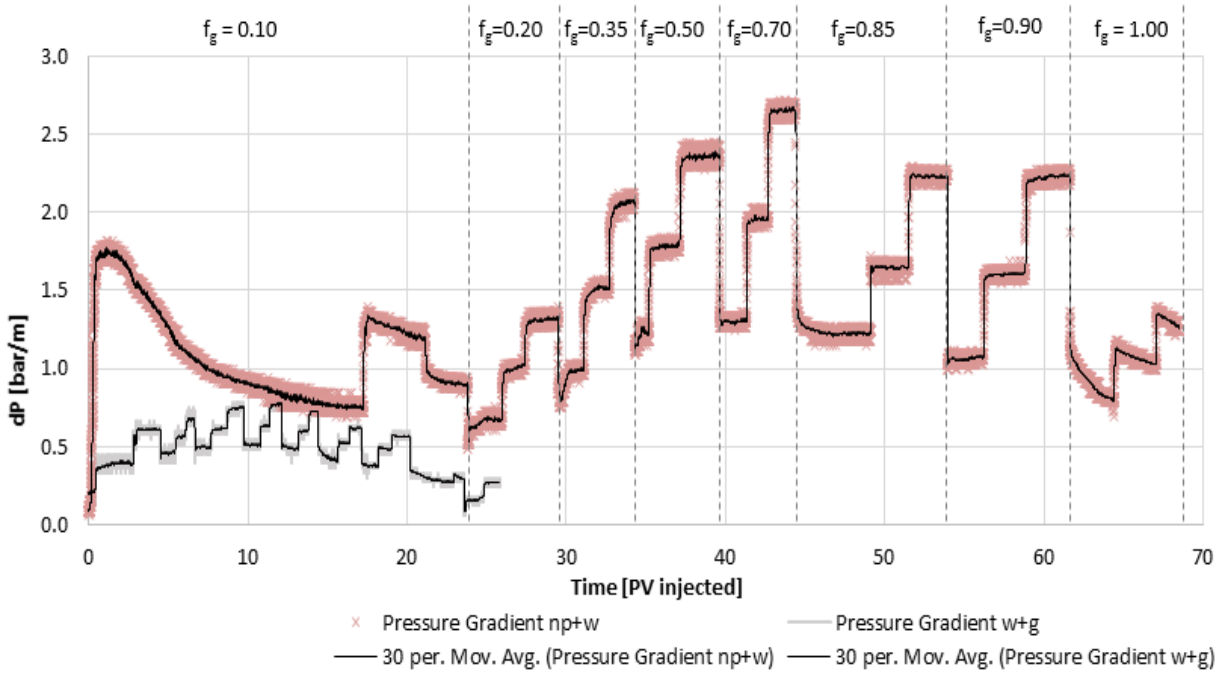

Figure 6-14 Differential pressure gradient versus pore volume injected co-injecting nanofluid and CO_2 in sandstone core. The gray graph is the baseline injection in figure 6.13 attached for comparison. Each plateau in the graph represent an injection rate for the given gas fraction. An increase in differential pressures were observed for the foam injection compared to the baseline injections.

Figure 6-15 shows the apparent viscosity for the baseline and the foam injections. The apparent viscosity, μ_{app}, was calculated for each rate and gas fraction where a steady pressure drop across the core was observed, using equation 4.2. Using the pressure drop across the whole core for the calculation ignores the issues of entrance effects. These effects describe the behaviour near the inlet of the core where the injected foam agent solution and gas generate foam. The effect extends a significant distance in the core, which could change with injected foam quality (gas fraction) (Ettinger and Radke 1992). In addition, the capillary end effects were ignored. These end effects attribute the injections to be time consuming reaching steady differential pressures. This is because they extend from the outlet of the core toward the inlet, in opposite flow direction (Apaydin and Kovscek 2000).

The foam viscosity at a given gas fraction showed minor differences (Figure 6-15). This indicated no shear-thinning or shear-thickening behaviour. These effects develop when fluid viscosity decreases (shear-thinning) or increases (shear-thickening) with increasing injection rate. A possible explanation why the viscosity is independent of rate is because the co-injection of nanofluid and CO_2 generated an emulsion, not a foam. An emulsion occurs when a liquid phase is dispersed in another liquid phase. Foam occurs when large amounts of a gas phase is dispersed in a liquid phase. When the injection rate increases for a foam injection, the gas bubbles becomes smaller and the foam texture is changed. This results in higher flow resistance, thus lower viscosity. Increasing the injection rates in an emulsion will likely not change the texture of the liquid dispersed in the liquid, and the apparent viscosity remains the same. Despite the possible generated emulsion, co-injection of CO_2 and nanofluid will be referred to as foam. The largest apparent viscosity for the co-injections occurred at the critical foam quality, f_g^*=0.7 for all total injection rates. One of the mechanisms nanoparticles enhance foam viscosity, is by reducing the rate the lamellae drain (Binks 2002) (Singh and Mohanty 2014, Roebroeks, Eftekhari et al. 2015) After reaching the critical foam quality the curves diverged. As mentioned, the foam reached the high quality regime (f_g>0.7) and the apparent viscosity decreased likely due to coalescence.

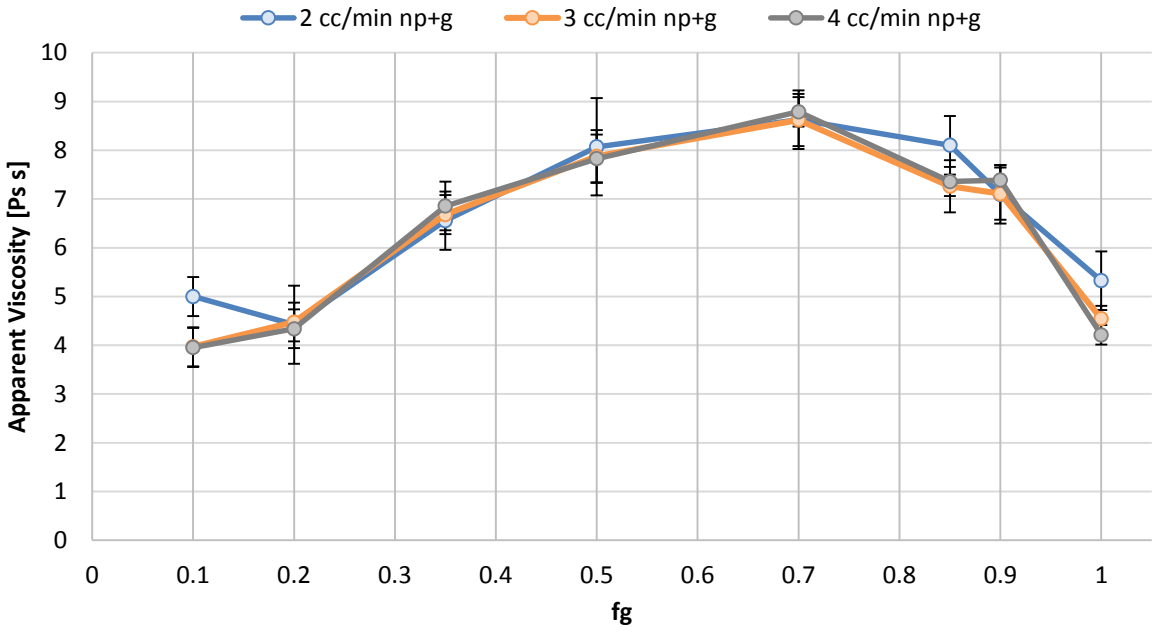

Figure 6-15 Apparent viscosity versus foam quality for three total injection rates co-injecting CO_2 and nanofluid (np+g). The line joining the points are simply for distinguishing between the data sets and are not measured values. The apparent viscosity showed independency of injection rates.

Figure 6-16 shows the mobility reduction factor, MRF, calculated using equation 4.3. Since the experiment and experimental setup made it difficult to quantify the water saturation, S_w, the calculation of MRF was performed assuming CO_2 and brine was not miscible. The apparent viscosity of CO_2 at 25^0 C and 91 bar is 0.071 cp (NIST 2011). The results showed a similar mobility reduction, within acceptable error, for all total injection rates. It was noted the mobility reduction values were remarkable high (Svorstøl, Vassenden et al. 1996). This is because the factor was calculated using pure CO_2 viscosity. The calculations should have been correlated with the apparent viscosity of the baseline injections. This is because at lower gas fractions the dominating viscosity is the brine viscosity. However, the highest mobility reduction was observed for the same gas fraction where the highest apparent viscosity and differential pressures were observed (f_g=0.70). The higher value obtained for rate 2 cc/min with f_g=0.10 could be because the differential pressure had not reached stable conditions completely. The differences between rate 2 and 4 cc/min injecting with f_g=1.0 might be caused by gas trapped in the cores.

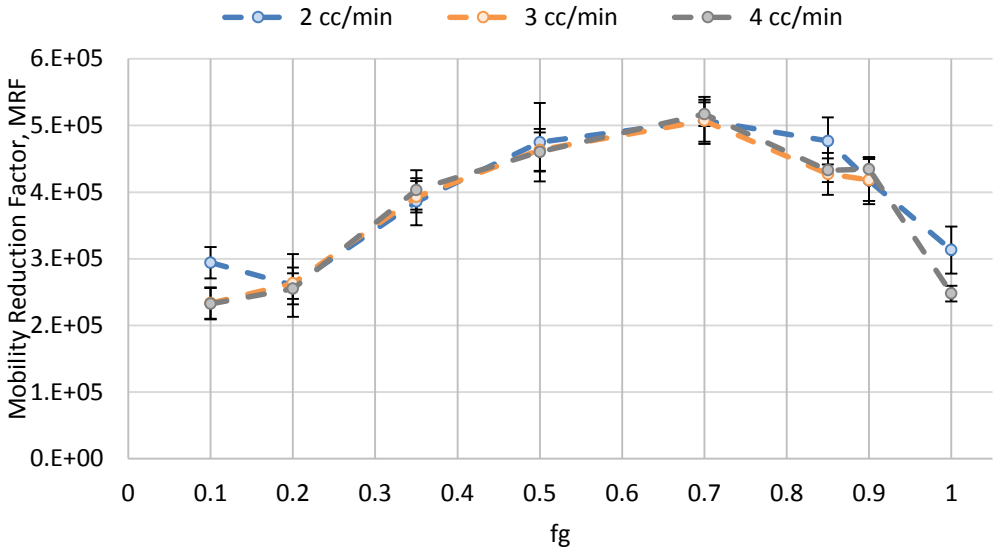

Figure 6-16 Mobility Reduction Factor, MRF, vs. foam quality (f_g) for three total injection rates.

Table 6-8 lists total injection rates, gas fractional flow, apparent viscosities, MRF and average pressure gradients for the baseline (brine/CO_2 injection) and the foam injection (nanofluid/CO_2). The pressure drops and apparent viscosities of the baseline compared with the foam injections achieved an average increase of about 200%, which indicated foam generation.

Table 6-8 Maximum results with associated percentage increase of foam apparent viscosities and pressure gradient for baseline injections(w+g) compared to foam injections(np+g).

Core ID	Q_T [cc/min]	f_g^*	ΔP_{max} [bAR/m]	% increase ΔP_{max}	$\mu_{app,max}$ [Pa s]	MRF_{max} $[10^5]$	% increase	Perm. [mD]
ST3 w+g	2	0.5	0.38	-	3.35	-	-	2252.3
	3	0.5	0.48	-	2.80	-	-	
	4	0.5	0.58	-	2.56	-	-	
ST3 np+g	2	0.7	1.30	169.5	8.63	5.08	157.30	
	3	0.7	1.96	223.9	8.62	5.07	208.18	
	4	0.7	2.66	268.9	8.79	5.17	242.75	

6.3.2 Total Injection Rate Effect

This subchapter investigates the effects of total injection rates on foam generation. CO_2 and nanofluid was co-injected in three sandstone cores for injection rates 1-4 cc/min. The injections were performed with increasing gas fractions. The highest differential pressures were observed for f_g^*=0.70 for all total injection rates. The majority of the foam apparent viscosities were similar comparing the injections in the cores, and were shown independent of injection rates.

Total injection rates have a significant role in the achieved pressure gradient over a core. Co-injections of nanofluid and CO_2 were performed in three sandstone core plugs, until steady differential pressures were achieved. The injections were performed with increasing gas fractions, following the drainage injection curve. The injections started with the lowest rates using 1-4 cc/min in core ST2, 1-2 cc/min in core ST4 and 2-4 cc/min in core ST7. Each rate achieved stable differential pressure for the gas fraction injected, before the gas fraction was increased.

Table 6-9 lists the obtained maximum differential pressures and apparent viscosities, with the corresponding gas fractions and total injection rates. Note the similar values of the maximum apparent viscosities for the injection rates.

Table 6-9 Maximum apparent viscosities and differential pressures from foam injections in core ST2, ST4 and ST7

Core ID	Q_T [cc/min]	f_g^*	max μ_{app} [Pa s]	ΔP_{max} [bar/m]	Perm. [mD]
ST2	1	0.70	3.89	0.38	1608.65
	2		3.41	0.66	
	3		3.33	0.97	
	4		3.35	1.30	
ST4	1		3.48	0.41	2257.6
ST7	2		4.40	0.59	2527.4
	3		3.69	0.75	
	4		3.18	0.86	

Figure 6-17 shows all injection rates in the three samples reached the maximum differential pressure for the same critical gas fraction, f_g^*=0.70. This was with acceptance of rate 4 cc/min in core ST7 where the reason is uncertain. The highest differential pressure was observed for rate 4 cc/min in core ST2. Core ST2 achieved in general higher differential pressures compared to core ST7. This can be explained by the permeability differences between the two cores, where core ST2 and ST7 had permeabilities 1.76 D and 2.53 D, respectively. Injection rate 1 cc/min in core ST4 (dashed, green graph) and 1 cc/min in core ST2 (green, solid graph) were fairly consistent, despite the high permeability differences between the cores. The permeability in core ST4 was 2.26 D. This can possibly be explained by the grain size distribution, which could make the foam generation more effective. The foam mobility is reported to decrease as the pore size increases, resulting in higher differential pressures. This is found regardless of core type and similar permeabilities (Yang and Reed 1989).

The differences in differential pressures could also be caused by adsorption of nanoparticles. The particles clog the pores making a larger resistant for the fluids to flow, thus an increase in differential pressure. The differential pressure did not reach stable state injecting f_g=1.0 with rate 1 and 2 cc/min in core ST2. This was because the CO_2 accumulator was emptied, and the experiment was ended. The obtained pressures are marked as red points in Figure 6-17. All total injection rates showed the behaviour of increasing pressure gradients with increasing gas fractions. This was observed until the foam began to diverge, reaching the higher gas fractions (f_g>0.7).

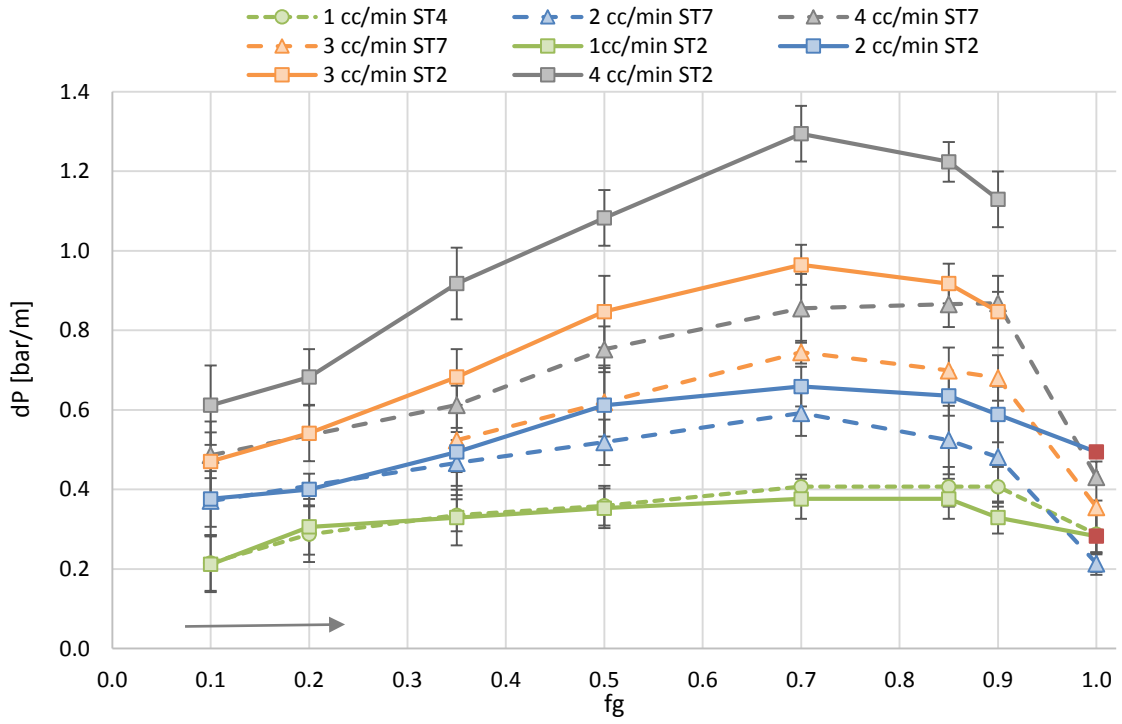

Figure 6-17 Pressure gradient versus gas fraction co-injecting nanofluid and CO_2 in three sandstone cores (ST2, ST4 and ST7). The cores are distinguished from each other by line styles and point geometries. Same colors represent same injection rates. The red points for injection rate 1 and 2 cc/min (f_g=1.0) in core ST2 indicate differential pressures not completely stabilized. The arrow points in the direction the injections were performed (increasing gas fractions).

Figure 6-18 shows the differential pressure for the foam injections conducted in core ST2 and ST7. Each plateau in the graphs represent a total injection rate, indicating achieved steady differential pressures for the corresponding gas fractions. Core ST2 achieved larger pressure differences between the rates for the same gas fraction, compared to core ST7. This can possibly be explained by foam blocking more high permeable channels within the core, forcing the fluids to flow in lower permeable areas where the flow resistant is higher.

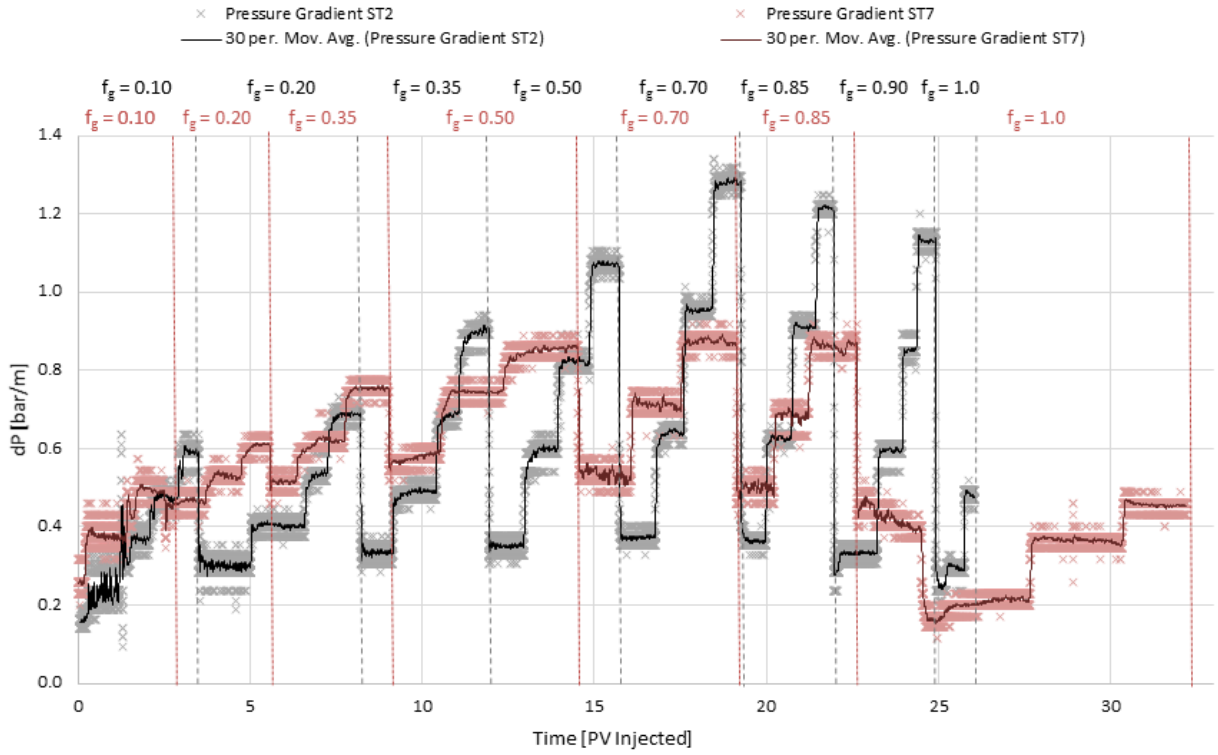

Figure 6-18 Differential pressure gradient vs. pore volume injected for core ST2 and ST7 at temperature 25°C. Pressure steady state was achieved for the injected gas fractions for each total injection rates (with excaptance of the injections with gas fraction 1.0 for core ST2). The largest value was reached for $f_g^* = 0.7$ for total injection rate 4 cc/min in core ST2. Each plateau in the graph represents steady differential pressure for an injection rate.

The apparent viscosity of CO_2 foam is reported to not only be dependent on foam agent, concentration and quality (gas fraction), but also the injection rate and the permeability of the porous media (Lee, Heller et al. 1991). Gas mobility in foam flow processes are shown to be a strong function of rock permeability. The mobility is more reduced and apparent viscosity more viscous in higher permeable formations (Hirasaki 1989). However, the opposite result have also been reported (Bernard, Holm et al. 1980, Hanssen and Dalland 1990, Lee, Heller et al. 1991).

Figure 6-19 shows the apparent viscosities for the injections in core ST2, ST4 and ST7. The viscosities are fairly consistent for all the rates, showing no shear-thinning or shear-thickening effects. This is with acceptance of rate 1 and 2 cc/min in core ST2, where the reason is unknown. Comparing the two injection rates (1 and 2 cc/min), a shear-thickening effect was observed. This effect occurs when the apparent viscosity decreases with lower injection rates, indicating a Newtonian fluid (Kamibayashi 2008). The decrease in apparent viscosity can be explained by the foam generation mechanisms (snap-off, etc.) being less effective at lower rates. The differences in the apparent viscosities could also be

caused by adsorption of the nanoparticles. When the walls inside the cores adsorb the foam agent (nanoparticles), it results in a lower foam agent concentration. This could have an effect on the foam generated, thus the apparent viscosity. However, the majority of the results showed that the foam apparent viscosity were independent of injection rates.

Significant lower apparent viscosities were observed in core ST4, ST2 and ST7 (Figure 6-19), compared to the results in core ST3 (Figure 6-15). This is caused by the differences in differential pressures for the injections. Core ST3 had possibly more gas trapped in the core, after the baseline injection, resulting in higher differential pressures. The saturation within the core gave likely better conditions for generation of a more viscous foam. Correlation of trapped gas saturation and permeabilities have been reported to not have any essential relationship (Keelan and Pugh).

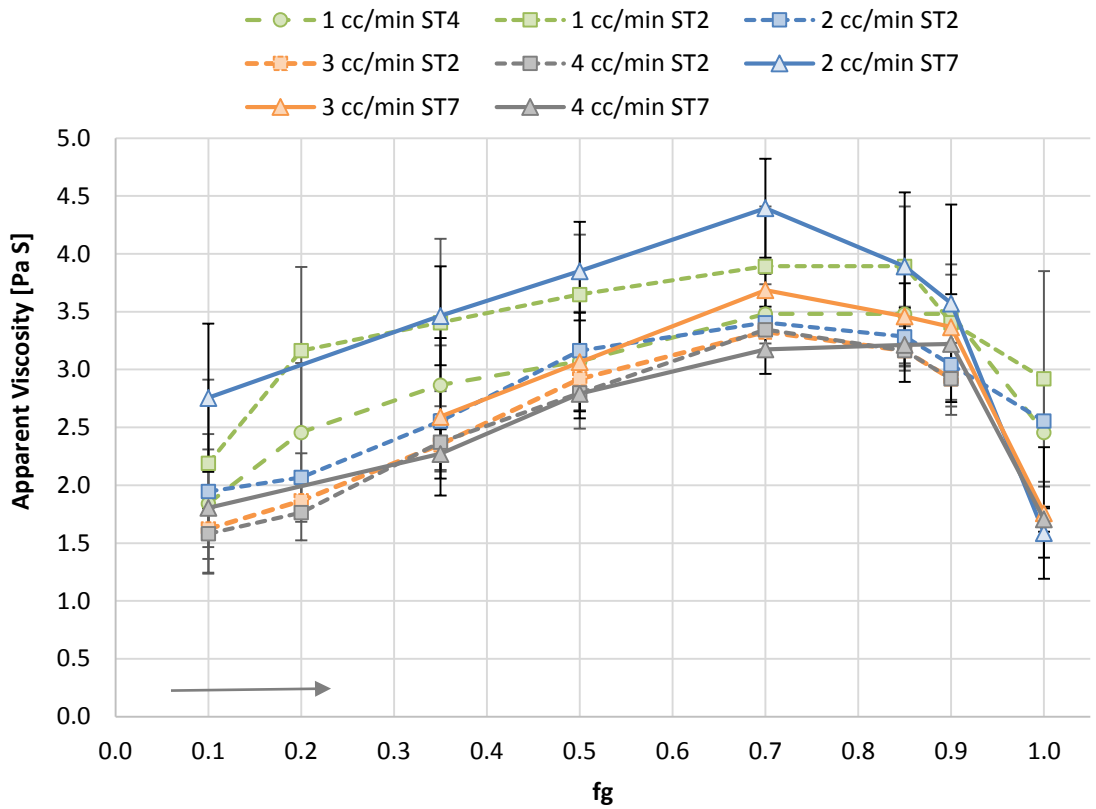

Figure 6-19 Apparent viscosity versus foam quality (gas fraction) for total injection rates in three sandstone cores. Same color represents the same rate, and the cores are distinguish with different point geometries and line styles. The highest foam apparent viscosity was seen for f_g=0.70.

6.3.3 The Effect of Hysteresis

This subchapter considers the hysteresis influence on nanofluid foam generation in sandstone core plugs. In total four cores were used for investigating this effect, where a significant hysteresis were observed for all injections in the cores. In addition, a drainage/imbibition hysteresis were observed, depending on the injections were performed with increasing (drainage curve) or decreasing (imbibition curve) gas fractions. For the injections with increasing gas fractions, the maximums differential pressures and apparent viscosities were observed for f_g^*=0.70, compared to f_g^*=0.35 for the decreasing gas fraction injections. The apparent viscosity behaviour showed independency of injection rates, except when both hysteresis and drainage/imbibition hysteresis were present (core ST7). A shear-thinning effect was then observed.

All experimental data and calculations are listed in Table 6-10. The following will describe injection strategies starting at different core saturations. The injection strategies were performed following the drainage injection curve (increasing gas fractions), or the imbibition injection curve (decreasing gas fractions).

Table 6-10 Critical gas fraction with associated maximum pressure gradient and apparent viscosities for the two injection strategies.

Core ID	Q_T [cc/min]	f_g^*	max μ_{app} [Pa s]	ΔP_{max} [bar/m]	Perm. [mD]	Injection strategy
ST3	2	0.70	8.63	1.30	2252.3	Drainage
	3	0.70	8.62	1.96		
	4	0.70	8.79	2.66		
ST4	1	0.70	3.48	0.41	2257.6	Drainage
	2*	0.35	43.92	10.27		Imbibition
ST5	1	0.35	12.58	1.47	1456.0	Imbibition
	2	0.35	11.75	2.75		
	3	0.35	11.55	4.05		
	4	0.35	11.19	5.23		
ST7	2	0.70	4.40	0.59	2527.4	Drainage
	3	0.70	3.69	0.75		
	4	0.90	3.22	0.87		
	2*	0.20	48.71	6.56		
	4	0.35	41.68	11.22		Imbibition

* The experimental values for the injection did not achieve pressure steady state and is only an approximate value.

Figure 6-20 shows differential pressures for co-injections of nanofluid and CO_2 using rate 1 cc/min with monotonic increasing gas fractions (green, solid curve), and rate 2 cc/min with decreasing gas fractions (blue, solid curve). Core ST2 are plotted for comparison, where the injections were performed with increasing gas fractions using the same rates (1 and 2 cc/min) (dashed curves). A hysteresis effect was observed for injection rate 2 cc/min in core ST4, compared to rate 1 cc/min in the same core and rate 2 cc/min in core ST2. An average of 7.2 PV was injected with rate 2 cc/min to establish stable differential pressures, in comparison to rate 1 cc/min where 2.5 PV was injected. The differential pressures injecting with decreasing gas fractions were more difficult to stabilize, than the injections with increasing gas fractions. The differences in the differential pressures between the two rates are likely caused by hysteresis effects. The hysteresis indicates the core performance is dependent on the history of the saturation change, i.e previous injections conducted in the core (Keelan and Pugh 1975). This effect impacts the foam behaviour. The two injections in core ST4, obtained maximum differential pressures for different foam qualities (gas fractions). For rate 1 cc/min the critical gas fraction, f_g^*, was 0.70. Injecting with rate 2 cc/min stable conditions for the maximum differential pressure was not reached because the accumulator, containing CO_2, was out of gas. The highest differential pressure is shown as a red point in Figure 6-20. The different gas fractions for the maximum differential pressures could be caused by an imbibition/drainage hysteresis. This is investigated and discussed later.

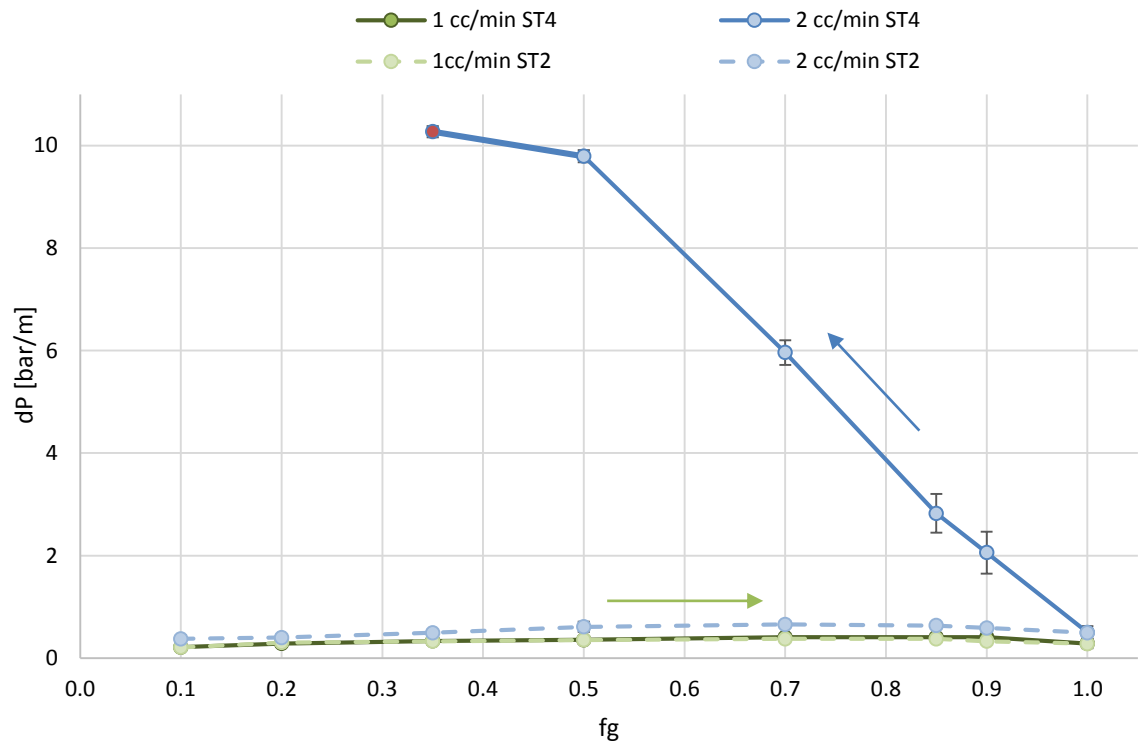

Figure 6-20 Pressure gradient versus foam quality, f_g, for two constant injection rates in sandstone core ST4 (solid lines). The experiment started at gas fraction 0.1 for injection rate 1cc/min (green graph) following the drainage curve (increasing gas fraction). Second injection rate, 2 cc/min, was injected following the imbibition curve (increasing gas fraction). The red point illustrates differential pressure not stabilized. Injections in core ST2 were performed following the drainage curve using the same rates, and is plotted for comparison. The arrows points the way the injections were performed. A large hysteresis effect was observed.

For confirming the hysteresis effect, another experiment was conducted in sandstone core ST7, shown in Figure 6-21. The injection started at the lowest gas quality, f_g=0.1, with the lowest injection rate 2 cc/min, at 100% water saturated core. The injection rate was increased before the gas fraction was increased, following the drainage curve. The maximum differential pressures were reached for the critical gas fraction, f_g^*=0.7, where the highest injection rate (4 cc/min) achieved the highest differential pressure. The injections were performed until f_g=1.0 was reached. Rate 2 and 4 cc/min was then injected with decreasing gas fraction, following the imbibition curve. The hysteresis effect was observed immediately for the first gas fraction (f_g=0.90), injecting with rate 4 cc/min (dashed graph). Rate 2 cc/min was within acceptable errors compared to the previous injection for the same rate and gas fraction. Continuing the injections following the imbibition curve, the hysteresis effect became larger for both rates. The maximum differential pressure for rate 4 cc/min was reached for f_g^*=0.35, and 0.20 for rate 2 cc/min. The different critical gas fractions for the two rates could be explained by stable differential pressure conditions was not completely reached. However, studying the differential pressure gradient versus pore volume injected in Figure B-3 (Appendix B), the pressure seemed to have reached steady state for injection rate 2 cc/min. An explanation might be because injecting at a higher rate flushed the core, starting the coalescence process. The injections following the imbibition curve were observed to be more time consuming for reaching steady differential pressures, compared to the injections following the drainage curve. It was also noticed a larger fluctuation in the differential pressures when injecting with decreasing gas fractions, compared to opposite. This might be caused by the foam generation mechanisms performing more frequently. The differential pressure injecting with rate 4 cc/min and gas fraction 0.20 was not stabilized due to the limiting timeframe of the experiment. The obtained pressure is shown as the red point in Figure 6-21.

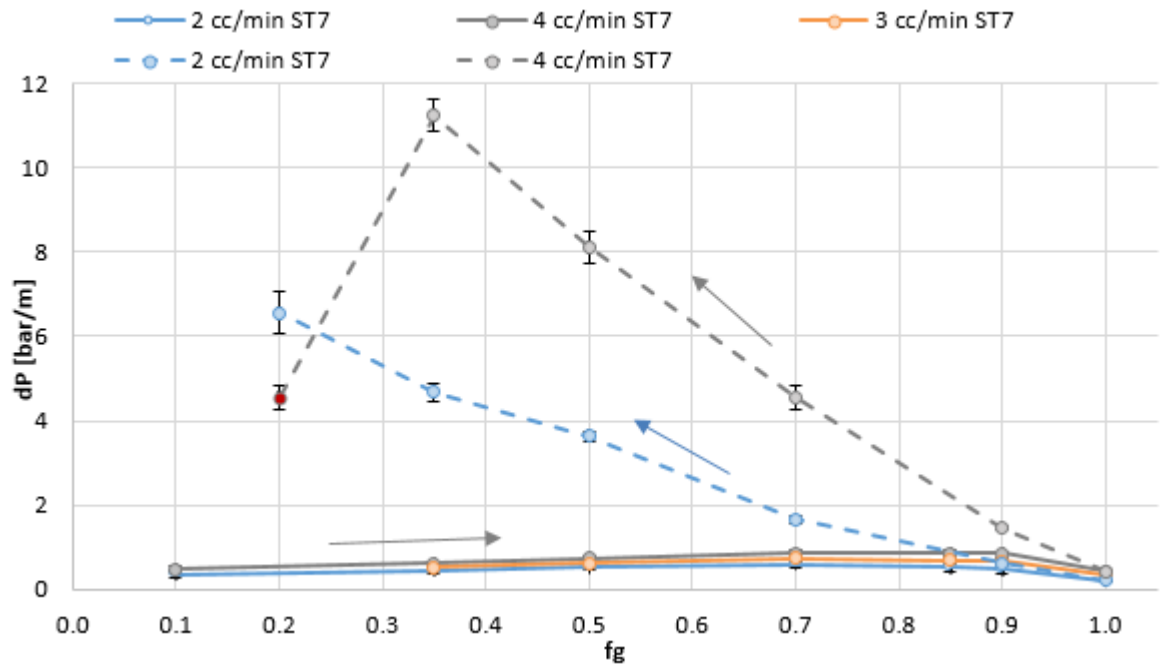

Figure 6-21 Differential pressure versus foam quality, f_g, for co-injecting nanofluid and CO_2 in sandstone core ST7. The injection started with f_g= 0.1 and continued to f_g= 1.0 for three constant total injection rates (solid lines, following the drainage injection curve). The injections were then performed following the imbibition injection curve for f_g=1.0-0.2 for two total injection rates (dashed lines). A large hysterics effect was observed.

Comparison of the hysteresis effects

The hysteresis effects from the injections in core ST4 and ST7 are compared and discussed.

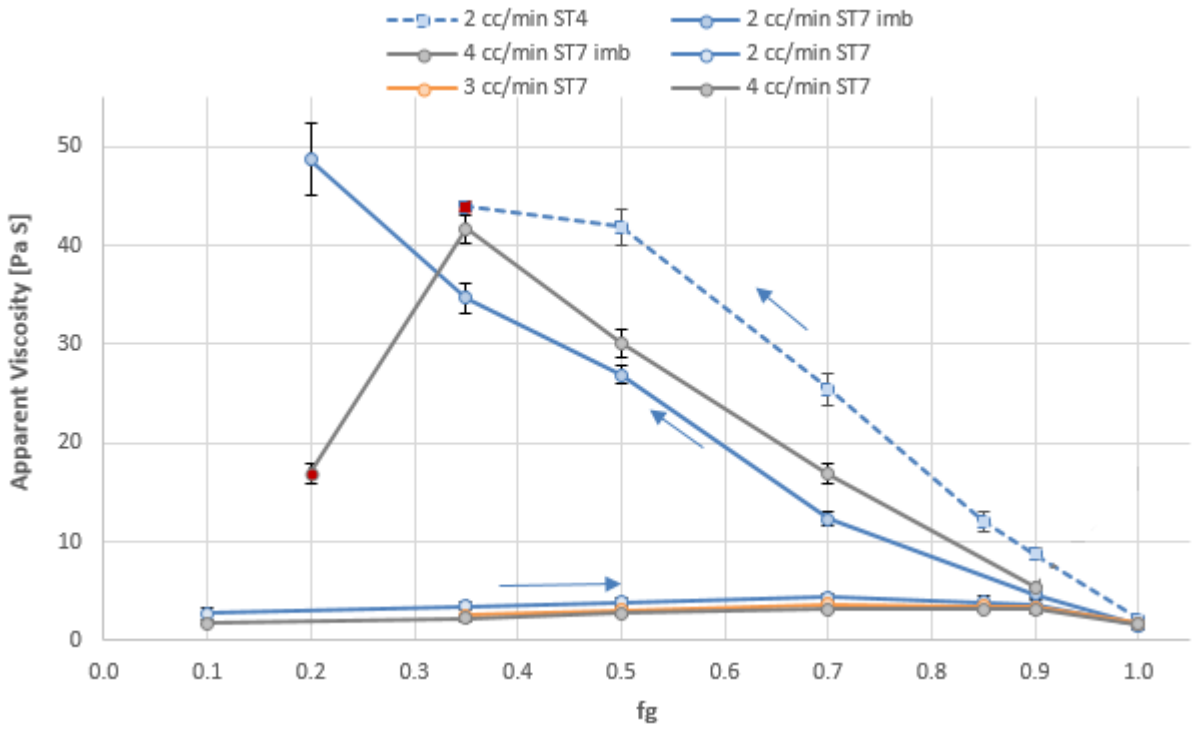

Figure 6-22 Apparent viscosity versus foam quality (f_g) for injections with increasing and decreasing gas fractions in core ST7 (solid graphs). The graphs are compared with the decreasing gas fraction injection in core ST4 (dashed lines). A higher apparent viscosity was observed for the rates injecting with decreasing gas fractions, and different gas fractions were achieved for the maximum apparent viscosities.

Figure 6-22 compares the apparent viscosity for the injections where a large increase in the viscosity were observed for the decreasing gas fraction injections (f_g=1.00-0.20), compared to the increasing gas fraction injections (f_g=0.10-1.00). For the latter case, the maximum apparent viscosity was reached for f_g^*=0.70. Injecting with decreasing gas fractions, the maximum was reached at f_g^*=0.35 (4 cc/min) and 0.20 (2 cc/min) in core ST7. In core ST4, the maximum value for rate 2 cc/min was not stabilized, but the injection showed the same trend as the two other decreasing gas fractions injections in core ST4. Consistency for the rates with increasing gas fractions were observed, and showed independency of injection rates. This was consistent with the previous obtained results in this study, and are possibly caused by the CO_2 and nanofluid generating an emulsion. The apparent viscosity for the injections following the imbibition curve, increased for higher injection rates. This indicated a shear-thickening effect, where the viscosities are dependent on injection rates. The viscosity differences are most likely caused by hysteresis, where the saturation of the core affect the nanofluid and CO_2 foam generation. For the decreasing gas fraction injections, more gas was likely present in the core due to trapped gas. The results indicated that this trapped gas gave larger reduction of CO_2-mobility, i.e larger apparent viscosity. The higher gas saturation in the core could also make more favourable conditions for generating higher viscosity foam. The foam mechanisms could also have performed more efficient. The foam generation is largely due to the snap-off mechanism controlled by capillary pressure in a high permeable porous medium (Falls, Hirasaki et al. 1988). The higher gas saturation might also be the explanation for the higher viscosity in core ST4 (2 cc/min), compared to the injection performed with the same rate in core ST7. The higher viscosity indicated generation of a more viscous foam in core

ST4, even though the permeability of the core was lower than core ST7. The foam mechanisms are reported to perform more frequently in high permeable cores (Hirasaki 1989). The high apparent viscosity obtained for rate 2 cc/min and f_g=0.20 was likely achieved because the coalescence process had not started. For rate 4 cc/min, the coalescence process had started, and the apparent viscosity was decreasing.

Drainage/Imbibition Hysteresis Effect

Hysteresis occur due to the previous injection history of a core. The following experiment investigates the effect of the injection strategy on foam generation, injecting with increasing or decreasing gas fractions. Figure 6-23 compares the results from co-injections of CO_2 and nanofluid in two sandstone cores, ST3 and ST5, following the two injection strategies. The co-injections were performed subsequently a CO_2 injection for both cores. Prior to the CO_2 injection in core ST3, a co-injection of brine and CO_2 were performed with increasing gas fractions. The injections followed with a CO_2 gas injection draining the core. These injections have previously been referred to as a baseline in section 6.3.1. Core ST5 was drained with pure CO_2 injected.

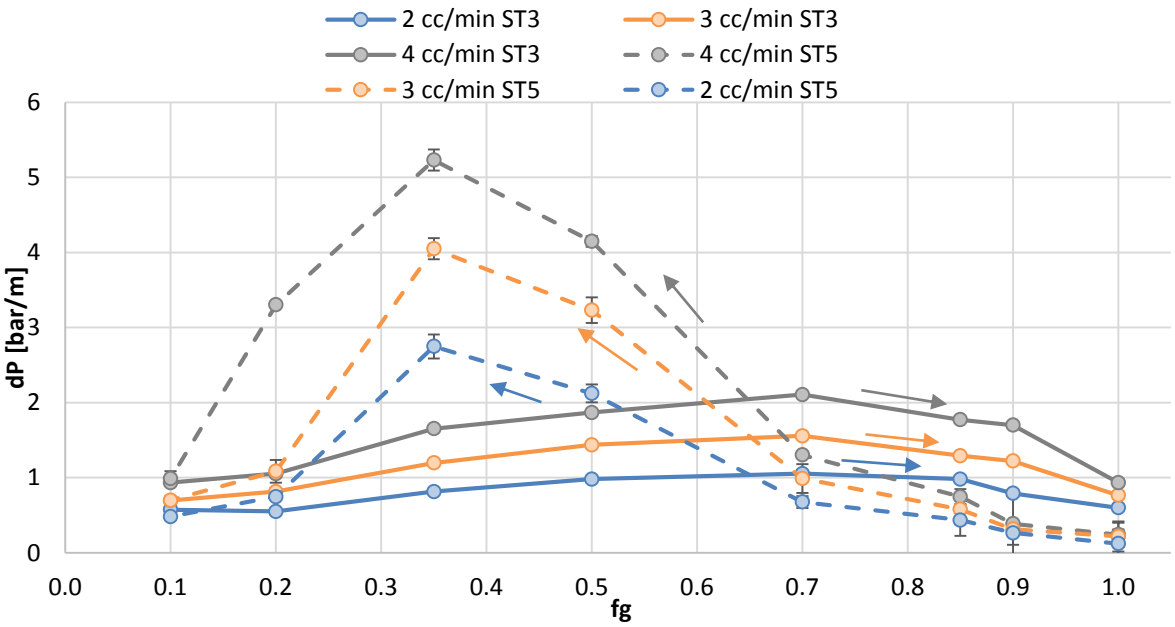

Figure 6-23 Differential pressure versus foam quality (f_g) for co-injection of CO_2 and nanofluid in sandstone core ST3 and ST5, subsequently a CO_2-injection. Foam injection in ST3 (solid lines) was started at gas quality 0.1, increasing gas fractions while the injections in core ST5 (dashed lines) started at gas quality 1.0 with decreasing gas fractions.

After the gas drainage in core ST3 and ST5, CO_2 and nanofluid were co-injected for three injection rates (2-4 cc/min). The co-injections in core ST3 were performed with increasing gas fraction (drainage injection curve), where the maximum differential pressures were reached for the critical gas fraction, f_g^*=0.7. The co-injections in core ST5 were performed with decreasing gas fractions (imbibition injection curve), and reached maximum differential pressures for f_g^*=0.35. The results show that the obtained critical gas fractions are most likely not only caused by hysteresis effects, but also the gas fraction injection strategy. Comparing the two injection strategies, a drainage/imbibition hysteresis was observed. This was the same result as reported by Sanchez (1986) (Sanchez, Schechter et al. 1986). The permeability of core ST3 was 2.25 D, and 1.46 D in core ST5. This could explain the differences in the obtained maximum differential pressures, but not the different gas fractions.

Figure 6-24 shows the apparent viscosity for the injections with increasing and decreasing gas fractions. The two injection strategies obtained different gas fractions for the maximum apparent viscosity, f_g^*=0.70 (increasing f_g) and f_g^*=0.35 (decreasing f_g). The injections with decreasing gas fractions resulted in higher apparent viscosity, compared to the increasing gas fraction injections. The decreasing gas fraction strategy also obtained the lowest apparent viscosity for high liquid (f_g=0.1-0.2) and gas fractions (f_g=0.7-0.9). A more rapid viscosity variation was also observed for 0.20<f_g<0.70, compared to the increasing gas fraction injection where the viscosity differences between the gas fractions were smaller. The differences are possible caused by the different foam behaviour due to the drainage/imbibition hysteresis. One important observation was the apparent viscosities were similar for all rates injected with the same strategy, thus the viscosity were independent of rates. It should be noted the higher viscosity when injecting with a decreasing gas fraction. These higher values are likely caused by trapped gas in the formation, resulting in a greater performance of the foam generation or better foam generation sites.

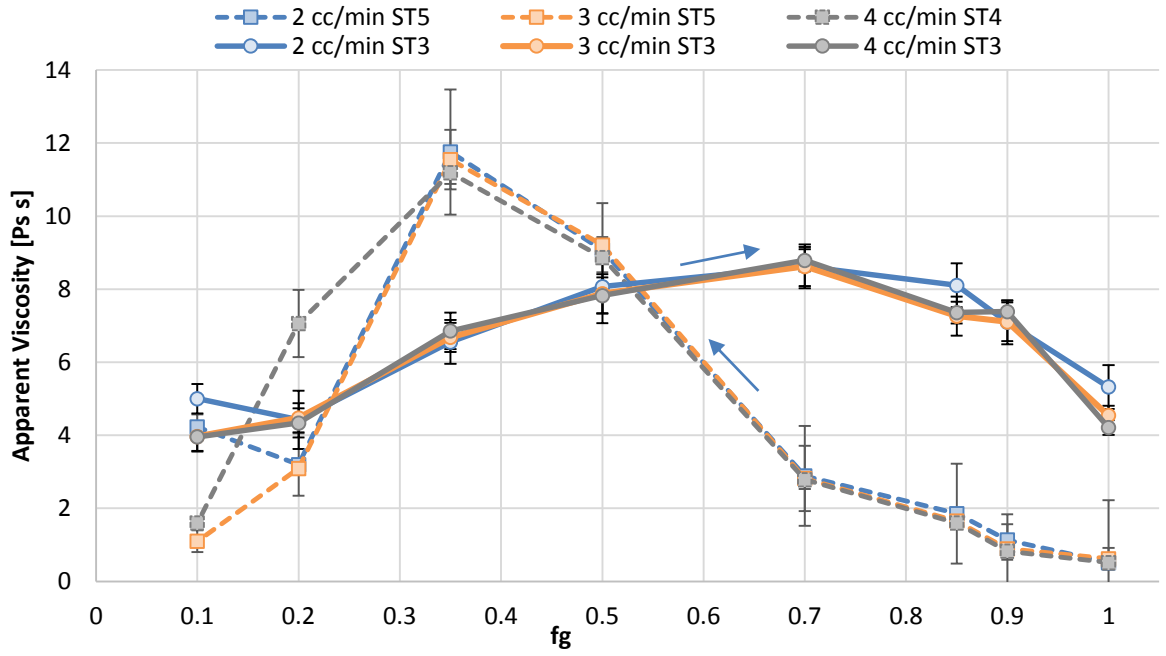

Figure 6-24 Apparent viscosity versus gas fraction for three injection rates in core ST3 (solid graphs) injecting with increasing gas fraction, and ST5 (dashed graphs), injecting with decreasing gas fraction. The maximum apparent viscosities are reach for two different gas fractions, f_g=0.70 and f_g=0.35.

Hysteresis effects have been observed by some researchers (Sanchez, Schechter et al. 1986) and not by others (Persoff, Radke et al. 1991). Other researches have reported both outcomes. Yaghoobi, H. et al. (1994) reported that the main factor effecting hysteresis was the type of foam agent used in the experiments (Yaghoobi 1994). An apparent drainage/imbibition hysteresis was seen which is consistent with previous observations by (Sanchez, Schechter et al. 1986). Sanchez *et.al* recommended for future steady differential pressure experiments to start injection of foam in the imbibition end, at foam quality 1.0, injecting with a decreasing gas fraction. This should ensure rapid and complete steady state pressure. However, injection performed with an increasing gas fraction ensured more rapid and accurate steady differential pressures for the experiments conducted in this study. These differences in results might be caused by the different foam agents.

6.3.4 The Effect of Gas Fraction Injection Sequence

One of the objectives in this subchapter was to investigate the residual water saturation in a sandstone core, after gas flooding was conducted. This was performed because fluid saturation within a core likely impacts the foam generation. The other objective was to investigate the effects on foam generation, co-injecting CO_2 and nanofluid with varied gas fraction sequences. This injection strategy was different from previous injections performed with either increasing gas fraction or decreasing gas fractions. The gas fractions were systematically varied in the following order, f_g= 0.10, 0.70, 0.20, 0.85, 0.50, 90. The obtained apparent viscosities showed fairly consistency compared with decreasing gas fractions injections. However, deviations were seen for the higher gas fractions (f_g>0.70).

A 100% gas injection was performed in sandstone core ST5. 7.8 PV CO_2 was injected distributed on four total injection rates (1-4 cc/min). The injections were performed with decreasing rates. All cores used in this thesis were assumed initially to be 100% saturated with brine. Using material balance on core ST5, the residual water saturation after the gas flooding was 0.54. This value would decrease for foam injection where the differential pressure is increased. Water saturation in sandstone cores have been reported to 0.30 with foam injection. The lowest liquid saturation was observed where the pressure gradient had its maximum (Persoff, Radke et al. 1991).

Figure 6-25 shows the calculated foam apparent viscosity for co-injections of nanofluid and CO_2, subsequently the gas injection, for four total injection rates (1-4 cc/min) (solid graphs). The injections were performed with decreasing injection rates and gas fractions. Each rate achieved steady differential pressure for the injected gas fraction, before the gas fraction was decreased. The maximum apparent viscosity was observed for the critical gas fraction, f_g^*= 0.35. Further, these injections were used for comparing the results obtained injecting with the varying gas fraction injection strategy.

After the co-injection of nanofluid and CO_2, a varying gas fraction injection strategy was performed for two injection rates (1 and 2 cc/min). The gas fractions were systematically varied in the following order, f_g= 0.10, 0.70, 0.20, 0.85, 0.50, 90. This strategy was different from previous performed injections injecting with increasing gas fractions or decreasing gas fractions. The calculated apparent viscosity for the injections are shown in Figure 6-25 as single points. Comparing the viscosity using the varying gas fraction injection strategy, with the injections performed with decreasing gas fractions were consistent for f_g=0.5 and 0.7 for both rates (1 and 2 cc/min). The other gas fractions (f_g=0.20, 0.85 and 0.90) showed higher apparent viscosities for the varying gas fraction injections. These results might be caused by hysteresis. The higher viscosity could also be explained by more gas trapped in the core, which likely changed the core saturation making it more suitable for a higher viscosity foam to be generated. Another explanation might be that the foam coalescence process did not have enough time to break down the foam, resulting in a higher differential pressure, thus larger foam viscosities. The trend show that the foam apparent viscosity was independent of injection rate, thus no shear-thinning or shear-thickening effects were observed. The absent of these effects might be explained by nanofluid and CO_2 generated an emulsion, not a foam.

The differential pressure versus pore volume injected is shown in Figure B-2, found in Appendix-B. The stable differential pressures were achieved for less pore volumes injected using the varying gas fraction injection strategy, compared with the decreasing gas fraction injections. This could be caused by hysteresis effects, based on that the same gas fractions had previous been injected in the core.

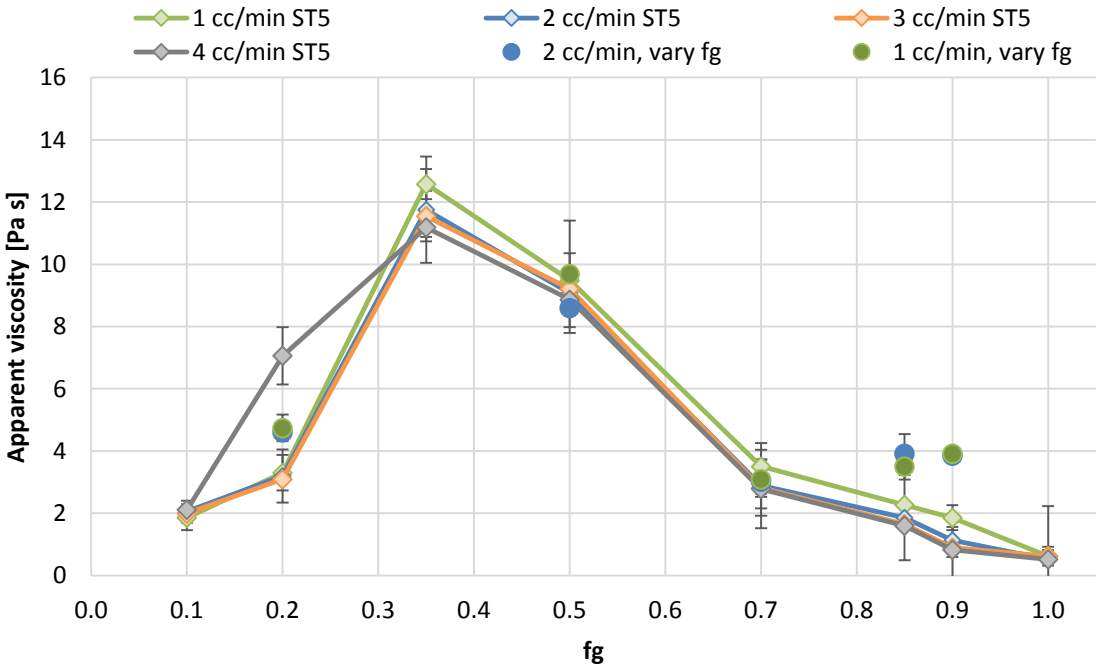

Figure 6-25 Apparent viscosity versus gas fraction for two injection strategies – injection following the imbibition curve (solid graphs) and injection with varying gas fraction (single points). The highest apparent viscosity was achieved for fg=0.35, for all injection rates.

6.3.5 Foam Generated in Carbonates

Carbonate reservoirs are often characterized as heterogeneous with large permeability differences dominating the fluid flow (Hirasaki, Miller et al. 2011). In this subchapter nanofluid are co-injected with CO_2 for foam generation in carbonate core plug with increasing gas fraction injections. An increase in differential pressures and apparent viscosity were observed for the co-injections, until f_g=0.35 was reach. Then, the generated foam started to diverge. A consistency was observed comparing the apparent viscosity with the results obtained in a sandstone core where co-injections with decreasing gas fractions were performed.

For investigating the performance of nanofluid foam generation in carbonates, co-injections of nanofluid and CO_2 were performed in 1”5 diameter core plug. The limestone core length was 7 cm. For achieving the approximate same length as the sandstone cores used in the previous experiments (30 cm), the cores were stacked as shown in Figure 6-26. The core was placed horizontally in the core holder, thus vertical fractures occurred as a result of the stacking of the cores. The average permeabilities of the cores, 27.8 mD, were used for calculations.

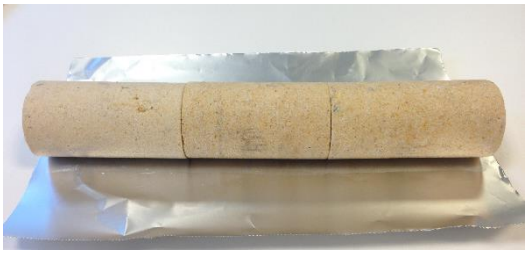

Figure 6-26 Preparation and stacking of limestone cores. Three cores were stacked after each other to achieve approximate same conditions as the previous experiments conducted in sandstone cores.

Co-injection of nanofluid and CO_2 using three injection rates (4, 2, 1 cc/min) was conducted with gas fractions, f_g=0.1-1.0. The injections were performed with increasing gas fractions, following the drainage injection curve. The rates were injected in a decreasing order (4, 2, 1 cc/min). Each rate achieved stable differential pressure for the injected gas fraction, before the gas fraction was increased. Figure 6-27 shows the differential pressures obtained for the rates and gas fractions. For rate 4 cc/min the injection was stopped at f_g=0.35 due to the safety pressure of the injecting QX-pump. The inlet pressure became so high that it almost reached the maximum pressure value the pump could handle, and the injection was stopped. The achieved, not stabilized, pressure is shown as a red point in Figure 6-27. Total injection rate 1 cc/min was introduced instead. The increase in differential pressure gradients indicated generation of foam, reaching a maximum differential pressure for f_g^*= 0.35 (2 cc/min). It is observed higher differential pressure over the limestone core compared to the injections conducted in sandstone core ST7 and ST2 (Figure 6-17). This can be explained by the hundred times larger permeability in the sandstone compared to the limestone cores. The pressure differences might also be explained by nanoparticles blocking the pore throats, resulting in a lager flow resistance through the core. The differential pressure versus pore volume injected is shown in Figure B-15 in Appendix – B.

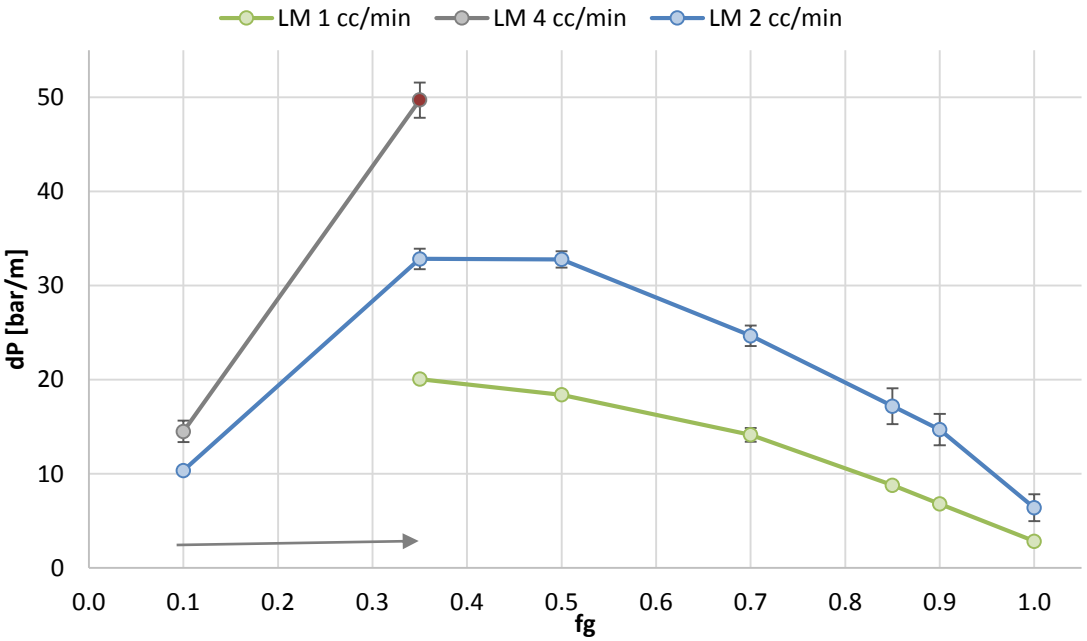

Figure 6-27 Differential pressure versus foam quality for co-injection of nanofluid and CO_2 for three total injection rates in limestone core. The red point for injection rate of 4 cc/min is not stabilized due to maximum pressure limit of the injection pump. A maximum value was seen for f_g=0.35.

Figure 6-28 shows foam apparent viscosity in limestone core, compared to foam generated under same conditions in two sandstone cores (Core ST2 and ST7). All injections where performed with increasing gas fractions. It is noted the maximum apparent viscosity for the injections in the limestone core was achieved for f_g=0.35, and f_g=0.70 for the sandstone cores. When the injections in the limestone continued with gas fractions above 0.35, the apparent viscosity decayed observed as a drop in the differential pressures. The foam started to coalescence and became more mobile. The difference in gas fractions for the maximum viscosity obtained in the cores is most likely due to the nanofluid foam generation behaving differently in other core materials. This might be due to the nanoparticles interaction with the pore walls. Foam is reported to performing better in high porous medium where the foam mechanisms (snap off, lamella division and leave behind) are more efficient. This could also be the reason why the apparent viscosity is higher in the high permeable sandstones (>1500 mD), compared to the low permeable limestone (27.8 mD) (Hirasaki 1989). The limestone core had vertical fractures as a result of the core stacking. The foam generation sites were likely not present in these fractures, which would make the foam generation less effective.

The generated foam seemed to appear with a shear-thinning effect. The increase in apparent viscosity with decreasing rates can be explained with gas bubble coalescence time decreases as the rate increases. This makes the thin films between the bubbles live shorter. Coalescence of bubbles results in less reduction of CO_2 mobility, and a decrease in the apparent viscosity. The snap-off mechanism can be more efficient at higher rates, but cannot offset the effect of bubble coalescence rate. For lower rates, the snap-off mechanism is less effective. However, the effect of snap-off is greater than the effect of coalescence (Yang and Reed 1989). For the gas fractions in the high quality regime (f_g>0.70), the viscosities were fairly similar which might be due to the high amount of gas flowing through the core with little resistance.

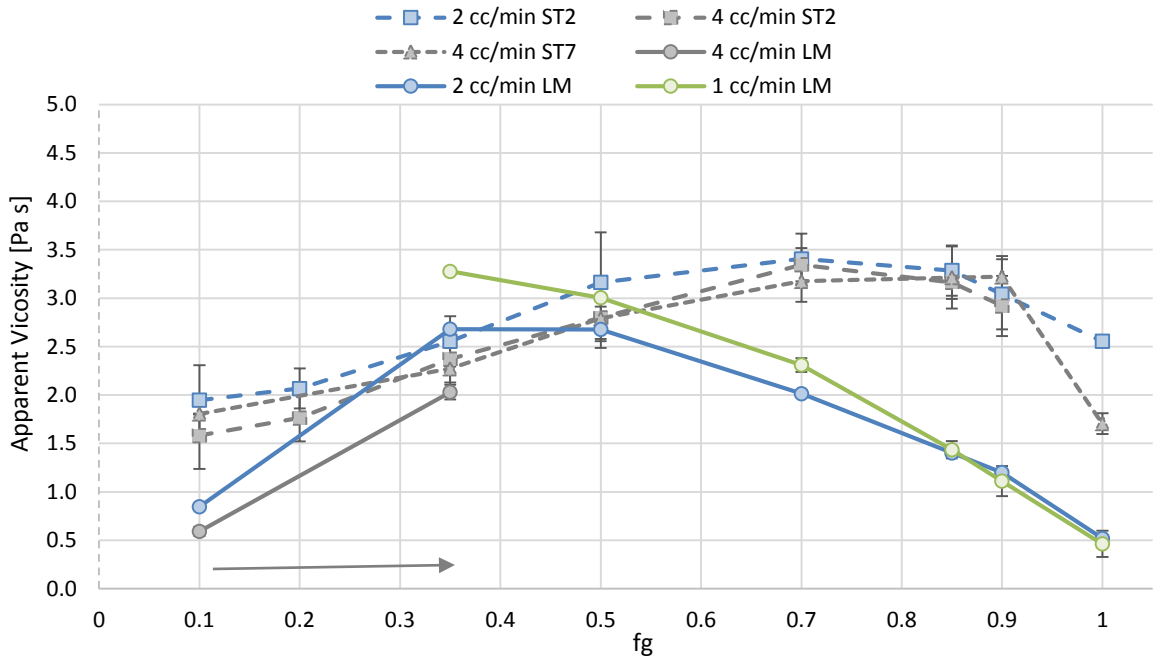

Figure 6-28 Apparent viscosity versus foam quality for experiments conducted in carbonate core (core LM, solid lines) and sandstone core (core ST2 and ST5, dashed lines). Injections started at 100% water saturated core with increasing gas fractions. The same colors represents the same injection rate.

Figure 6-29 shows nanofluid injections in the limestone core (solid graphs) with increasing gas fractions, compared to injections with decreasing gas fractions in sandstone core ST5 (dashed graphs). All the injections obtained maximum apparent viscosity for f_g^*=0.35. The gas fraction reaching the maximum values was consistent with results reported by (Roebroeks, Eftekhari et al. 2015). Roebroeks also reported the nanofluid might not perform as well in carbonates. Experiments conducted in a carbonate (K=0.1 D) revealed very small pore geometries which prevented the nanoparticles from propagating into the core sample. The nanoparticles were significantly filtrated by the core (Roebroeks, Eftekhari et al. 2015). When the nanoparticles are filtrated, they are not present in the liquid phase making them unable to generate foam. This could explain the lower apparent viscosity values for the limestone injections compared to the sandstone injections. These values are shown on secondary y-axis in Figure 6-29. The trend comparing the injections in the two cores are consistent, but the apparent viscosity in the sandstone showed a more rapid increase and decrease when the injected gas fractions changed for $0.20<f_g<0.70$.

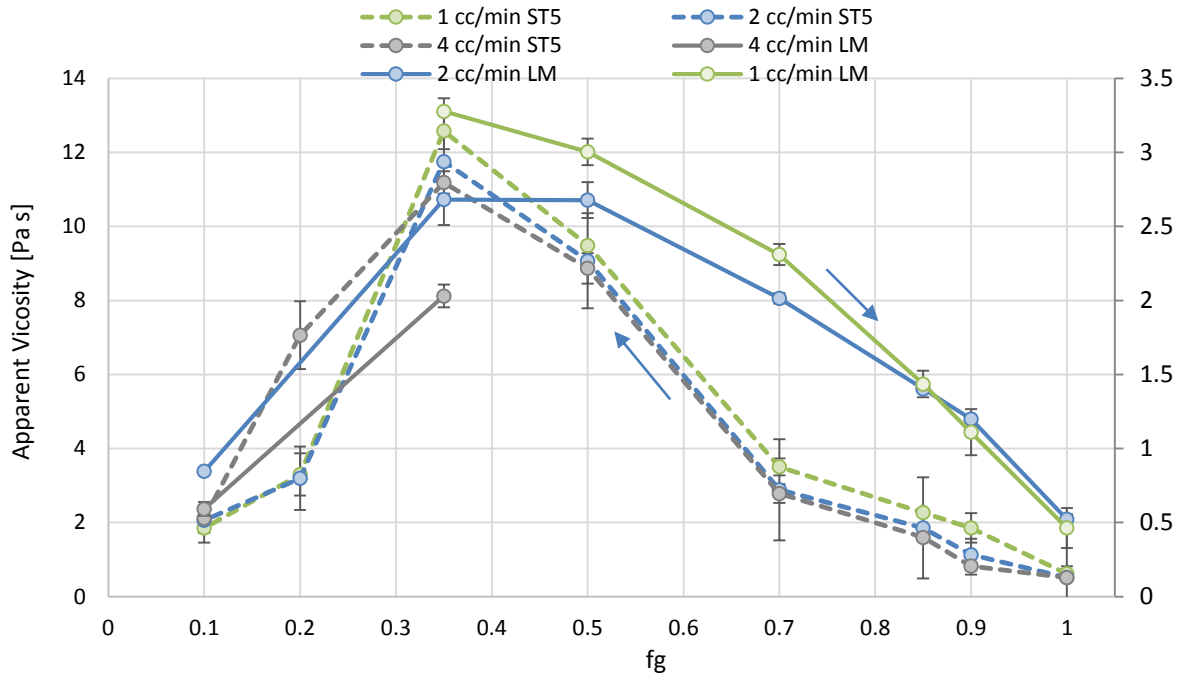

Figure 6-29 apparent viscosity versus foam quality for co-injection of nanofluid and CO_2 in limestone core (solid lines) and sandstone core (dashed lines). The experiment conducted in sandstone core was started after f_g=1.0 injecting with decreasing foam quality while the experiment in the limestone core was started at f_g=0.1 with increasing foam quality.

6.3.6 Surfactant Generated Foam in Sandstone Core

This subchapter presents co-injection of AOS surfactant and CO_2 in sandstone core. The objective of the injections was to investigate the performance of foam generated with surfactant as foam stabilizers, compared to nanofluid stabilized foam in the same core material. The results showed the maximum differential pressures and apparent viscosity were found for gas fraction 0.90. The foam showed a shear-thinning effect, where the apparently viscosities increased with higher injection rates. No clear hysteresis were observed compared to the nanofluid stabilized foam where this effect was seen clearly.

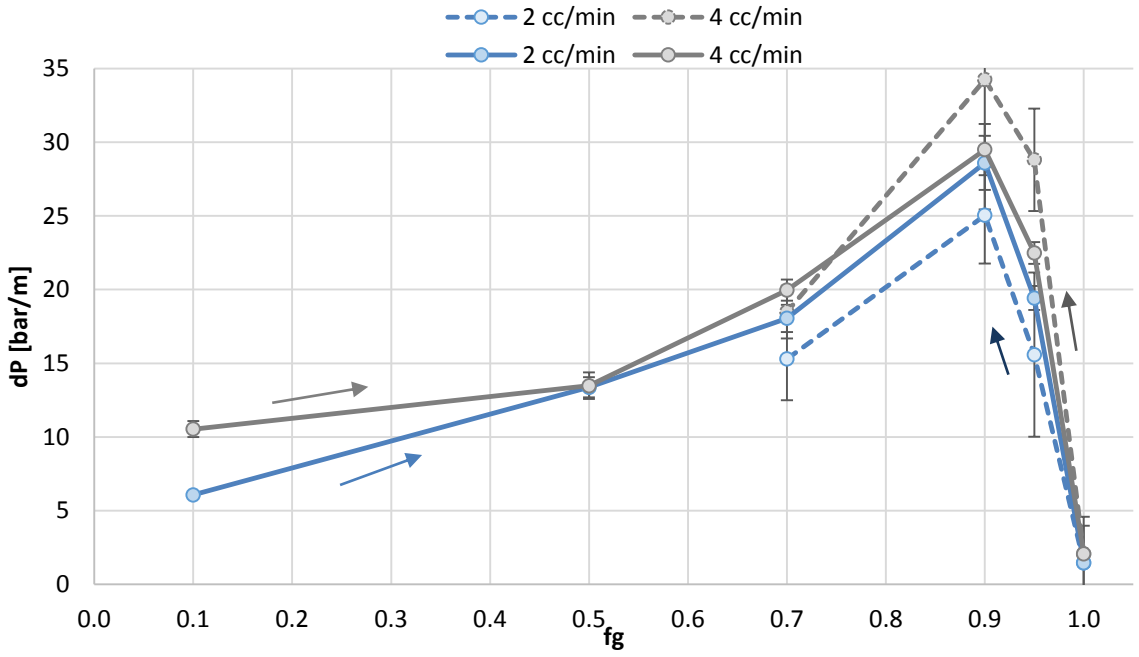

Figure 6-30 Pressure gradient versus foam quality (f_g) for co-injection of surfactants and CO_2 in sandstone core for two total injection rates. The solid lines represents injection with increasing foam quality starting at f_g=0.1. Dashed lines represent injections with decreasing foam quality starting with f_g=1.0. The highest differential pressure was observed for f_g=0.90.

Figure 6-30 shows the achieved differential pressure gradients for injections with increasing gas fractions (solid lines) and decreasing fractions (dashed lines) using rate 2 and 4 cc/min. The injection started at 100% water saturated core, and was performed following the drainage curve (increasing gas fraction). Increasing pressure gradients with increasing gas fractions were observed for both rates (2 and 4 cc/min). This increase continued until the critical gas fraction, f_g^*, was reached for 0.9, and a sudden pressure drop occurred. The foam bubble shape has been reported changing from round to polyhedral with gas fraction 0.9. This change of shape makes it harder to mobilize the foam bubbles, resulting in an increase in differential pressure. From previous work, smaller bubbles have resulted in larger pressure gradients and flow resistance (Ettinger and Radke 1992) This might be similar for this surfactant foam injection. After reaching f_g^*, a sudden decrease in pressure drop was observed. The foam became dry and started coalescence. This behaviour corresponded to work reported on foam mobility in fractured systems (Pancharoen, Fernø et al. 2012, Ferno, Gauteplass et al. 2014). The decreasing pressure was more rapid and steeper than the foam injections using nanofluid as foam agents (Figure 6-17). For the injections, the differential pressures stabilized faster at smaller foam qualities (f_g<0.7) compared with higher foam qualities (f_g>0.7).

After the co-injection of surfactant and CO_2 was injected with increasing gas fraction, the injections were performed with decreasing gas fraction. Both injection strategies resulted in the same gas fraction for the maximum differential pressure for both rates. The drainage/imbibition hysteresis effect was not observed. This was in contrast to the injections performed using nanofluid as foam agent. For these injections, the maximum differential pressures were reach for different gas fractions depending on the injection strategy (increasing or decreasing gas fraction), and previous injections in the core (hysterises). However, it was observed that the differential pressures did not reach the same value for the two injection strategies. This could be caused by the differential pressures not reaching steady state completely. Another explanation might be that small hysteresis caused the differences in the differential pressures. However, a consistency between the results were not observed. The pressures from the decreasing gas fraction injections were both higher (4 cc/min) and lower (2 cc/min) then the pressures from the increasing gas fraction injections.

Stabilizing the differential pressures using surfactants as foam agent was time consuming and difficult because the pressures had large fluctuation. These fluctuations were observed to be larger compared to the injections using nanofluid as foam agent. The large fluctuations might be explained by surfactants entering and leaving the interface between the gas and liquid continuously for stabilizing the foam bubbles. This behaviour is different from nanoparticles, where the particles are constantly placed at the interface. It is well known that foam propagation in porous media is a process of breaking and reforming the lamellae (Mo, Yu et al. 2012). Apaydin and Kovscek (2000) reported that the end effect was similar to classic capillary end effect for low surfactant concentrations. For larger concentrations, another end effect was observed building from the outlet towards the inlet, against the flow direction (Apaydin and Kovscek 2000). Many pore volumes injected was necessary to achieve pressure steady state for the co-injections of surfactant and CO_2, and this was likely attributed by such end effects. The surfactant generated foam gave higher differential pressures than for the nanofluid, which can indicate the foam generating mechanisms likely was different and more efficient. The efficiency of foam generation might also explain the large fluctuations. The obtained results using surfactant as foam agent was in agreement with Sanchez (1986); pressure steady state was easier reached injecting with decreasing gas fraction, than injecting with increasing gas fraction (Sanchez, Schechter et al. 1986). This was also reported by (Yaghoobi 1994).

Figure 6-31 shows the foam apparent viscosity for the injections using surfactants as stabilizers, compared with the injections using nanofluid as stabilizers. The notations NP and surf represents nanoparticles and surfactants, respectively. The maximum apparent viscosity of the surfactant generated foam was significantly higher compared to the nanofluid stabilized foam. This higher value was observed for the injections with both increasing and decreasing gas fractions. For injection rate 2 cc/min the surfactant foam achieved a 41 times larger maximum viscosity, than the nanofluid generated foam. This indicated that the surfactants generated a more viscous foam, resulting in a larger reduction of the CO_2 mobility. The behaviour of the foams was also different injecting with decreasing gas fraction, subsequently an increasing gas fraction injection. The nanofluid reached the largest apparent viscosity for a different gas fraction (f_g=0.35), while it remained the same for the surfactant injection (f_g=0.90), indicating no imbibition/drainage hysteresis. The apparent viscosity of the surfactant generated foam showed clearly a shear-thinning effect where the viscosity increased as the rate decreased. This was a deviation compared to the nanofluid stabilized foam where the majority of the experiments showed independency of injection rate. A few results showed a shear-thickening effect.

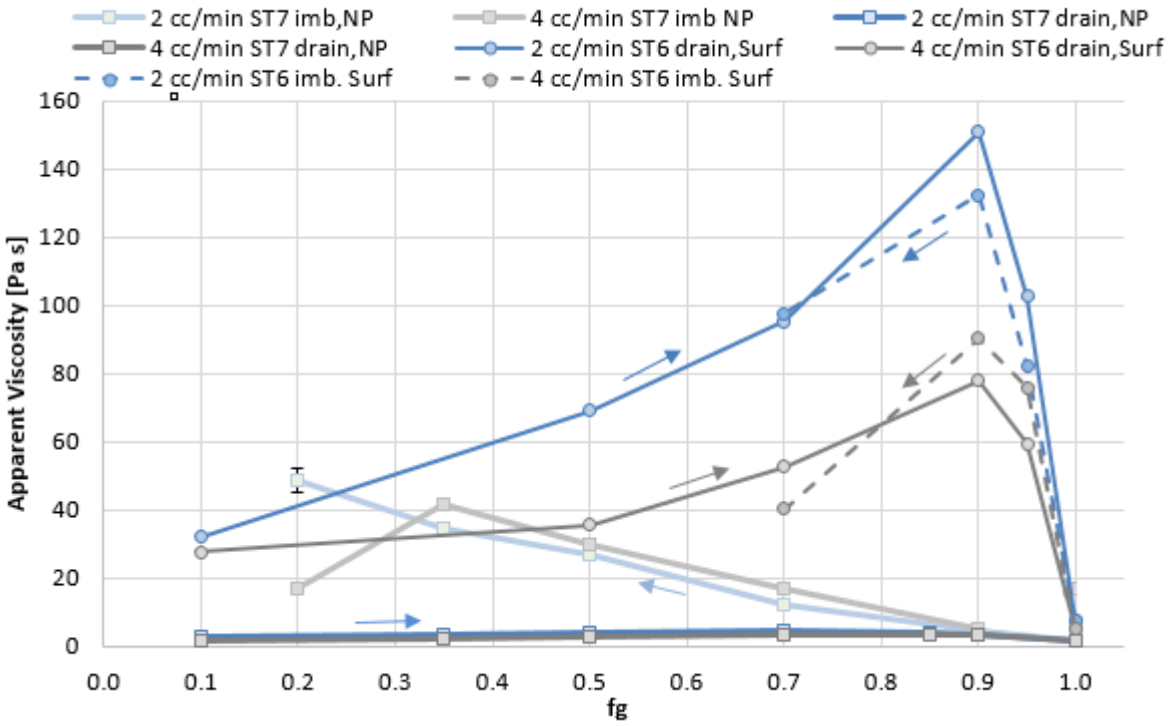

Figure 6-31 Apparent viscosity versus foam quality for co-injection of surfactant and CO_2. Dashed lines represents injection with decreasing gas fraction, following the imbibition injection curve. The solid lines represents injection with increasing foam quality, following the drainage injection curve. The injections were compared to nanoparticle co-injection in sandstone core ST7. The arrows point in the injected gas fraction direction.

6.3.7 Adsorption of Foam Agents

The adsorption of nanoparticles to the core surfaces are briefly discussed in this subchapter. Physiochemical attraction between particles and pore walls may lead to significant retention and adsorption of a foam agent (Nowack and Bucheli 2007). The adsorption capacities depends on concentration, flow rates, clay content, type of porous media, foam agent and coating of nanoparticles. The cores used in this experimental work were not flushed with the foam agent solution prior to the foam injections. This should have been done to ensure the adsorption of the foam agent to the rock surfaces did not affect the results. Based on this, the experimental results might contain an error caused by adsorption that could have been mitigated.

Table 6-11 lists the permeability of the cores used in the experiments before and after the experiments were conducted. All the cores showed a decrease in permeability. Core LM11 had a larger permeability decrease (25%), then core LM14 (19%). For the sandstone cores, core ST4-ST7 achieved approximate the same percentage decrease of 28-32%, regardless of foam agent injected (surfactant or nanofluid). Core ST5 achieved a lower percentage change (16%). The injected nanofluid for foam generation did not have calcium carbonate added to the water. This caused a corrosive effect on the limestone cores during co-injection of brine and CO_2. This effect was visually observed as small holes in core LM10. The permeability measured for core LM10 was not taken into consideration, since the core was damaged from the experiment. The limestone cores (LM10, LM11, LM14) were stacked after each other, placing core LM10 at the inlet and core LM14 at the outlet. This explains why core LM10 was most damaged by the injected fluids. The permeability reductions could be caused by adsorption of nanoparticles to the core wall. These adsorptions are reported to not be permanent. The foam agents are possible to remove by passage of several pore volume of water (Bernard, Holm et al. 1980). Zhang *et.al* performed experiments showing both reversible and irreversible adsorption of nanoparticles occurring during transport through a water saturated porous media (Zhang, Murphy et al. 2014). The irreversible adsorbed nanoparticles are reported to increase with smaller flow rate, less clay and larger injection concentrations (Zhang, Murphy et al. 2014).

The decreased permeabilities might be caused by foam agent adsorption, or by gas trapped in the pores. The cores have likely contained trapped gas after the foam injections, resulting in a higher flow resistance of the injected brine when the permeabilities were measured. The relative permeability is naturally lower than the effective permeability due to larger flow resistance in a two phase system (brine and gas). Since the cores most likely contained trapped gas after the injections of foam, the measured permeabilities were relative permeabilities. The gas was tried displaced by injecting 5 PV of water at 90 bar pressure condition, before the permeability measurements were conducted in atmospheric pressure. However, the measured permeabilities might indicate gas was still in the cores. After the foam injections in core ST2 and ST3, the cores were dried and re-saturated with brine. The permeability was measured, and both cores had significant lower change in percentage, compared to core ST4-ST7. This indicated less adsorption of the nanoparticles to the rock wall and that the permeabilities of the other cores (core ST4-ST7) were measured with large amount of gas present. However, the adsorption of the nanoparticles to a porous medium needs further investigation.

Table 6-11 Permeability measurements of sandstone and limestone cores

Core ID	Initial effective perm. [mD]	Relative perm. [mD]	% decrease	
ST2***	1608.65	1514.35	5.86	Nanoparticle
ST3***	2252.25	2079.29	7.67	
ST4	2257.6	1623.3	28.10	
ST5*	2067.7	1722.8	16.67	
ST6	1798.2	1244.5	30.79	Surfactant
ST7	2527.4	1713.5	32.21	
LM10	22.45	20.59**	8.32	Nanoparticle
LM11	30.29	22.51	25.67	
LM14	30.70	24.75	19.40	

*The differential pressure was measured with ESI pressure transducer, pressure range 0-40 bar.

** After the experiment, the first limestone in the core stack was dissolved due to injection of brine and CO_2 without calcium carbonate present. The permeability measured after the experiment is not representative.

***The cores were dried after the experiments and re-saturated with brine before the permeabilities after the experiments were measured.

Table 6-12 lists all the maximum values for the experiments, the injection strategy and the foam agent used. The listed differential pressure gradient is the average pressure between minimum and maximum value within a single fluctuation.

Table 6-12 Maximum apparent viscosity with associated maximum pressure gradient and critical foam quality for each core

Core ID	U_T [cc/min]	f_g^*	max μ_{app} [Pa s]	ΔP_{max} [bar/m]	Perm. [mD]	Injection direction	Foam agent
ST1**	1	0.70	-	-	2487.0	Drainage	Nanoparticle
ST2	1	0.70	3.89	0.37	1608.7	Drainage	
	2	0.70	3.41	0.66			
	3	0.70	3.33	0.97			
	4	0.70	3.35	1.29			
ST3 w+g	2	0.50	3.35	0.38	2252.3	Drainage	Brine
	3	0.50	2.80	0.48			
	4	0.50	2.56	0.58			
ST3	2	0.70	8.63	1.30			Nanoparticle
	3	0.70	8.62	1.96			
	4	0.70	8.79	2.66			
ST4	1	0.70	3.48	0.40	2257.6	Drainage	
	2	0.35*	43.92	10.27		Imbibition	
ST5	1	0.35	12.58	1.47	1456.0	Imbibition	
	2	0.35	11.75	2.75			
	3	0.35	11.55	4.05			
	4	0.35	11.19	5.23			
ST6	1	0.70	179.51	16.99	1798.2	Drainage	Surfactant
	2	0.90	151.00	28.59			
	4	0.90	77.90	29.50			
	2	0.90	132.27	25.04		Imbibition	
	4	0.90	90.46	34.25			
LM (10,11,14)	1	0.35	3.29	20.06	27.8	Drainage	Nanoparticle
	2	0.35	2.68	32.82			
ST7	2	0.70	4.40	0.59	2527.4	Drainage	
	3	0.70	3.69	0.75			
	4	0.35	3.22	0.87			
	2	0.20	48.71	6.56		Imbibition	
	4	0.35	41.68	11.23			

* The pressure gradient did not achieve steady state before the experiment had to be determinate due to the safety pressure of the injection QX-pump.

** Experiments conducted in core ST1 has not been evaluated due to lost data.

7 Uncertainties related to Experiments

A summary of the uncertainties in this experimental study are briefly discussed in this chapter. Uncertainties related to the experiments conducted in this study can be divided into two categories; experimental and equipment uncertainties. The overall uncertainty in an experiment is the total of errors related to the many steps in preparing the experiment, and the uncertainties in the equipment. The main contributor related to the experiments error is the experimental uncertainty. This uncertainty is hard to control and is related to leakage, BPR, temperature variations etc. It can, however, be reduced by reproduction of the conducted experiment. The equipment uncertainties are always specified, and are listed in Table 7-1 for this experimental work. FS is notation for full scale, and is the maximum value the equipment can measure.

Table 7-1 Uncertainties of the equipment used in the conducted experiments

Equipment	**Uncertainty**
Caliper	± 0.01 mm
Weight	± 0.02 g
***ESI* pressure transducers**	± 0.015% FS
***Validyne* pressure transducer**	± 0.25% FS
***Quizix* injection pump**	± 0.1% of injection rate

7.1 Uncertainties related to Routine Core Analysis

- *Volumetric Measurements*
  It was assumed the cores geometry was a perfect cylinder when measuring the cross section area of the cores. This assumption was also made for the porosity, permeability and pore volume measurements. After the cores were drilled and cut using a circular saw, the perfect geometry is not always the case.

- The pore volume of the cores was found when the cores were saturated with brine, after they were dried in the heating cabinet. The vacuum pump removed air from the cores (Figure 5-3), and 100%water saturation was assumed. If air was left in the pore space, the calculated pore volume would become smaller than the absolute value. With the presence of air, a two phase system would occur since the cores then were saturated with two fluids (brine and air). The measured absolute permeabilities would then be relative permeabilities. The equipment used for the permeability measurements and drainage of the cores have uncertainties listed in

  Table **7-1**. When the cores were fractured, an additional error had to be considered in the calculation of the fractured pore volume. Using these errors, the uncertainties for the porosity and permeability measurements can be calculated. These calculations are presented in Appendix A.

7.2 Uncertainties related to EOR Core Flooding Experiments

During the EOR core flooding experiments presented in section 6.2, some difficulties occurred regarding the experimental set-up. These difficulties are discussed as uncertainties for the experiment in following key parameter

- *System Pressure*
  Difficulties related to constant pressure maintenance in the system occurred. Maintaining a constant backpressure using the BPR was difficult because the production pressure was either above or below the decided backpressure. Because of the pressure variation the experiments were conducted in a pressure range of 88 – 98 bar. Fluctuations in the differential pressure were observed. These fluctuations could be caused by the BPR since the BPR alternated between open and closed, depending on the pressure in the system.

- *Dead Volume*
  Oil was used to pressurize the experimental system before the injections of CO_2/CO_2-foam. Measuring the dead volume of the system was difficult, and is one of the major contributors to the uncertainty in the oil saturation and recovery. Making sure all the oil was removed from the dead volume before the injections were performed was challenging. An underestimation of the dead volume would result in a overestimation of oil production. The build-up pressure factor was also difficult to obtain. This factor is the addition of oil injected into the system for reaching 90 bar pressure conditions.

- *Temperature*
  Maintaining a constant temperature during the experiments was important since the fluid properties and pressure strongly depend on thermal conditions. The temperature was kept constant in a heating cabinet holding 35^{o}C. To minimize temperature variances the cabinet door was kept closed during the experiments. Exceptions were when valves located inside the cabinet had to be turned. A variation of ±1 ^{o}C was observed due to opening of the cabinet door.

- *Leakage*
  Possible system leaks have to be mentioned as a source of error. Leaks occur often in system with high pressures, and are difficult and time consuming to find. Leaks increase the uncertainty in an experiment, and are usually so significant that the experiments are aborted.

- *Oil Production Measurements*
  The produced oil was accumulated downstream the BPR in a graded cylinder. Measuring the produced oil volume was dependent on sight angle and the individual readings. The uncertainty of the readings was assumed to be ± 0.05 ml, which had a great impact on the oil recovery.

- *Uncertainties caused by Equipment*
  All the equipment uncertainties used in these experiments are listed in
  Table 7-1. The uncertainty in pump rate provided error in pore volumes injected. The pressure transducers errors results in an uncertainty in the line pressure of the system, in addition to the differential pressures across the cores. The *ESI* pressure transducers, ranging from 0-250 bar, had an uncertainty of ±0.38 bar. This is a large number with respect to the measured differential pressure ranging from 0-0.21 bar. The Quizix-pump injection rate uncertainty gave an error in the pore volumes injected and the fractional flow rate. The uncertainty to the pump was ±0.1% of flow rate.

7.3 Uncertainties related to Nanoparticle Sensitivity Analysis

The potential uncertainties in the sensitivity analysis of the nanoparticle foam generation are discussed in following key parameters

- *Measuring Differential Pressures*
  In the nanoparticle experiments the differential pressures were measured using a *Validyne* pressure transducer. The transducer had a pressure range of 0-14 bar, and an uncertainty of ±0.035 bar. However, the uncertainties in the differential pressures were dominated by the pressure fluctuations at the given rate and gas fraction. Reaching a stable differential pressure was at times difficult, and large fluctuations were observed for some of the injections. This contributed to an error in the achieved differential pressure.

- *Temperature*
  The experiments were conducted in room temperature of 25^{o}C, where the temperature was not controlled or systematically measured. The temperature variations were set to ±2^{o}C.

- *Saturation*
  Calculating the water saturation for one core (core EOR5), a large uncertainty was related to the system line volume, which contained brine. In addition, the water volume in the ST-pump, where the fluids accumulated, was a source of error. The calculated saturation in the core could be overestimated or underestimated.

- *Adsorption*
  The influence in adsorption of foam agents to the rock walls is unknown, and could have a remarkable effect on the results. The cores should have been flushed with the foam agent solutions prior to the experiments. This should have been performed to ensure the adsorption in the cores were kept to a minimum, and would have reduced this source of error.

- *Concentration*
  An uncertainty is also present in the mixing of the nanoparticle dispersion and brine concentrations. A weight was used for measuring the volumes of the fluids. Small differences in the nanofluid concentrations could have impact on the generated foam.

8 Conclusion

In this experimental study, foam stabilization and EOR has been evaluated using two types of foam agents: surfactants and nanoparticles. Miscible CO_2 and CO_2-foam generated *in-situ,* was injected for EOR in fractured limestone core plugs, using surfactants as foam agent. Sensitivity analysis of *in-situ* generated CO_2-foam in sandstone with nanoparticles was also performed.

Key observations from foam EOR in fractured carbonate core plugs

- Tertiary CO_2 and CO_2-foam injections in strongly water-wet limestone cores resulted in incremental oil recovery compared with water injection (R_F=16-36% OOIP). Similar recoveries were observed for pure CO_2 (R_F=47-59% OOIP) and CO_2-foam (R_F=44-63.1% OOIP) injections. The recovery mechanism in both whole and fractured core plugs was predominantly by molecular diffusion during CO_2 and CO_2-foam injection above the MMP between the CO_2 and oil.

- On average, 3.5 PV CO_2 was injected to reach the maximum recoveries during tertiary CO_2 and CO_2-foam injections, mainly a result of the decreased diffusion rate between oil and CO_2 due to the presence of water. Injection of CO_2-foam compared to pure CO_2 required less CO_2 injected.

- Injection of CO_2-foam, subsequent to a CO_2 injection, produced more oil compared with separate injections of CO_2 and CO_2-foam. All injections were tertiary, after a waterflood. These results demonstrate the adverse effect oil has on foam generation: oil saturation was lower for a CO_2-foam injection subsequent a CO_2 injection and a waterflood, hence, foam was generated and increased oil recovery.

- CO_2-foam was generated in whole cores, as observed by the increasing pressure gradient. Due to short cores and presence of oil, stable foam was not reached for the injection tests in this thesis. Foam did not generate *in-situ* in fractured systems mainly due to lack of foam generation sites and the presence of oil.

Key observations from foam generation using nanoparticles in sandstone cores

- Co-injection of CO_2 and nanoparticles increased the apparent viscosity to the CO_2 compared with co-injection of CO_2 and brine. The apparent viscosity increase with increasing gas fractional flow until 0.7, for all injection rates, then the apparent foam viscosity decreases with further increase in gas fraction.

- A hysteresis effect was observed during CO_2-foam generation using nanoparticles, where difficulty to establish a stable pressure and long injection times were observed using the imbibition injection strategy (decreasing gas fraction), compared to following the drainage strategy (increasing gas fraction). During the imbibition injection strategy, the highest apparent viscosity was observed at a gas fraction of 0.7, compared with 0.35 using the drainage injection strategy. This hysteresis effect was not observed when using surfactant as a foaming agent.

- Larger fluctuations in the differential pressures were observed when injecting from higher foam qualities to lower foam qualities. The fluctuations were larger co-injecting CO_2 with surfactant solution than with nanofluid. Sensitivity analysis should be performed with increasing gas fraction injecting nanofluid, and decreasing gas fraction injecting surfactant solution.

- The majority of reported results show that apparent viscosity for CO_2-foam using nanoparticles did not change with the total injection rates, but some experiments showed the apparent viscosity varied with the total injection rate. A clear conclusion cannot be drawn based on this work alone, and the changes in apparent viscosity with variations in injection rate using nanoparticles must be investigated further.

- Measuring the cores permeabilities after the experiments showed a significant reduction compared to the absolute permeability measured before the experiments were conducted. The permeability reduction was in the range of 16-32% injecting nanofluid in the sandstones. The permeability reduction was 31% injecting surfactant solution. This indicated adsorption of the foam agents to the rock walls. However, two cores re-saturated with brine after the experiments were conducted, showed a permeability decrease in the range of 6-8%. This indicate the adsorption of the nanoparticles to the rock walls are either irreversible, or the measurement after the experiments had large amount of gas present in the pore space resulting in a high differential pressure. The effect of adsorption needs further investigations.

- Foam was sucessfully generated in both sandstone and carbonate core material, using nanoparticles as foam stabilizer. Indications showed that adsopsion of nanoparticles onto the pore wall surfaces was minimal.

9 Future work

- Foam injections for EOR using surfactants in fractured limestone cores should be performed in cores of larger dimensions. Both areal cross section and length of the cores should be changed. The foam generating mechanisms should be investigated for better performance, not interrupted by inlet effects when the cores are longer.

- The cores used in future experiments should be flushed with the foam agent solution prior to the experiments. This should be performed to ensure the adsorption in the cores are kept to a minimum, and not having a large effect on the results.

- Further work on foam generation using nanofluid should be carried out under reservoir conditions. The objective should be to find the nanoparticles quality and stability under high temperature and salinity conditions. A better understanding of how nanofluid-generated foam behaves with oil present should be performed and tested for oil displacement efficiency.

- CO_2/nanofluid foam generation should be tested in fractured porous networks. Different dimensions should be tested to observe if it has any impact on the generated foam. If the dimensions do not have a large influence, smaller cores could be using being more time and material efficient. This is because it would require less fluid injected for each core flood experiment. Using small cores, the volume of the experimental system should be kept to a minimum for making the errors smaller.

- Constant total injection rates were used in this experimental study. The nanofluid should be investigated with constant liquid rates, varying the gas fraction and total injection rate. The objective would be to investigate the foam stability in the high and low foam flow regimes found by Osterloh and Jante, 1992,(Osterloh and Jante 1992)
- The differential pressure across the core should be measured at smaller intervals, not only across the whole core for being able to evaluate the impact of inlet effects.

- The effect of nanoparticle and surfactant concentrations should be considered with the objective of finding an optimal concentration for a given system.

10 Nomenclature

φ	Porosity
V_p, V_b	Pore and bulk volume, respectively
ρ	Fluid density
o	Oil
w	Water
g	Gas
Q	Flow rate
A	Areal
D	Diameter
μ	Fluid Viscosity
μ_{app}	Foam Apparent Viscosity
P	Pressure
T	Temperature
L	Core length
K	Permeability
P_c	Capillary Pressure
K_{abs}	Absolute permeability
K_{rel}	Relative permeability
K_{eff}	Effective permeability
R_f	Recovery Factor
MMP	Minimum Miscibility Pressure
EOR	Enhanced Oil Recovery
OOIP	Original Oil in Place
IFT	Interfacial tension
f_g	Gas fraction
S_g	Gas Saturation

S_w	Water Saturation
S_o	Oil Saturation
S_{wi}	Initial Water Saturation
$S_{or,w}$	Residual Oil Saturation after Waterflooding
$S_{or\ g}$	Residual Oil Saturation after CO_2 flooding
$S_{or,foam}$	Residual Oil Saturation after foam flooding
R_f	Total Recovery Factor (% OOIP)
$R_{f,w}$	Recovery Factor from Waterflooding (% OOIP)
$R_{f,CO2}$	Recovery Factor from CO_2 flooding (% OOIP)
$R_{f,foam}$	Recovery Factor from foam flooding (% OOIP)
SWW	Strongly Water Wet
BPR	Back Pressure Regulator
DV	Distillated Water
CO_2	Carbon dioxide
MRF	Mobility Reduction Factor
wt%	Weight Percent
M	Mobility Ratio

11 References

Abrams, A. (1975). "The Influence of Fluid Viscosity, Interfacial Tension, and Flow Velocity on Residual Oil Saturation Left by Waterflood."

Adkins, S. S., D. Gohil, J. L. Dickson, S. E. Webber and K. P. Johnston (2007). "Water-in-carbon dioxide emulsions stabilized with hydrophobic silica particles." Phys Chem Chem Phys **9**(48): 6333-6343.

Alvarez, J. M., H. J. Rivas and W. R. Rossen (2001). "Unified Model for Steady-State Foam Behavior at High and Low Foam Qualities."

Apaydin, O. G. and A. R. Kovscek (2000). Transient Foam Flow in Homogeneous Porous Media: Surfactant Concentration and Capillary End Effects, Society of Petroleum Engineers.

Aronofsky, J. S. (1952). "Mobility Ratio - Its Influence on Flood Patterns During Water Encroachment."

Asghari, K. and F. Torabi (2008). Effect of Miscible and Immiscible CO2 Injection on Gravity Drainage: Experimental and Simulation Results, Society of Petroleum Engineers.

Ayirala, S. C. and D. N. Rao (2006). "Fluid Phase Equilibrium."

Bernard, G. C., L. W. Holm and C. P. Harvey (1980). "Use of Surfactant to Reduce CO2 Mobility in Oil Displacement."

Bijeljic, B. and M. J. Blunt (2006). A Physically-Based Description of Dispersion in Porous Media, Society of Petroleum Engineers.

Binks, B. P. (2002). "Particles as surfactants—similarities and differences." Current Opinion in Colloid & Interface Science **7**(1–2): 21-41.

Blaker, T., M. G. Aarra, A. Skauge, L. Rasmussen, H. K. Celius, H. A. Martinsen and F. Vassenden (2002). "Foam for Gas Mobility Control in the Snorre Field: The FAWAG Project."

Blunt, M., M. , J. Fayers and O. F. M. (1993). Carbon Dioxide in Enhanced Oil Recovery Department of Petroleum Engineering, Stanford University, Stanford, California, USA: 1197-1204.

Brattekas, B., A. Haugen, G. Ersland, O. Eide, A. Graue and M. A. Ferno (2013). Fracture Mobility Control by Polymer Gel- Integrated EOR in Fractured, Oil-Wet Carbonate Rocks, Society of Petroleum Engineers.

Brautaset, A., G. Ersland and A. Graue (2010). "In Situ Phase Pressures and Fluid Saturation Dynamics Measured in Waterfloods at Various Wettability Conditions."

Burger, J. E., G. Springate and K. K. Mohanty (1996). " Experiments on Bypassing During Gasfloods in Heterogeneous Porous Media."

Campbell, B. T. and F. M. Orr, Jr. (1985). "Flow Visualization for CO2/Crude-Oil Displacements."

Chatzis, I. and M. N. R. (1984). "Correlation of Capillary Number Relationships for Sandstone."

CO2CRC. (2015). "Carbon Dioxide Molecule." Retrieved 01/15, 2015, from www.co2crc.com.au/imagelibrary3/general.php?screen=2

Contreras, J. D., D. G. Durst and A. Al-Qaissy (2010). Maximizing Well Life and Optimizing Exploitation Strategies with Solid Expandable Tubulars, Society of Petroleum Engineers.

Corbett, P. W. M., P. S. Ringrose, J. L. Jensen and K. S. Sorbie (1992). Laminated Clastic Reservoirs: The Interplay of Capillary Pressure and Sedimentary Architecture, Society of Petroleum Engineers.

Craze, R. C. (1950). "Performance of Limestone Reservoirs."

Darvish, G. R. (2007). "Physical Effects Controlling Mass Transfer in Matrix Fracture System during CO2 Injection Into Chalk Fractured Reservoirs." (Norwegian University of Science and Technology, Department of Petroleum Engineering and Applied Geophysics).

Dautriat, J., N. F. Gland, s. Youssef, E. Rosenberg and S. Bekri (2007). Stress-Dependent Permeabilities of Sandstones and Carbonates: Compression Experiments and Pore Network Modelings, Society of Petroleum Engineers.

David, A. and S. S. Marsden, Jr. (1969). The Rheology of Foam, Society of Petroleum Engineers.

Dickson, J. L., B. P. Binks and K. P. Johnston (2004). "Stabilization of Carbon Dioxide-in-Water Emulsions with Silica Nanoparticles." (Langmuir 2004, 20, 7976-7983).

Dooley, J. J., R. T. Dahowski and C. L. Davidson (2010). "CO2-driven Enhanced Oil Recovery as a Stepping Stone to What?" U.S. Department of Energy.

Duerksen, J. H. (1986). "Laboratory Study of Foaming Surfactants as Steam-Diverting Additives."

Esmaeilzadeh, P., A. Bahramian and F. Z (2011). Adsorption of Anionic, Cationic and Nonionic Surfactants on Carbonate Rock in Presence of ZrO2 Nanoparticles, Petroleum Industries Processes Design, Tehran South Branch, Azad University, Tehran, Iran.

Espinoza, D. A., F. M. Caldelas, K. P. Johnston, S. L. Bryant and C. Huh (2010). Nanoparticle-Stabilized Supercritical CO2 Foams for Potential Mobility Control Applications, Society of Petroleum Engineers.

Ettinger, R. A. and C. J. Radke (1992). "Influence of Texture on Steady Foam Flow in Berea Sandstone."

Falls, A. H., G. J. Hirasaki, T. W. Patzek, D. A. Gauglitz, D. D. Miller and T. Ratulowski (1988). "Development of a Mechanistic Foam Simulator: The Population Balance and Generation by Snap-Off."

Farajzadeh, R., A. Andrianov, R. Krastev, G. Hirasaki and W. R. Rossen (2012). Foam-Oil Interaction in Porous Media: Implications for Foam Assisted Enhanced Oil Recovery, Society of Petroleum Engineers.

Farajzadeh, R., A. Andrianov and P. Zitha (2009). Foam Assisted Oil Recovery at Miscible and Immiscible Conditions, Society of Petroleum Engineers.

Farajzadeh, R., A. Andrianov and P. L. J. Zitha (2010a). Investigation of Immiscible and Miscible Foam for Enhanced Oil Recovery, Shell International Exploration and Production, Rijiswik, The Netherlands and Delft University and Technology, Delft, The Netherlands. Ind. Eng. Chem. Res. 2010, 49, 1910-1919.

Ferno, M. A., J. Gauteplass, M. Pancharoen, A. Haugen, A. Graue, A. R. Kovscek and G. J. Hirasaki (2014). Experimental Study of Foam Generation, Sweep Efficiency and Flow in a Fracture Network, Society of Petroleum Engineers.

Fried, A. N. (1961). "The Foam Drive Process for Increasing the Oil Recovery of Oil." (US. Bureau of Mines. Rep. Inv 5866).

Friedmann, F. and J. A. Jensen (1986). Some Parameters Influencing the Formation and Propagation of Foams in Porous Media, Society of Petroleum Engineers.

Gabitto, J. F. (1998). Matrix-Fracture Mass Transfer, Society of Petroleum Engineers.

Graue, A., K. Nesse, B. A. Baldwin, E. A. Spinler and D. P. Tobola (2002). Impact of Fracture Permeability on Oil Recovery in Moderately Water-Wet Fractured Chalk Reservoirs, Society of Petroleum Engineers.

Grigg, R. B., M. D. Gregory and J. D. Purkaple (1997). "The Effect of Pressure on Improved Oilflood Recovery from Tertiary Gas Injection."

Grigg, R. B., R. K. Svec, Z. Zeng, B. Bai, L. B. Bethapudi, S. Ganda, D. B. Gupta and Y. Liu (2003). Improving CO2 Efficiency for Recovering Oil in Heterogeneous Reservoirs Annual Technical Progress Report, New Mexico Petroleum Recovery Research Center, New Mexico Institue of Mining and Technology.

Grogan, A. T., V. W. Pinczewski, G. J. Ruskauff and F. M. J. Orr (1988). "Diffusion of CO2 at Reservoir Conditions: Models and Measurements."

Grogan, A. T. and W. V. Pinczewski (1987). "The Role of Molecular Diffusion Processes in Tertiary CO2 Flooding."

Grundmann, S. R. and D. L. Lord (1983). "Foam Stimulation."

Habermann, B. (1960). The Efficiency of Miscible Displacement as a Function of Mobility Ratio, Society of Petroleum Engineers.

Hansford, J. and Q. Fisher (2009). "The Influence of Fracture Closure from Petroleum Production from Naturally Fractured Reservoirs: A Simulation Model Approach."

Hanssen, J. E. and M. Dalland (1990). Foams for Effective Gas Blockage in the Presence of Crude Oil, Society of Petroleum Engineers.

Harpole, K. J., W. T. Siemers and M. G. Gerard (1994). CO2 Foam Field Verification Pilot Test at EVGSAU: Phase IIIC--Reservoir Characterization and Response to Foam Injection, Society of Petroleum Engineers.

Haugen, Å., M. A. Fernø, A. Graue and H. J. Bertin (2012). Experimental Study of Foam Flow in Fractured Oil-wet limestone for Enhanced Oil Recovery, SPE Reservoir Evaluation and Engineering.

Haugen, Å., N. Mani, S. Svenningsen, B. Brattekås, A. Graue, G. Ersland and M. A. Fernø (2013). Miscible and Immiscible Foam Injection for Mobility Control and EOR in Fractured Oil-Wet Carbonate Rocks, Department of Physics and Technology, University of Bergen, Norway.

Haugen, K. B. and A. Firoozabadi (2006). Measuring Molecular and Thermal Diffusion Coeffi cients in Multicomponent Mixtures by the Beam Deflection Technique, Society of Petroleum Engineers.

Healy, R. N., E. D. Holstein and J. P. Batycky (1994). [7]3 Status of Miscible Flooding Technology, World Petroleum Congress.

Hirasaki, G., C. A. Miller and M. Puerto (2011). "Recent Advances in Surfactant EOR."

Hirasaki, G. J. (1989). "The Steam-Foam Process."

Hirasaki, G. J. (1989). Supplement to SPE 19505, The Steam-Foam Process--Review of Steam-Foam Process Mechanisms, Society of Petroleum Engineers.

Hirasaki, G. J. and J. B. Lawson (1985). Mechanisms of Foam Flow in Porous Media: Apparent Viscosity in Smooth Capillaries, Shell Development Co.

Hjartnes, T. N. (2015). An Experimental Study of Tertiary CO2 Injection Startegies in Fractured Limestone". Master University of Bergen.

Holm, L. W. (1970). "Foam Injection Test in the Siggins Field, Illinois."

Holm, L. W. (1986). "Miscibility and Miscible Displacement." Journal of Petroleum Technology.

Holm, L. W. and V. A. Josendal (1974). "Mechanisms of Oil Displacement By Carbon Dioxide."

Holm, L. W. and V. A. Josendal (1982). "Effect of Oil Composition on Miscible-Type Displacement by Carbon Dioxide."

Hoteit, H. and A. Firoozabadi (2009). "Numerical Modeling of Diffusion in Fractured Media for Gas-Injection and -Recycling Schemes."

Hudgins, D. A. and T. H. Chung (1990). Long-Distance Propagation of Foams, Society of Petroleum Engineers.

Hustad, C. W. and J. M. Austell (2004). Mechanisms and Intensives to Promote the Use and Storage of CO2 in the North Sea, CO2-Norway AS.

Jensen, T. B., K. J. Harpole and A. Østhus (2000). EOR Screening for Ekofisk, Society of Petroleum Engineers.

Jones, S. A., V. van der Bent, R. Farajzadeh, W. R. Rossen and S. Vincent-Bonnieu (2015). "Small Core Flood Experiments for Foam EOR- Screening Surfactant Applications."

Kam, S. I., W. W. Frenier, S. N. Davies and W. R. Rossen (2003). Experimental Study of High-Temperature Foam for Acid Diversion, Society of Petroleum Engineers.

Kamibayashi, M. (2008). "Shear-thickening Flow of Nanoparticle Suspensions flocculated by Polymer Bridging." (Department of Urban Environment Systems, Faculty of Engineering, Chiba University, Japan).

Keelan, D. K. and V. J. Pugh (1975). "Trapped-Gas Saturations in Carbonate Formations."

Khatib, Z. I., G. J. Hirasaki and A. H. Falls (1988). "Effects of Capillary Pressure on Coalescence and Phase Mobilities in Foams Flowing Through Porous Media."

Kim, J., Y. Dong and W. R. Rossen (2005). "Steady-State Flow Behavior of CO2 Foam."

Koval, E. J. (1963). "A Method for Predicting the Performance of Unstable Miscible Displacement in Heterogeneous Media."

Kovscek, A. R. and C. J. Radke (1994). Fundamentals of Foam Transport in Porous Media, In: Foams: Fundamentals and Applicantions in the Petroleum Industry, ACS Advances in Chemistry Series, N.242, American Society.

Kovscek, A. R., D. C. Tretheway, P. Persoff and C. J. Radke (1995). "Foam Flow Through a Transparent rough-walled Fracture." Journal of Petroleum Science and Engineering.

Kulkarni, M. M. and D. N. Rao (2004). Experimental Investigation of Various Methods of Tertiary Gas Injection, Society of Petroleum Engineers.

Lake, L. W. (1984). A technical Survery of Micellar Polymer Flooding. presented at Enhanced Oil Recovery A symposium for the Independent Producer, Southern Methodist University, Dallas, Texas.

Lake, L. W. (1989). "Enhanced Oil Recovery." (Prentice Hall Incorporate. Englewood Cliffs, New Jersey).

Lam, A. C., R. S. Schechter and W. H. Wade (1983). "Mobilization of Residual Oil Under Equilibrium and Nonequilibrium Conditions."

Lee, H. O., J. P. Heller and A. M. W. Hoefer (1991). "Change in Apparent Viscosity of CO2 Foam With Rock Permeability."

Li, R. F., R. B. Le Bleu, S. Liu, G. J. Hirasaki and C. A. Miller (2008). Foam Mobility Control for Surfactant EOR, Society of Petroleum Engineers.

Lindeberg, E. and T. Holt (1994). EOR by Miscible CO2 Injection in the North Sea, Society of Petroleum Engineers.

Liu, Y., R. B. Grigg and R. K. Svec (2005). CO2 Foam Behavior: Influence of Temperature, Pressure, and Concentration of Surfactant, Society of Petroleum Engineers.

Mo, D., B. Jia, J. Yu, N. Liu and R. Lee (2014). Study Nanoparticle-stabilized CO2 Foam For Oil Recovery At Different Pressure, Temperature, And Rock Samples, Society of Petroleum Engineers.

Mo, D., J. Yu, N. Liu and R. Lee (2014). The Application of Nanoparticle-Stabilized CO Foam for Oil Recovery, Society of Petroleum Engineers.

Mo, D., J. Yu, N. Liu and R. L. Lee (2012). Study of the Effect of Different Factors on Nanoparticle-Stablized CO2 Foam for Mobility Control, Society of Petroleum Engineers.

Möbius, D. and R. Miller (1998). Foam and Foam Films, Studies in Interfacial Science, Dotchi Exerowa Institute of Physical Chemistry, Bulgarian Academy of Science, Sofia, Bulgaria and Pyotr M. Kruglyakov (State Academy of Archetecture and Building, Penza, Russia).

Muller, T. and L. W. Lake (1991). "Theoretical Study of Water Blocking in Miscible Flooding."

Nagarajan, N. and R. L. Robinson (1986). (J. Chem. Eng. 31 168).

NIST. (2011). "Thermophysical Propertirs of Fluid Systems." from http://webbook.nist.gov/chemistry/fluid/.

NOAA. (2014). "Greenhouse Gases." from http://www.ncdc.noaa.gov/monitoring-references/faq/greenhouse-gases.php.

Nowack, N. and T. D. Bucheli (2007). Occurrance, Behavior and Effects of Nanoparticles in the Environment. Environmental Pollution**:** 5-22.

NPD, T. N. P. D. (2015). "Nasjonalbibliotek for Sokkelen." Retrieved 06/10/2015, 2015, from http://www.npd.no/.

Ogolo, N. A., O. A. Olafuyi and M. O. Onyekonwu (2012). Enhanced Oil Recovery Using Nanoparticles, Society of Petroleum Engineers.

Opdal, I. (2014). Mobility Control by CO2-foam Injection for Integrated EOR. Master Degree, University of Bergen.

Osterloh, W. T. and M. J. J. Jante (1992). "Effects of Gas and Liquid Velocity on Steady-State Foam Flow at High Temperature."

Pancharoen, M., M. A. Fernø and A. R. Kovsceka (2012). "Modeling Foam Displacement in Fractures." Journal of Petroleum Science and Engineering.

Perkins, T. K. a. O. C. J. (1964). "A Review of Diffusion and Dispersion in Porus Media."

Persoff, P., C. J. Radke, K. Pruess, S. M. Benson and P. A. Witherspoon (1991). "A Laboratory Investigation of Foam Flow in Sandstone at Elevated Pressure."

Picha, M. S. (2007). Enhanced Oil Recovery By Hot CO2 Flooding, Society of Petroleum Engineers.

Pomeroy , R. D., W. N. Lacey, N. F. Nathan F. Scudder and F. P. Stapp (1933). "Rate of Solution of Methane in Quiescent Liquid Hydrocarbons." Ind. Eng. Chem.

Puerto, M. C. and R. L. Reed (1983). "A Three-Parameter Representation of Surfactant/Oil/Brine Interaction."

Ramsden, W. (1903). "Separation of Solids in the Surface-Layers of Solution and Suspensions." Retrieved 01/15, 2015, from http://www.jstor.org/stable/pdfplus/116458.pdf?acceptTC=true.

Ransohoff, T. C. and C. J. Radke (1988). "Mechanisms of Foam Generation in Glass-Bead Packs."

Roebroeks, J., A. A. Eftekhari, R. Farajzadeh and S. vincent-Bonnieu (2015). "Nanoparticle Stabilized Foam in Carbonate and Sandstone Reservoirs."

Roebrokes, J., A. A. Eftekhari, R. Farajzadeh and S. vincent-Bonnieu (2015). "Nanoparticle Stabilized Foam in Carbonate and Sandstone Reservoirs."

Rossen, W. R. and Q. Lu (1997). Effect of Capillary Crossflow on Foam Improved Oil Recovery, Society of Petroleum Engineers.

Safouane, M., D. Langevin and B. P. Binks (2007). Effect of Particle Hydrophobicity on the Propeties of Silica Particle Layers at the Air-Water Interface, Laboratoire de Physique des Solides, Université Paris 11, 91405 Orsay, France, and Surfactant & Colloid Group, Department of Chemistry, University of Hull, Hull HU6 7RX, United Kingdom.

Sanchez, J. M., R. S. Schechter and A. Monsalve (1986). The Effect of Trace Quantities of Surfactant on Nitrogen/Water Relative Permeabilities, Society of Petroleum Engineers.

Schramm, L. L. (1994). Foams: Fundamentals and Applications in the Petroleum Industry, Petroleum Recovery Institute, American Chemical Society, Washington, DC.

Schweitzer, P. (2015). "Mineral Resources On-line Spatial Data - Edward Limestone." Available from [http://tin.er.usgs.gov/geology/state/sgmc-unit.php?unit=TXKed%3B0](U. S Department of the Interior).

Sheng, J. J. (2013). Enhanced Oil Recovery Field Case Studies. Bob L. Herd Department of Petroleum Engineering, Texas Tech University.

Sheng, J. J., B. B. Maini, R. E. Hayes and W. S. Tortike (1997). "Experimental Study of Foamy Oil Stability."

Singh, R. and K. K. Mohanty (2014). Synergistic Stabilization of Foams by a Mixture of Nanoparticles and Surfactants, Society of Petroleum Engineers.

Skarrestad, M. and A. Skauge (2011). "Re. Fluid properties and Recovery Methods."

Skarrestad, M. and A. Skauge (2012). Reservoir Technique II, Fluid Properties and Recovery Methods PTEK213 Course Compendium, University of Bergen.

Skauge, A., M. G. Aarra, L. Surguchev, H. A. Martinsen and L. Rasmussen (2002). Foam-Assisted WAG: Experience from the Snorre Field, Society of Petroleum Engineers.

Skjæveland, S. M. and J. Kleppe (1992). SPOR - Recent Advances in Improved Oil Recovery Methods For North Sea Sandstone Reservoirs, Stavanger, Norwegain Petroleum Directorate.

Song, Y. C., N. J. Zhu, Y. Liu, J. F. Zhao, W. G. Liu, Y. Zhang, Y. C. Zhao and L. L. Jiang (2011). "Magnetic Resonance Imaging Study on the Miscibility of a CO2/n-decane System."

(Key Laboratory of Ocean Energy Utilization and Energy Conservation of Ministry of Education, Dalian University of Technology, Dalian 116024).

Svorstøl, I., F. Vassenden and K. Mannhardt (1996). Laboratory Studies for Design of a Foam Pilot in the Snorre Field, Society of Petroleum Engineers.

Taber, J. J. (1969). "Dynamic and Static Forces Required To Remove a Discontinuous Oil Phase from Porous Media Containing Both Oil and Water."

Taber, J. J., F. D. Martin and R. S. Seright (1997). "EOR Screening Criteria Revisited - Part 1: Introduction to Screening Criteria and Enhanced Recovery Field Projects."

Takahashi, S., H. Okabe, H. Mitsuishi, H. Kawahara, H. R. Al-Shehhi and H. M. Al-Hammadi (2012). Phase behavior and displacement characteristics for CO2 EOR with a reservoir fluid from a Middle Eastern offshore reservoir, Society of Petroleum Engineers.

Tanzil, D., G. J. Hirasaki and C. A. Miller (2000). Mobility of Foam in Heterogeneous Media: Flow Parallel and Perpendicular to Stratification, Society of Petroleum Engineers.

Tiffin, D. L. and W. F. Yellig (1983). "Effects of Mobile Water on Multiple-Contact Miscible Gas Displacements."

Turta, A. T. and A. K. Singhal (1998). Field Foam Applications in Enhanced Oil Recovery Projects: Screening and Design Aspects, Society of Petroleum Engineers.

UoA. (2005, Visited [04/21/2015]). "Geology - Rocks and Minerals, Limestone." Retrieved The University of Auckland, New Zealand, from http://flexiblelearning.auckland.ac.nz/rocks_minerals/rocks/limestone.html

Uren, L. D. and E. H. Fahmy (1927). "Increasing Oil Recovery by Flooding ".

van Lingen, P. P. and S. Knight (1997). Evaluation of Capillary Entrapment within Reservoir Flow Units, Society of Petroleum Engineers.

Whaley, J. (2008). "Pyrenees Holds Clues to Fractured Carbonate Reservoirs." Retrieved 10/06/15, 2015, from http://assets.geoexpro.com/legacy-files/articles/Pyrenees%20Hold%20Clues%20to%20Fractured%20Carbonate%20Reservoir.pdf

Willhite, G. P. (1986). "Waterflooding." (Society of Petroleum Engineers).

Worthen, A., H. Bagaria, Y. Chen, S. L. Bryant, C. Huh and K. P. Johnston (2012). Nanoparticle Stabilized Carbon Dioxide in Water Foams for Enhanced Oil Recovery, Society of Petroleum Engineers.

Worthen, A., H. Bagaria, Y. Chen, S. L. Bryant, C. Huh and K. P. Johnston (2012). Nanoparticle Stabilized Carbon Dioxide in Water Foams for Enhanced Oil Recovery, Society of Petroleum Engineers.

Yaghoobi, H. (1994). Laboratory Investigation of Parameters Affecting CO2-Foam Mobility in Sandstone at Reservoir Conditions, Society of Petroleum Engineers.

Yang, S. H. and R. L. Reed (1989). Mobility Control Using CO2 Forms, Society of Petroleum Engineers.

Yu, J., C. An, D. Mo, N. Liu and R. L. Lee (2012). Foam Mobility Control for Nanoparticle-Stabilized Supercritical CO2 Foam, Society of Petroleum Engineers.

Yu, J., S. Wang, N. Liu and R. Lee (2014). Study of Particle Structure and Hydrophobicity Effects on the Flow Behavior of Nanoparticle-Stabilized CO2 Foam in Porous Media, Society of Petroleum Engineers.

Zhang, T., D. Davidson, S. L. Bryant and C. Huh (2010). Nanoparticle-Stabilized Emulsions for Applications in Enhanced Oil Recovery, Society of Petroleum Engineers.

Zhang, T., M. Roberts, S. L. Bryant and C. Huh (2009). Foams and Emulsions Stabilized With Nanoparticles for Potential Conformance Control Applications, Society of Petroleum Engineers.

Zhang, T., M. J. Murphy, H. Yu, H. G. Bagaria, K. Y. Yoon, B. M. Nielson, C. W. Bielawski, K. P. Johnston, C. Huh and S. L. Bryant (2014). "Investigation of Nanoparticle Adsorption During Transport in Porous Media."

Zhang, Y. P., S. G. Sayegh and S. Huang (2007). Effect of Oil/Brine Ratio on Interfacial Tension in Surfactant Flooding, Petroleum Society of Canada.

Zolotukhin, A. B. and J.-R. Ursin (2000). "Introduction to Petroleum Engineering." (Kristiansand, Høyskoleforelaget AS - Norwegian Academic Press): 402.

Zuta, J., I. Fjelde and R. Berenblyum (2009). Oil Recovery During CO2-foam Injection in Fractured Chalk Rock at Reservoir Conditions, International Research Institute of Stavanger (IRIS).

Zuta, J. F. (2010). "Improve Macroscopic Sweep Efficiency in CO2-Flooding of Fractured Carbonate Reservoirs."

Appendix A - Uncertainties Calculations

The uncertainty of value R given by variables, x, y, z....., i, where the uncertainty for each variable is given by $\boldsymbol{S_{\bar{x}}}$, $\boldsymbol{S_{\bar{y}}}$, $\boldsymbol{S_{\bar{z}}}$,……,$\boldsymbol{S_{\bar{i}}}$ can be calculated by equation

$$S_{\bar{R}} = \sqrt{\left(\frac{\partial R}{\partial x}\mathrm{S}_{\bar{\mathrm{x}}}\right)^2 + \left(\frac{\partial R}{\partial y}\mathrm{S}_{\bar{\mathrm{y}}}\right)^2 + \left(\frac{\partial R}{\partial z}\mathrm{S}_{\bar{\mathrm{z}}}\right)^2 + \cdots + \left(\frac{\partial R}{\partial i}\mathrm{S}_{\bar{\mathrm{i}}}\right)^2}$$

[A-1]

Where x,y,z,….,i are uncorrelated variables and $\bar{x}, \bar{y}, \bar{z}, \ldots . . \bar{i}$, are the arithmetical middle value of the measured variables given by

$$\bar{x} = \frac{x_1+x_2+x_3+\cdots..x_N}{N} = \frac{1}{N}\sum_{i=1}^{N} x_i \qquad \text{[A-2]}$$

If the value R is given as a product of variable: $R = x^n + y^m + z^k$ the uncertainty, ∂R, can be written as

$$\partial \bar{R} = R\sqrt{\left(n\frac{\partial x}{x}\right)^2 + \left(m\frac{\partial y}{y}\right)^2 + \left(k\frac{\partial z}{z}\right)^2}$$

[A-3]

Uncertainty in porosity

The uncertainty in the porosity measurement is contributed by the use of the calliper. The bulk volume of the cores is calculated by using the volume equation for a circular tube

$$V_{bulk} = \pi \cdot r^2 \cdot L \qquad \text{[A-4]}$$

where *r* is the radius and *L* is the length of the core.

The uncertainty in the bulk volume is given by

$$\partial_{\overline{V_{bulk}}} = \sqrt{(2 \cdot \pi \cdot L \cdot \partial_{\bar{r}})^2 + (\pi \cdot r^2 \cdot \partial_{\bar{L}})^2}$$

[A-5]

The formula for pore volume is

$$V_p = \frac{m}{\rho} \qquad \text{[A-6]}$$

where the uncertainties are in the mass of the core, *m,* and in the density of the saturating fluid, ρ.

$$\partial_{\bar{v}_p} = \sqrt{\left(\partial_{\bar{m}} \frac{\partial v_p}{\partial m}\right)^2 + \left(\partial_{\bar{\rho}} \frac{\partial v_p}{\partial \rho}\right)^2} \quad \text{[A-7]}$$

The uncertainty in the porosity is based on equation 5.1, and is found by combining equation A-5 and A-7 giving equation

$$\partial_{\bar{\varphi}} = \sqrt{\left(\partial_{\overline{V_p}} \frac{1}{V_{bulk}}\right)^2 + \left(\partial_{\overline{V}_{bulk}} \frac{V_p}{V_{bulk}}\right)^2} \quad \text{[A-8]}$$

Uncertainty in permeability

The contribution to the uncertainty regarding permeability is the variation in Darcy's law (equation 2.1) Using equation A-3 the uncertainty can be calculated by

$$\partial \overline{K} = K \sqrt{\left(\frac{\partial \bar{Q}}{\bar{Q}}\right)^2 + \left(\frac{\partial \bar{\mu}}{\bar{\mu}}\right)^2 + \left(\frac{\partial \bar{L}}{\bar{L}}\right)^2 + \left(\frac{\partial \bar{A}}{\bar{A}}\right)^2 + \left(\frac{\partial \overline{\Delta p}}{\overline{\Delta p}}\right)^2} \quad \text{[A-9]}$$

Calculation example of permeability error in core ST4

Table A-1 Values for calculating the permeability and corresponding error for core ST4

	Value	**Uncertainty**
K [D]	2.30	-
Q [ml/h]	800.00	± 0.80
A	11.16	± 0.01
L [cm]	0.28	± 0.05
ΔP [bar]	0.29	± 0.04
μ [cP]	1.08	± 0.01

$$\partial \overline{K} = 2303 \sqrt{\left(\frac{0.80}{800}\right)^2 + \left(\frac{0.01}{11.16}\right)^2 + \left(\frac{0.05}{0.28}\right)^2 + \left(\frac{0.04}{0.29}\right)^2 + \left(\frac{0.01}{1.08}\right)^2} = \underline{5.23 \text{ mD}}$$

The uncertainty for the Validyne pressure transducer, measuring the differential pressures in the experiments, was $\pm$0.04 bar. Even though the error in the pressure transducer was low, the uncertainties in the experiments were dominated by the fluctuation of the pressures at the given rate and gas fraction.

Table A-2 Maximum apparent viscosities, differential pressures and permeabilities with corresponding uncertainties

Core ID	U_T [cc/min]	f_g^*	max μ_{app} [Pa s]	ΔP_{max} [bar/m]	Perm. [mD]
ST2	1	0.70	3.89 ± 0.15	0.377 ± 0.05	1608.7 ± 3.8
	2	0.70	3.41 ± 0.08	0.659 ± 0.05	
	3	0.70	3.33 ± 0.05	0.965 ± 0.05	
	4	0.70	3.35 ± 0.04	1.294 ± 0.05	
ST3 w+g	2	0.50	3.35 ± 0.40	0.38 ± 0.06	2252.3 ± 5.17
	3	0.50	2.80 ± 0.27	0.48 ± 0.06	
	4	0.50	2.56 ± 0.10	0.58 ± 0.03	
ST3	2	0.70	8.63 ± 0.60	1.30 ± 0.09	
	3	0.70	8.62 ± 0.53	1.96 ± 0.12	
	4	0.70	8.79 ± 0.30	2.66 ± 0.09	
ST4	1	0.70	0.70 ± 0.08	0.40 ± 0.03	
	2	0.35*	12.65 ± 0.06	10.27 ± 0.24	2257.6 ± 5.2
ST5	1	0.35	12.6 ± 0.3	1.47 ± 0.07	1456.0 ± 4.7
	2	0.35	11.8 ± 0.5	2.7 ± 0.2	
	3	0.35	11.6 ± 0.8	4.1 ± 0.1	
	4	0.35	11.2 ± 1.7	5.2 ± 0.1	
ST6	1	0.70	179.5 ± 4.8	17.0 ± 0.5	1798.2 ± 4.1
	2	0.90	151.0 ± 10.5	28.6 ± 0.9	
	4	0.90	77.9 ± 4.5	29.5 ± 0.7	
	2	0.90	132.3 ± 17.3	25.0 ± 2.1	
	4	0.90	90.5 ± 4.6	34.3 ± 1.9	
LM (10,11,14)	1	0.35	3.27 ± 0.09	20.06 ± 0.06	27.8 ± 0.1
	2	0.35	2.68 ± 0.02	32.8 ± 1.1	
ST7	2	0.70	4.4 ± 0.4	0.60 ± 0.05	2527.4 ± 5.8
	3	0.70	3.7 ± 0.1	0.75 ± 0.06	
	4	0.90	3.2 ± 0.2	0.87 ± 0.06	
	2	0.20	48.8 ± 3.6	6.6 ± 0.2	
	4	0.35	41.7 ± 1.4	11.2 ± 0.4	

Table A-3 Initial permeabilities and permeabilities measured after nanofluid injections with corresponding uncertainties.

Core ID	Initial perm. [mD]	Relative perm. [mD]
ST2	1608.65 ± 3.84	1514.35 ± 3.62
ST3	2252.25 ± 5.17	2079.29 ± 4.76
ST4	2257.6 ± 5.2	1623.3 ± 3.7
ST5	2067.7 ± 4.7	1722.8 ± 3.9
ST6	1798.2 ± 4.1	1244.5 ± 2.8
ST7	2527.4 ± 5.8	1713.5 ± 3.9
LM10	22.45 ± 0.05	20.59± 0.05
LM11	30.29 ± 0.07	22.51 ± 0.05
LM14	30.70 ± 0.07	24.75 ± 0.06

Appendix B – Differential Pressures

The developing differential pressure for the experiments are plotted and added in this appendix for core ST5, ST6, ST7 and the limestone core.

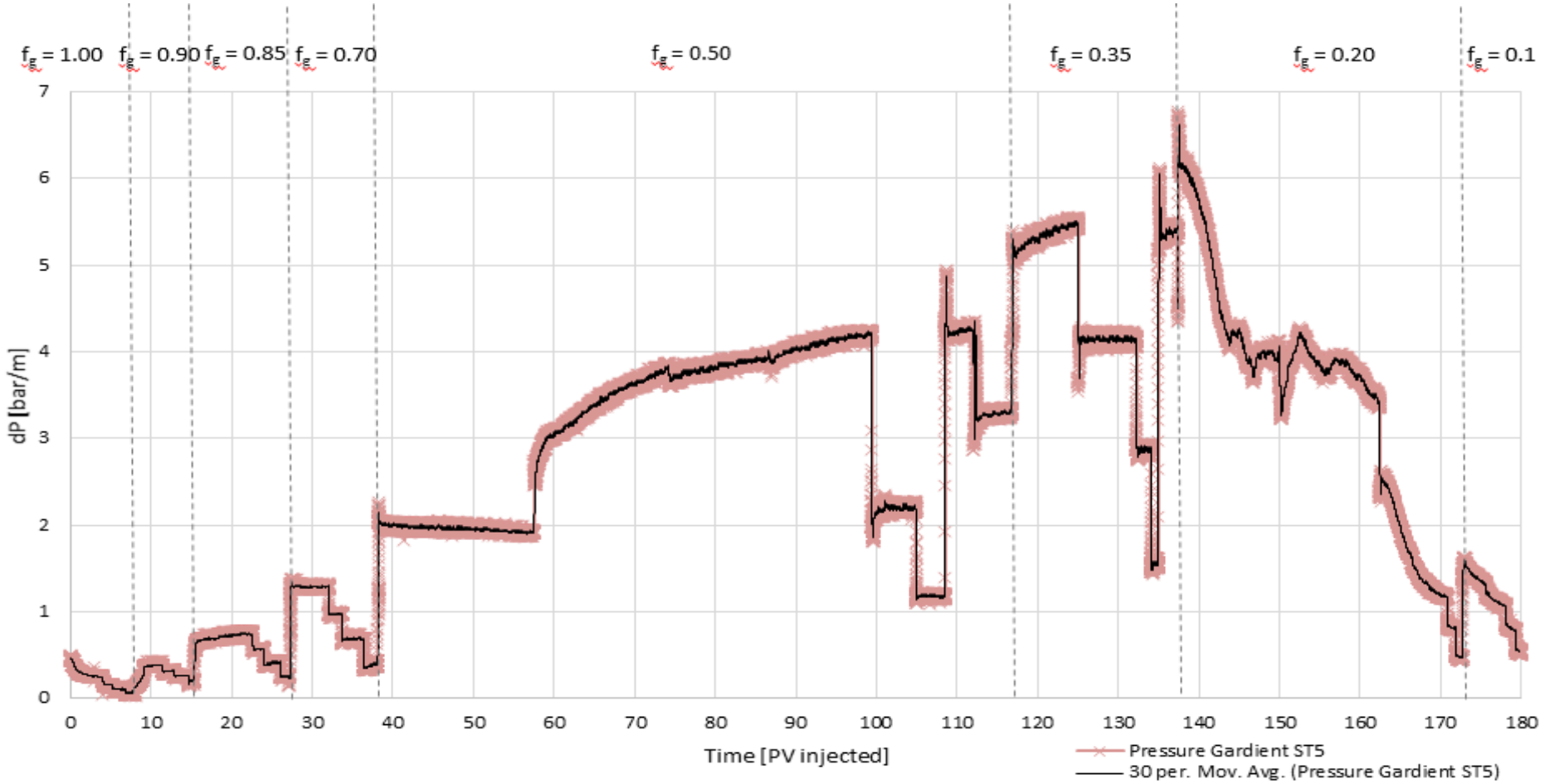

Figure B-1 Pressure gradient versus pore volume injected for sandstone core ST5 with decreasing foam quality, f_g, from 1.0 to 0.1 for four total constant injection rates. Pressure steady state was easily achieved in the low quality regime, (f_g<0.70) where as in the transition phase of high quality regime (f_g>0.70) the differential pressures varied more due to coalesce of the generated foam.

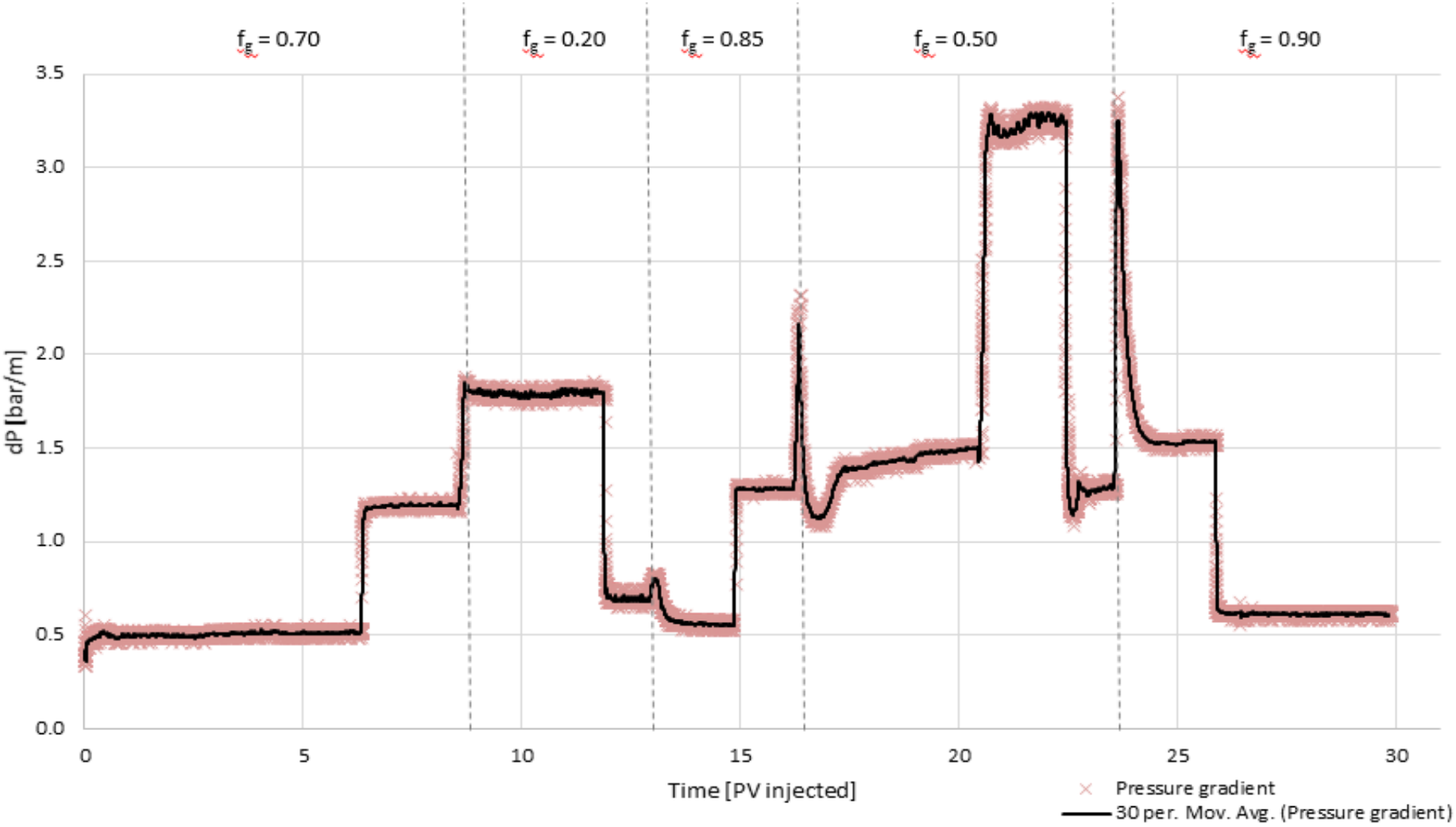

Figure B-2 Differential pressure gradient versus pore volume injected for varying gas quality injection in sandstone core ST5. The foam quality was changed from higher to lower continuously changing between two constant total injections. Pressure steady state is easy obtained for each rate and foam quality. Each step in the graph correspond to a injection rate. On the other hand, looking at the developing differential pressure gradient for the varying gas fraction injections in Figure B-2 the differential pressure has achieved steady state for all injection rates and foam qualities.

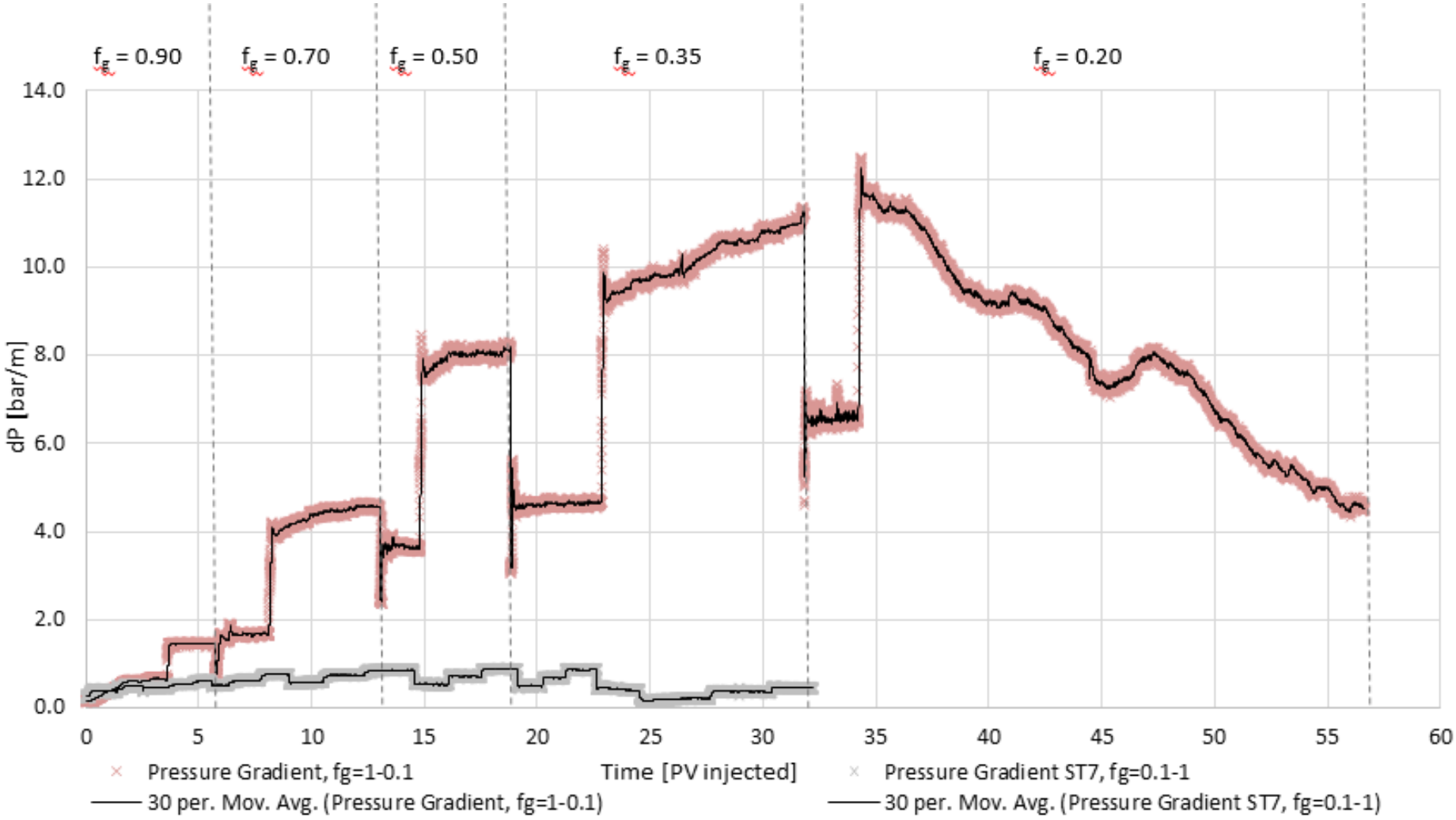

Figure B-3 Differential pressure gradient versus pore volume injected for sandstone core ST7. The pink graph represent co-injection of nanofluid and CO_2 following the imbibition curve (decreasing gas fraction), while the grey pressure gradient represents the co-injection following the drainage curve (increasing gas fraction). The latter graph is for comparison only and is shown better in Figure 6-18.

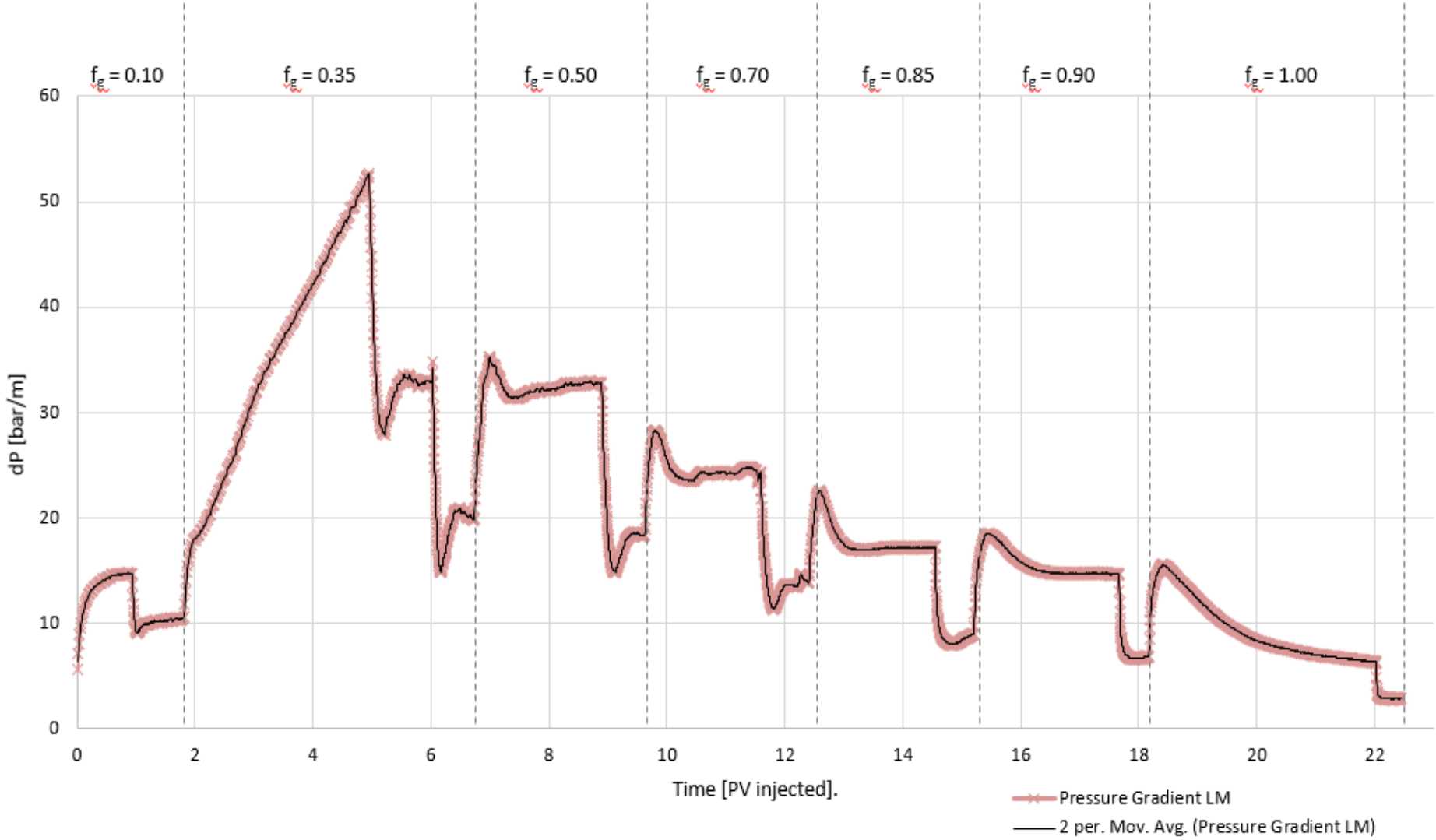

Figure B-5 Differential pressure gradient versus pore volume injected for co-injection of nanofluid and CO_2 in limestone carbonate core. Three total injection rates were used where each plateau in the graph corresponds to one injection rate within the given foam quality